Copy No. 35

RESTRICTED

RM No. L8D29

NACA

RESEARCH MEMORANDUM

WIND-TUNNEL INVESTIGATION OF HIGH-LIFT AND STALL-CONTROL

DEVICES ON A 37° SWEPTBACK WING OF ASPECT RATIO 6

AT HIGH REYNOLDS NUMBERS

By

William Koven and Robert R. Graham

Langley Aeronautical Laboratory
Langley Field, Va.

NATIONAL ADVISORY COMMITTEE
FOR AERONAUTICS

WASHINGTON
September 2, 1948

RESTRICTED

NATIONAL ADVISORY COMMITTEE FOR AERONAUTICS

———

RESEARCH MEMORANDUM

———

WIND-TUNNEL INVESTIGATION OF HIGH-LIFT AND STALL-CONTROL

DEVICES ON A 37° SWEPTBACK WING OF ASPECT RATIO 6

AT HIGH REYNOLDS NUMBERS

By William Koven and Robert R. Graham

S U M M A R Y

Results are presented of an investigation in the Langley 19-foot pressure tunnel of the longitudinal characteristics of a semispan model wing having 37° sweepback of the leading edge, an aspect ratio of 6, and NACA 64_1-212 airfoil section perpendicular to the 27-percent-chord line. Several types of stall-control devices including extensible round-nose leading-edge flaps, a leading-edge slat, and a drooped leading edge were investigated; partial- and full-span trailing-edge split and double slotted flaps were also tested. In addition, various combinations of the aforementioned leading- and trailing-edge flaps were investigated. The tests covered a range of Reynolds numbers between 2.00×10^6 and 9.35×10^6.

The wing with or without trailing-edge split or double slotted flap was longitudinally unstable near maximum lift due to tip stalling. The addition of an outboard half-span leading-edge flap or a leading-edge slat to the plain wing or wing with inboard half-span split flaps eliminated tip stalling and resulted in stable moment variations at the stall. The drooped leading edge, on the other hand, was only effective when used in conjunction with an upper-surface fence.

The combination of an outboard leading-edge device and inboard half-span double slotted flap resulted in an undesirable loop in the pitching-moment curve near maximum lift in spite of an inboard stall. The loop is attributed to the section characteristics of the double slotted flap. Air-flow surveys behind the wing indicated that a suitably placed horizontal tail would eliminate the loop in the moment curve.

For combinations with split flaps, upper and lower limits exist for the span of the leading-edge device between which stability at the stall can be obtained; a critical span of the leading-edge device was found, however, below which reductions in maximum lift resulted.

The maximum lift coefficient of the plain wing was about 1.27.
Maximum lift coefficients of about 1.5 and 2.0 were obtained for
combinations of an outboard half-span leading-edge device with inboard
half-span split and double slotted flaps, respectively. The highest
maximum lift coefficients were obtained with drooped leading edge
plus fence combinations with trailing-edge flaps. An increase in
trailing-edge flap span from half to full span did not produce appreciable
increases in maximum lift when the accompanying changes in trim were
taken into account.

INTRODUCTION

Numerous investigations have been devoted to a study of the low-
speed longitudinal characteristics of swept wings. (For example, see
references 1 to 3.) As indicated by these studies, two of the major
difficulties associated with sweptback wings are low values of maximum
lift coefficient compared with unswept wings and instability at the
stall due to tip stalling.

As far as maximum lift is concerned, the available data are confined
mainly to investigations of plain wings and wings with split flaps.
Even with split flaps, the maximum lift coefficients have been relatively
low and it is indicated that investigation of additional high-lift devices
such as a double slotted flap would be desirable.

One method of eliminating tip stalling which has been used suc-
cessfully (reference 4) involves the use of a leading-edge device located
on the outboard sections of the wing span. Several types of leading-edge
devices have been tried, that is, extensible round-nose leading-edge
flap, leading-edge slat, and so forth; but no direct comparison to assist
in the selection of the most satisfactory device has been made.

With the above considerations in mind, an investigation has been
conducted in the Langley 19-foot pressure tunnel on a wing having 37°
sweepback of the leading edge and an aspect ratio 6. It should be
pointed out that the wing plan-form variables were such that, according
to the stability boundary presented in reference 1, tip stalling and
instability at the stall would be expected. In addition to the basic
wing characteristics at high Reynolds number, the investigation was
concerned mainly with (a) the effectiveness of double slotted flaps
and split flaps, (b) whether a leading-edge device would eliminate tip
stall on the particular plan form used, (c) the determination of the
relative merits of several types of leading-edge devices, and (d) the
magnitude of maximum lift coefficients and the type of stall associated
with various combinations of leading- and trailing-edge devices.

The semispan reflection-plane model was equipped with three types of leading-edge or stall-control devices, namely, a round-nose extensible leading-edge flap, a leading-edge slat, and a drooped leading edge. In addition, the wing was provided with partial- and full-span split and double slotted flaps. Additional devices, such as a fence and outboard pitch flaps, were also investigated. The model configurations were tested alone and in combination through a large angle-of-attack range at Reynolds numbers varying from 2.00×10^6 to 9.35×10^6. Lift, drag, and pitching-moment data and stall studies are given for some of the more important configurations.

C O E F F I C I E N T S   A N D   S Y M B O L S

The data are referred to the wind axes with the origin at the quarter chord of the mean aerodynamic chord. The data have been reduced to standard NACA nondimensional coefficients which are defined as follows:

C_L lift coefficient $\left(\dfrac{L}{qS}\right)$

$C_{L_{max}}$ maximum lift coefficient

C_D drag coefficient $\left(\dfrac{D}{qS}\right)$

C_m pitching-moment coefficient $\left(\dfrac{M}{qS\bar{c}}\right)$

R Reynolds number $\left(\dfrac{\rho V \bar{c}}{\mu}\right)$

M_O stream Mach number

α angle of attack of root chord line, degrees

α_{max} angle of attack at $C_{L_{max}}$

C_{L_α} lift-curve slope $\left(\dfrac{dC_L}{d\alpha}\right)$

ϵ downwash angle, degrees

Z vertical distance above chord plane extended

L lift

D   drag

M   pitching moment about $0.25\bar{c}$

S   wing area

b   wing span

b_f flap span

$\bar{c}$ mean aerodynamic chord $\left(\dfrac{2}{S} \displaystyle\int_0^{b/2} c^2 dy \right)$

c   local wing chord parallel to plane of symmetry

y   lateral coordinate

$\bar{y}$ lateral coordinate of centroid of lift

q   dynamic pressure $\left(\dfrac{\rho V^2}{2} \right)$

q_t dynamic pressure at tail

V   free-stream velocity

μ coefficient of viscosity

ρ density of air

δ flap deflection

Subscripts:

n   nose

a   aileron

MODEL AND TESTS

MODEL

The model used in the investigation was a semispan wing mounted on a reflection plane and single strut as shown in figure 1. It was of steel construction and had an aspect ratio of 6, a taper ratio of 0.50, and 37° sweepback of the leading edge. The airfoil section perpendicular

to the 27-percent-chord line was the NACA 64_1-212 profile. The general
plan form and some of the principal dimensions of the model are given in
figure 2(a).

Details of the geometry of the various stall-control devices are
shown in figures 2(b) to 2(d). The drooped leading edge (which could be
deflected to three positions) and the leading-edge slat covered half
the wing semispan extending from $0.45\frac{b}{2}$ to $0.95\frac{b}{2}$. The round-nose extensible
leading-edge flap, on the other hand, was constructed so that several
flap spans could be investigated at one deflection. The leading-edge
flap was of constant chord, whereas both the slat and the drooped leading
edge were of constant percent chord.

The model was so constructed that when the leading edge was drooped,
the slat was in the retracted position. Thus, slight discontinuities in
contour existed at 0.14c and 0.02c of the upper and lower surfaces of
the wing, respectively, for the drooped leading-edge configurations.
No such discontinuities were present, however, on configurations without
stall-control devices or configurations with leading-edge flap where a
different leading edge was used.

The stall-control fence is shown in figures 2(e) and 2(f). The
fence was located at $0.50\frac{b}{2}$, had a constant height of 0.60 the maximum
thickness of the wing at that spanwise location, and extended over the
chord as indicated on the figure.

The model was equipped with two types of trailing-edge flaps,
namely, split and double slotted, both of which could be tested half and
full span. The design parameters for the double slotted flap were
chosen on the basis of two-dimensional wind-tunnel data given in
reference 5. A schematic drawing showing the design details of these
flaps is presented in figures 2(g) and 2(h).

Photographs of the model and reflection plane mounted in the tunnel
and of the various stall-control devices installed on the model are
presented as figure 3.

For model configurations with leading-edge roughness, No. 60
(0.011-inch diameter) carborundum particles were applied by means of
a thin coat of shellac to the forward 8- and 2-percent of the wing
upper and lower surfaces, respectively. Roughness for the slat-extended
configuration was applied in the same manner to the leading edge of the
slat and to the leading edge of the inboard sections of the wing.

TESTS

Tests were made in the Langley 19-foot pressure tunnel with the air compressed to approximately 33 pounds per square inch. In order to cover as wide a range of Reynolds numbers as possible, several tests were made at atmospheric pressure. The Reynolds numbers and their corresponding Mach numbers obtained in this investigation are as follows:

R	M_O
2.00×10^6	0.08
3.00	.12
4.36	.08
5.30	.10
6.80	.13
8.10	.15
9.35	.18

Lift, drag, and pitching moment were measured through an angle-of-attack range extending well beyond maximum lift. In addition, stall studies of some of the more interesting configurations were made by visual observation and from motion-picture records of the behavior of wool tufts attached to the upper surface of the wing. The majority of the tests and the stall studies were conducted at a Reynolds number of about 6,800,000. Downwash and dynamic-pressure surveys were made behind the wing for the slat and half-span double-slotted-flap configuration.

CORRECTIONS TO DATA

The lift, drag, and pitching-moment data presented herein have been corrected for air-stream misalinement but have not been corrected for support tare and interference effects. Previous experience on complete models indicates that corrections for the effects of the tare and interference caused by the model supports consist of (a) a constant shift in the pitching-moment curve (about -0.008), (b) a slight increase in lift-curve slope (about 0.0008), and (c) a decrease in drag in the low lift range.

Jet-boundary corrections obtained by combining the methods of references 6 and 7 were made to the angle of attack and to the drag coefficient and are as follows:

$$\Delta\alpha = 1.12C_L$$
$$\Delta C_D = 0.0164C_L^2$$

The correction to the pitching-moment coefficient caused by the tunnel-induced distortion of the loading is

$$\Delta C_m = 0.0101 C_L$$

All corrections were added to the data.

RESULTS AND DISCUSSION

The results of the investigation of the plain wing and wing with trailing-edge flaps are presented in figures 4 to 7. Figures 8 to 12 show the effect of leading-edge devices, and figures 13 to 22 show the effect of various combinations of leading-edge and trailing-edge devices. Several additional tests were made to determine the effect of varying the leading-edge flap span; only the maximum lift and pitching-moment characteristics of these configurations are presented (fig. 16). The spanwise location of the centroid of lift is presented for several configurations in figure 23. A summary of the more important results of the investigation is presented as table I.

PLAIN WING AND HIGH-LIFT DEVICES

Lift Characteristics

The data for the plain wing and wing with split and double slotted flaps are presented in figures 4 to 7. The lift curves for all conditions were relatively linear up to maximum lift except for a slight rounding at high angles of attack. In all cases the maximum lift coefficient and angle of attack at maximum lift were very well defined indicating a rather sudden breakdown of the flow at the critical angle.

Lift-curve slope.- The lift-curve slope was calculated from two-dimensional data using the method suggested in reference 8 where the aspect ratio is based on the true length of the quarter-chord line. The lift-curve slope was also obtained from the charts of reference 9 which assume a section lift-curve slope of 2π. The two methods predicted values of lift-curve slope of 0.071 and 0.066, respectively, as compared with the value of 0.070 obtained experimentally.

Effect of flap deflection.- Increments in lift at zero angle of attack and at maximum lift are presented in figure 5 as a function of flap span. The data for the half- and full-span flaps were taken from figure 4; in order to obtain more complete data on the effects of flap

span, some additional tests on intermediate split-flap spans were made. Only the lift increments for the supplementary tests are presented.

An attempt was made to estimate the increments in lift at zero angle of attack from two-dimensional data utilizing a method for unswept wings outlined in reference 10. The equation was modified and sweep taken into account as follows:

$$\Delta C_L = J \, \Delta c_l \, C_{L_{\alpha_\Lambda}} \cos \Lambda$$

where

J factor depending on aspect ratio, taper ratio, and flap span (reference 10)

Δc_l two-dimensional lift increment

$C_{L_{\alpha_\Lambda}}$ calculated lift-curve slope of the swept wing

Λ angle of sweep of quarter-chord line

It is believed that the form of the revised equation represents the first-order effects of sweepback. The calculated curves are given in figure 5 as the dashed lines.

Considering the split-flap configurations, it can be seen that the effect of inboard spans up to $0.5\frac{b}{2}$ was calculated with reasonable accuracy. For spans greater than $0.5\frac{b}{2}$, on the other hand, the theory greatly overestimated the contribution of the flap. No such noticeable departure from theory has been obtained on unswept wings; this abnormal loss of outboard flap effectiveness may be typical of split flaps on sweptback wings.

The data for the double-slotted-flap configurations are considerably different from those for the split flap. The double slotted flap produced larger increments in lift throughout the flap-span range than the theory predicted, and the outboard span did not lose its effectiveness beyond what might be expected from the simplified theory.

The reason for this difference between the split and double slotted flap is not apparent. The effects of sweepback on the variation with flap span of the increment in lift due to flap deflection appear to be dependent on the type of flap under consideration.

Figure 5 also shows that the increments in lift at maximum lift are considerably less than at zero angle of attack. The magnitude of this effect, however, appears to be of the same order as on unswept wings of similar airfoil section. (See reference 11.)

Maximum lift.- As far as the maximum lifts are concerned, they can best be summarized in the following table. The values of $C_{L_{max}}$ listed below are untrimmed values:

Flap	$C_{L_{max}}$
None	1.27
$0.5\frac{b}{2}$ split	1.55
$0.5\frac{b}{2}$ double	1.92
$1.0\frac{b}{2}$ split	1.65
$1.0\frac{b}{2}$ double	2.32

Pitching-Moment Characteristics

Except for the full-span double-slotted-flap condition, the pitching-moment curves were fairly linear, and for the most part, parallel to one another (fig. 4). In all cases the moment at the stall broke in an unstable direction, that is, in a nose-up direction.

The trim changes brought about as a result of flap deflection are of special interest. A comparison of the data from figure 4 with similar data from reference 11 shows that the full-span split and double slotted flaps produced changes in trim which were of the same magnitude as on an unswept wing with approximately the same airfoil section. The semispan flaps, however, produced considerably smaller trim changes than was noted on the unswept wing. The half-span split flaps caused practically no change in trim, and the half-span double slotted flaps effected less change than the full-span split flaps. (See fig. 4(b).) The smaller trim changes associated with the half-span flaps are a result of the increased lift over the inboard portions of the wing ahead of the $0.25\bar{c}$ point.

The changes in trim would require a balancing down load at the tail which would reduce the available lift. For example, assuming a tail length of $2.0\bar{c}$ and a center-of-gravity location of $0.25\bar{c}$, the available lift at $0.85C_{L_{max}}$ will be reduced as indicated in the following table:

Flap	$0.85C_{L_{max}}$	$0.85C_{L_{max}}$ (trim)
None	1.08	1.05
$0.5\frac{b}{2}$ split	1.32	1.28
$0.5\frac{b}{2}$ double	1.63	1.54
$1.0\frac{b}{2}$ split	1.40	1.29
$1.0\frac{b}{2}$ double	1.97	1.66

It appears that little gain in the usable maximum lift coefficient is obtained from an increase in flap span from half to full span.

Drag Characteristics

Referring to the drag polars (fig. 4), it can be seen that, in general, the effects of the flaps are similar to those on unswept wings; that is, for a given lift coefficient the half-span split flap had lower drag than the same span double slotted flap, and the full-span split flap had higher drag than the full-span double slotted flap.

Stalling Characteristics

The stalling characteristics for the plain wing and half-span trailing-edge flap configurations are presented in figure 6. For all configurations the stall occurred rather suddenly, encompassing the entire outer half of the wing semispan. Prior to the stall a marked outflow along the wing trailing edge was observed. This cross flow was most severe for the plain wing and resulted in a region of rough, but not stalled, flow at the trailing edge of the tip sections. This apparently reduced the lift effectiveness of the outboard sections because, upon examination of the pitching-moment and lift curves, it can be seen that a noticeable nosing-up tendency and rounding of the lift curve occurred concurrently with the rough flow. Similar but less severe conditions prevailed with double slotted flaps but did not occur with split flaps.

Scale and Roughness Effect

The effects of a fairly wide variation in Reynolds number on lift, drag, and pitching moment of the plain wing are shown in figure 7. At low Reynolds numbers the lift curves were well rounded near maximum lift,

whereas at Reynolds numbers of 4,350,000 and higher the curves were characterized by sharp peaks. As might be expected, $C_{L_{max}}$ increased with increasing Reynolds number, the rate of increase being greatest between Reynolds numbers of 3,000,000 and 4,350,000.

There were no important scale effects on the pitching-moment curves near $C_{L_{max}}$; in all cases the moment broke in an unstable direction.

One test was made to determine the effects of leading-edge roughness on the aerodynamic characteristics of the model at a Reynolds number of 6,800,000. The results (fig. 7) show that the leading-edge roughness caused a reduction in $C_{L_{max}}$ and a decrease in the lift-curve slope in the high lift range. The roughness also caused irregularities in the pitching-moment-coefficient curve near maximum lift. The reduction in $C_{L_{max}}$ was not so large as that obtained in similar tests of a 42° sweptback wing reported in reference 12. The smaller reduction in $C_{L_{max}}$ is believed to be, in part, due to the smaller relative size of the carborundum grains used for the roughness in the present investigation. The reasons for the peculiar behavior of the pitching-moment curve are not apparent.

STALL-CONTROL DEVICES

The data for the various stall-control devices are presented in figures 8 to 11. It should be remembered that the slat was present in the retracted position for all the tests with the leading edge drooped (including zero angle of droop). The irregularities in profile due to the presence of the slat had a noticeable effect on maximum lift as can be seen from the comparison with the plain wing (fig. 8). In evaluating the effect of the drooped leading edge, reference should therefore be made to the zero droop angle condition and not to the configuration possessing the continuous profile.

The previous remarks do not apply to the leading-edge flap or slat configurations; the data for these conditions should be compared directly with the data for the wing without the discontinuities.

Lift Characteristics

In general, the effect of the drooped leading edge was to shift the lift curve so as to make the angle of zero lift more positive (fig. 8) and to increase the angle of attack for maximum lift. The maximum lift coefficient was increased approximately 0.11 and was, in the main, independent of the angle of droop.

Figure 9 shows a comparison between the round-nose leading-edge flap and the leading-edge slat; it also shows the effect of two spans of the leading-edge flap. The addition of the leading-edge flap increased the lift-curve slope an amount approximately proportional to the increase in area caused by the flap; the slat, on the other hand, had a negligible effect on C_{L_α}. With the leading-edge flap or slat, the maximum lift coefficient was not a very well defined parameter in that the lift curves near $C_{L_{max}}$ were fairly well rounded. The effects of varying the span of the leading-edge flap on $C_{L_{max}}$ can be obtained from figure 16. It can be seen that extension of the leading-edge flap inboard from the $0.95\frac{b}{2}$ station caused a decrease in maximum lift until the inboard end of the flap reached the 0.60 semispan station; further extensions inboard, however, produced increases in $C_{L_{max}}$. The loss in maximum lift obtained with the smaller span flaps is attributed to premature stalling behind the inboard end of the flap which apparently counteracts the increase in lift contributed by the flapped portion of the wing. Although similar premature stalling occurs with the larger span flaps, the increment in lift effected by the large span flap is great enough to produce a net increase in maximum lift. Unpublished data indicate that the effects of varying the span of the slat would probably be similar to those shown for the leading-edge flap.

Pitching-Moment Characteristics

The primary function of the stall-control devices is to delay tip stalling and to cause the inboard sections to stall first. This presumably would produce a nose-down pitching moment at the stall. Thus, insofar as the stall-control devices are concerned, the greatest interest centers about their effect on wing pitching moments near maximum lift.

With the drooped leading edge, for all the angles of droop, the pitching-moment curves showed a marked but gradual destabilizing trend several degrees prior to the stall similar to that for the no-droop configuration. At the stall, however, the curves broke in a stable direction except in the case of the 40° droop. In general, it might be said that the drooped leading edge did not display satisfactory stall-control qualities.

The leading-edge flap and the slat proved to be adequate with regard to stabilizing the moment near the stall. There was no appreciable tendency toward instability prior to the stall except for the larger span leading-edge flap. This destabilizing effect for the $0.70\frac{b}{2}$ flap, although not so marked as for the drooped leading edge, might be considered undesirable.

The effects of varying the leading-edge flap span over a fairly wide range are shown in figure 16(b). It can be seen that flap spans between $0.375\frac{b}{2}$ and $0.70\frac{b}{2}$ provided stable pitching-moment variations at the stall. The pitching moment at the stall for the full-span flap was unstable similar to that obtained with the plain wing.

Data on a 42° sweptback wing of aspect ratio 4 (reference 4), having an outboard leading-edge slat differing from the present slat, indicated that the particular slat configuration used was not completely satisfactory as a stall-control device. If the difference in angle of sweep between the present wing and that of reference 4 can be considered of secondary importance, the inference may be drawn that very careful attention must be given to the slat-position parameters if the full benefits of the slat are to be realized.

Stalling Characteristics

The stalling characteristics of the wing with the various stall-control devices are presented in figure 10.

The drooped leading edge did not produce a satisfactory stall pattern. Although the origin of the stall was inboard (behind the inboard end of the droop), the stall itself moved outboard rather suddenly as the angle of attack was increased.

Comparing the leading-edge flap and slat it can be seen that, in general, the origin and progression of the stall were very similar. In both cases the stall originated behind the inboard end of the device and spread inboard and outboard. The outward movement of the stall, however, was not so great for the slat as it was for the flap configuration. A stall pattern such as produced by either the leading-edge flap or slat is believed satisfactory from the standpoint of wing longitudinal stability at or near maximum lift.

Drag Characteristics

When the stall-control devices are used, the drag characteristics are mainly of interest at high lift coefficients. Figure 8 shows that, for lift coefficients above 0.70, the drooped leading edge had very little effect on the drag of the plain wing. Comparison of the drag curves for the $0.50\frac{b}{2}$ leading-edge flap and slat (fig. 9) indicates that, for all practical purposes, the drag characteristics of the two devices are the same at high lift coefficients. Although the drag was less for the drooped leading-edge configuration than either the flap or the slat, the differences in drag do not appear to be of major importance.

Additional Stall-Control Devices

Fence.- The stall studies with the leading edge drooped indicated
that the droop was effective in displacing the initial point of stall
inboard but was not adequate in preventing the separated region of flow
from moving outboard. In an effort to prevent this outward shift,
an investigation was made to determine the effects of an upper-surface
fence. This fence was of constant height and placed slightly outboard
of the inboard end of the droop. The data for this configuration are
shown in figure 8.

The lift and drag characteristics of the drooped leading-edge
configuration were not noticeably altered by the addition of the fence;
the pitching-moment characteristics near and at the stall, on the other
hand, were markedly improved. In spite of a slight destabilizing trend
several degrees prior to the stalling angle, the general shape of the
pitching-moment curve was such that the combination of droop plus
fence might be considered satisfactory. The fence in combination with
the droop apparently straightened the cross flow to such an extent
that outward spread of the stalled region was delayed. From a comparison
of the stall studies showing the effects of the fence on the wing with
leading edge drooped and neutral (fig. 11), it can be seen that the fence
did not materially influence the origin of the stall but only prevented
the outward progression once the stall had started. The tip stalling
associated with the unflapped wing was relatively unaffected by the
addition of the fence.

Wing twist.- Some interest has been shown toward the possibility
of incorporating washout in the outer wing panels of sweptback wings
as a means of eliminating tip stalling. Since the model in this
investigation could be equipped with a plain 0.20-chord aileron extending
over the outboard 50 percent of the wing span (for use in a subsequent
lateral control investigation), an opportunity arose to simulate wing
twist by deflecting the ailerons. Although aileron deflection does
not exactly reproduce the effect of twist, it is believed that some
correlation does exist for wings of moderate camber and thickness.

Figure 12 shows the characteristics of the plain wing as affected
by several aileron deflections. The data show that a definite improve-
ment in the wing pitching-moment characteristics several degrees prior
to the stalling angle was effected by the 20° and 25° up aileron
deflections, but that no improvement at the stall itself was produced.
The magnitude of the twist at high angles of attack corresponding to
25° up aileron is difficult to estimate. The data of reference 13, however,
indicate that 20° up aileron on a similar airfoil are equivalent to
about 9° at low angles of attack but only about 3.5° of twist at the stall.
It would appear, therefore, that large amounts of twist would be required
to effect any appreciable change in the wing stalling characteristics.

COMBINATIONS OF HIGH-LIFT AND STALL-CONTROL DEVICES

The previously discussed data have shown that tip stalling was eliminated by use of the various stall-control devices and that reasonably high values of maximum lift were obtained with either the half-span split or double slotted flap. In the case of the former, the maximum lifts realized were comparatively low, and for the latter, the wing was still longitudinally unstable at $C_{L_{max}}$. Consequently, the various high-lift and stall-control devices were tested in combination to obtain an indication of the highest maximum lift coefficient obtainable with a stable pitching-moment variation at the stall. The data for the combinations are shown in figures 13 to 22.

Lift Characteristics

Combinations with split flaps.- Figure 13 shows the data for the half-span split flap in combination with leading-edge flaps of several spans. The variation of $C_{L_{max}}$ with the span of the leading-edge flap when the half-span split flaps were deflected is shown in figure 16.

The leading-edge flap caused reductions in $C_{L_{max}}$ until the span was extended inboard to about the 0.4 semispan station. Extension of the flap inboard of the 0.4 semispan station produced increases in $C_{L_{max}}$ The action of the flap in the presence of the split flap was similar to its action when no trailing-edge flaps were on the wing. The reductions in $C_{L_{max}}$ due to the short-span leading-edge flaps, however, were considerably larger with the trailing-edge flaps deflected.

A comparison of the lift characteristics for three equal-span leading-edge devices is shown on figure 14. Comparing figures 8 and 14, it is evident that the drooped leading-edge combination produced the highest increments in maximum lift. The increments in maximum lift due to the combinations of leading- and trailing-edge devices were 0.38, 0.31, 0.19, 0.16 for the drooped leading edge, the droop plus fence, the leading-edge flap, and the slat, respectively.

Combinations with double slotted flaps.- Figure 15 shows the effect of two spans of the leading-edge flap and also compares the droop, slat, and flap. The variation of $C_{L_{max}}$ with span of leading-edge flap is shown in figure 16.

As was true with the split flap, the addition of leading-edge flaps reduced $C_{L_{max}}$ until the span of the flap was extended inboard to about the 0.4 semispan station. Extension of the flap inboard of that station increased $C_{L_{max}}$.

Comparing the droop, slat, and flap, it can be seen that (a) the maximum lift coefficients for the equal span flaps and slat were about the same and (b) that the drooped-leading-edge combination produced the highest increments in maximum lift coefficient. Unlike the split-flap configurations, however, the addition of the fence to the droop configuration effected a noticeable increase in maximum lift.

Although the data are not presented, it should be mentioned that extending the slat on the 30° drooped leading edge caused a reduction in maximum lift as compared to the drooped leading edge without the slat extended.

Pitching-Moment Characteristics

Combinations with split flaps.- The data indicate that stability at the stall can be obtained when a leading-edge device and a split flap are used together if the span of the leading-edge device is suitably chosen. For example, figures 13 and 16(b) show that the $0.50\frac{b}{2}$ leading-edge flap produced a nosing-down moment at the stall, whereas the $0.70\frac{b}{2}$ flap combination caused the pitching-moment-coefficient curve to break in a stable direction at $C_{L_{max}}$ but in an unstable direction as the lift dropped off in the stall. This unstable break was eliminated by a reduction in flap span from $0.70\frac{b}{2}$ to $0.65\frac{b}{2}$. The data also indicate that a minimum flap span exists below which unsatisfactory longitudinal stability characteristics at maximum lift will result. The combinations with $0.375\frac{b}{2}$ or $0.25\frac{b}{2}$ leading-edge flap displayed a nosing-up tendency at $C_{L_{max}}$ followed by a nosing-down tendency as the lift decreased in the stall. This loop was eliminated when the span of the leading-edge flap was extended to $0.50\frac{b}{2}$. It is believed that the leading-edge slat would act in a similar manner.

The slat and leading-edge flap configurations behaved similarly at the stall in that a nosing-down moment was obtained. The drooped leading edge, however, was not as effective as the flap or slat, as was indicated by a marked destabilizing trend several degrees prior to the stall. As in the case of the droop alone, the addition of the fence resulted in a pitching-moment curve that was satisfactory at the stall (fig. 14).

Combinations with double slotted flaps.- For all of the combinations with double slotted flaps, a typical loop in the moment curve (fig. 15) was noted at high lift coefficients. The loop was such that it showed nosing-up moments at $C_{L_{max}}$ but reversed to give stable moments as the lift dropped off in the stall. The stall studies for these configurations

(fig. 18) show the same type of stall progression as was obtained by the stable combinations with split flaps and indicate that the initial instability was not caused by a loss in lift over the outer portions of the wing. Two-dimensional data for the airfoil and double-slotted-flap configuration used on the subject wing show decided instability at the stall. (See reference 5.) This instability has also been noted on other double-slotted-flap airfoil sections and appears to be characteristic of that type of flap. Thus the initial stall occurred over a portion of the wing where the predominant factor in the wing pitching moment was the instability of the double-slotted-flap section. As the angle of attack was increased, the stall progression was such that the moment due to the loss in lift over the inboard portions of the wing exceeded the unstable moments due to the flap, resulting in the nose-down portion of the loop.

The effects of varying the leading-edge flap span on the pitching-moment characteristics of the double-slotted-flap combinations (fig. 16(b)) are somewhat obscured by the characteristics of the double slotted flaps. The pitching-moment characteristics are similar for all combinations of leading-edge flap and double slotted flap regardless of leading-edge flap span.

Drag Characteristics

In the high-lift-coefficient range there were no important differences in the drag characteristics of the various combinations with split flaps other than the lift coefficient at which the sharp drag rise occurred. The onset of the drag rise is associated with a break in the lift curve.

Similar results were obtained for the combinations with double slotted flaps.

The drag was higher for the double-slotted-flap configurations than for the split-flap configurations. In the high lift range (below the drag-rise lift coefficient) the greater drag of the double-slotted-flap combinations does not appear to be of great importance from the standpoint of relative sinking speeds. In particular, assuming a wing loading of 40 pounds per square foot and sea-level conditions, the sinking speeds at $0.85C_{L_{max}}$ are about 20 and 22 feet per second for the split- and double-slotted-flap configurations, respectively.

Stalling Characteristics

The stall patterns for the several combinations are illustrated in figures 17 and 18. In general, the discussions of the stall progressions given in connection with the leading-edge devices alone apply to the combinations with trailing-edge flaps.

Downwash and Dynamic-Pressure Measurements

In order to determine whether a suitably placed horizontal tail would eliminate the unfavorable loop in the pitching-moment curve for the double-slotted-flap combinations, downwash and dynamic-pressure surveys were made behind the wing. The particular combination used was the leading-edge slat plus double slotted flap.

A plane approximately $2.0\bar{c}$ behind the $0.25\bar{c}$ point of the wing was surveyed; the area surveyed was from about $0.9\bar{c}$ above to $0.3\bar{c}$ below the chord plane extended and from $0.15\frac{b}{2}$ to $0.37\frac{b}{2}$ out from the plane of symmetry. The data were obtained by means of the survey apparatus described in detail in reference 14 and are presented in figures 19 and 20. To obtain tail-on pitching-moment curves, a constant-chord tail of area $0.15S$ and aspect ratio 3 was assumed. Average values of downwash and dynamic pressure were obtained by integrating the survey data across the span of the assumed tail.

Pitching-moment data were computed for three vertical locations of the horizontal tail and are presented in figure 21. The data show that, although the three tail locations selected for illustration eliminated the loop in the moment curves near maximum lift, some instability was present. Of the three tail heights investigated, it appears that the high position offered the most satisfactory characteristics.

Scale and Roughness Effect

In order to obtain an indication of the effects of scale and roughness on a typical combination, several additional tests on the slat and double-slotted-flap configuration were made. The data are presented in figure 22.

In general, the scale effect was very similar to that obtained on the plain wing; maximum lift coefficient increased as the Reynolds number was increased, and no important effects on stability at $C_{L_{max}}$ were observed. The effect of roughness was to reduce maximum lift and to cause a slight rounding of the lift curve at the high angles of attack. Unlike the plain wing, no irregularities in the pitching-moment curve occurred.

Spanwise Position of Centroid of Lift

Information concerning the spanwise location of the center of the load distribution over a wing is desirable from the structural standpoint. Inasmuch as the model used in this investigation was a semispan model, it was possible to determine the centroid of the loading from the force and rolling-moment data without resorting to pressure-distribution measurements.

The variation of the spanwise position of the centroid of the loading with lift coefficient for several wing configurations is presented in figure 23. The centroid given in figure 23 is that due to the total loading, that is, the basic and additional loadings. The data show that (a) up to the stall there was a negligible change in the load centroid for the basic wing and wing with half-span leading-edge slat, (b) deflection of the inboard trailing-edge flaps moved the centroid inboard, and (c) with flaps deflected the centroid of the load moved outboard with increasing lift coefficient. These results are in qualitative agreement with those expected from theoretical considerations.

Some computations were made to determine the degree of accuracy to which the spanwise position of the centroid of the loading could be calculated. The charts of reference 9 were used to determine the position of the centroid for the plain wing. Agreement between theory and experiment was very good, the theory predicting $\frac{\bar{y}}{b/2} = 0.452$ and experiment yielding values varying between $\frac{\bar{y}}{b/2} = 0.458$ and $\frac{\bar{y}}{b/2} = 0.451$.

The variation of $\frac{\bar{y}}{b/2}$ with C_L for the half-span trailing-edge flap was calculated for the split-flap condition from the following equation:

$$\frac{\bar{y}}{b/2} = \frac{C_{l(C_L=0)_{\Lambda=0^\circ}} \cos^2\Lambda}{C_L} + \left(\frac{\bar{y}}{b/2}\right)_a$$

where

$\left(\dfrac{\bar{y}}{b/2}\right)_a$ spanwise position of centroid for additional loading with sweepback taken into account (reference 9)

$C_{l(C_L=0)_{\Lambda=0^\circ}}$ rolling-moment coefficient at zero lift due to basic loading on one panel of unswept wing

For purposes of comparison, the above equation was used to compute the variation for an unswept wing of the same aspect ratio and taper ratio. The calculated curves are shown by the dashed lines in figure 23.

The results indicate that, for the given condition, the spanwise variation of the centroid with lift coefficient was calculated with reasonable accuracy. It should be pointed out that the equation given above was based on the assumption that sweep did not affect the distribution of the basic lift but only affected the effectiveness of the flap. From the close agreement between experiment and theory it appears as if the assumption was relatively valid.

SUMMARY OF RESULTS

The results of the wind-tunnel investigation of high-lift and stall-control devices on a 37° sweptback semispan wing of aspect ratio 6 may be summarized as follows: •

1. The wing with or without trailing-edge split or double slotted flaps was longitudinally unstable near maximum lift due to tip stalling.

2. The addition of an outboard half-span leading-edge flap or leading-edge slat to the plain wing or wing with inboard half-span split flaps eliminated tip stalling and resulted in stability at the stall. The drooped leading edge, on the other hand, was only effective when used in conjunction with an upper-surface fence.

3. The combination of an outboard leading-edge device and inboard half-span double slotted flap resulted in an undesirable loop in the pitching-moment curve near maximum lift in spite of an inboard stall. The loop is attributed to the section characteristics of the double slotted flap. Air-flow surveys behind the wing showed that a suitably placed tail would eliminate the loop in the moment curve.

4. For combinations with split flaps, upper and lower limits exist for the span of the leading-edge device between which stability at the stall can be obtained; a critical span of the leading-edge device was found, however, below which reductions in maximum lift resulted.

5. The maximum lift coefficient of the plain wing was about 1.27. For combinations of an outboard half-span leading-edge device with an inboard half-span split flap or double slotted flap, maximum lift coefficients of the order of 1.5 and 2.0, respectively, were obtained. It is also indicated that the drooped leading edge plus fence combinations with trailing-edge flaps would give the highest maximum lift.

6. An increase in trailing-edge flap span from half to full span did not produce appreciable increases in maximum lift when the accompanying changes in trim were taken into account.

Langley Aeronautical Laboratory
      National Advisory Committee for Aeronautics
            Langley Field, Va.

R E F E R E N C E S

1. Shortal, Joseph A., and Maggin, Bernard: Effect of Sweepback and Aspect Ratio on Longitudinal Stability Characteristics of Wings at Low Speeds. NACA TN No. 1093, 1946.

2. McCormack, Gerald M., and Stevens, Victor I., Jr.: An Investigation of the Low-Speed Stability and Control Characteristics of Swept-Forward and Swept-Back Wings in the Ames 40- by 80-Foot Wind Tunnel. NACA RM No. A6K15, 1947.

3. Sweberg, Harold H., and Lange, Roy H.: Summary of Available Data Relating to Reynolds Number Effects on the Maximum Lift Coefficients of Swept-Back Wings. NACA RM No. L6L20a, 1947.

4. Graham, Robert R., and Conner, D. William: Investigation of High-Lift and Stall-Control Devices on an NACA 64-Series 42° Sweptback Wing with and without Fuselage. NACA RM No. L7G09, 1947.

5. Cahill, Jones F., and Racisz, Stanley F.: Wind-Tunnel Investigation of Seven Thin NACA Airfoil Sections to Determine Optimum Double-Slotted-Flap Configurations. NACA TN No. 1545, 1948.

6. Sivells, James C., and Deters, Owen J.: Jet-Boundary and Plan-Form Corrections for Partial-Span Models with Reflection Plane, End Plate, or No End Plate in a Closed Circular Wind Tunnel. NACA TN No. 1077, 1946.

7. Eisenstadt, Bertram J.: Boundary-Induced Upwash for Yawed and Swept-Back Wings in Closed Circular Wind Tunnels. NACA TN No. 1265, 1947.

8. Letko, William, and Goodman, Alex: Preliminary Wind-Tunnel Investigation at Low Speed of Stability and Control Characteristics of Swept-Back Wings. NACA TN No. 1046, 1946.

9. DeYoung, John: Theoretical Additional Span Loading Characteristics of Wings with Arbitrary Sweep, Aspect Ratio, and Taper Ratio. NACA TN No. 1491, 1947.

10. Pearson, Henry A., and Anderson, Raymond F.: Calculation of the Aerodynamic Characteristics of Tapered Wings with Partial-Span Flaps. NACA Rep. No. 665, 1939.

11. Sivells, James C., and Spooner, Stanley H.: Investigation in the Langley 19-Foot Pressure Tunnel of Two Wings of NACA 65-210 and 64-210 Airfoil Sections with Various Type Flaps. NACA TN No. 1579, 1948.

12. Neely, Robert H., and Conner, D. William: Aerodynamic Characteristics of a 42° Swept-Back Wing with Aspect Ratio 4 and NACA 64_1–112 Airfoil Sections at Reynolds Numbers from 1,700,000 to 9,500,000. NACA RM No. L7D14 1947.

13. Underwood, William J., Braslow, Albert L., and Cahill, Jones F.: Two-Dimensional Wind-Tunnel Investigation of 0.20-Airfoil-Chord Plain Ailerons of Different Contour on an NACA 65_1-210 Airfoil Section. NACA ACR No. L5F27, 1945.

14. Furlong, G. Chester: Downwash and Dynamic Pressure at the Horizontal Tail of a Six-Engine Pusher-Propelled Airplane. NACA RM No. L8F21, 1948.

TABLE I.— SUMMARY OF RESULTS OF INVESTIGATION OF HIGH LIFT AND
STALL CONTROL DEVICES ON A 37° SWEPTBACK SEMISPAN WING

Configuration	T.E. device (b/2)	L.E. device (b/2)	Untrimmed $C_{L_{max}}$	α_{max} (deg)	D/L at 0.85$C_{L_{max}}$	C_m characteristics	Fig. No.
	Off	Off	1.27	19.0	0.081		4
	Off	0.500	1.42	26.0	.123		9
(a)	Off	.500	1.28	20.0	.084		8
(a)	Off	.500	1.28	18.9	.085		8
	Off	.500	1.39	24.0	.102		9
	Off	.700	1.41	25.0	.093		9
	0.500	Off	1.55	17.1	.134		4
	.975	Off	1.65	15.1	.157		4
	.500	.500	1.43	15.0	.124		14
(a)	.500	.500	1.55	18.1	.124		14
(a)	.500	.500	1.49	16.0	.122		14

a Leading edge drooped 30°; slat in retracted position

TABLE I.— SUMMARY OF RESULTS OF INVESTIGATION OF HIGH LIFT AND STALL

CONTROL DEVICES ON A 37° SWEPTBACK SEMISPAN WING — Concluded

Configuration	T.E. device (b/2)	L.E. device (b/2)	Untrimmed $C_{L_{max}}$	α_{max} (deg)	D/L at $0.85C_{L_{max}}$	C_m characteristics	Fig. No.
	0.500	0.500	1.46	15.0	.121		13
	.500	.650	1.63	18.2	.128		13
	.500	.700	1.69	21.3	.129		13
	.500	off	1.92	14.3	.141		4
	.975	off	2.32	11.9	.146		4
	.500	.500	1.85	14.3	.141		15
(a)	.500	.500	1.94	15.3	.141		15
(a)	.500	.500	2.02	17.4	.144		15
	.500	.500	1.87	13.4	.142		15
	.500	.650	2.06	16.4	.145		15

[a] Leading edge drooped 30°; slat in retracted position.

All Dimensions in inches

Plan View

Reflection Plane

Tunnel Wall
(228.36 Diam.)

13.5

56.25

$\frac{3}{8}$ gap

63.00

15.50

Horizontal axis of tunnel

Model

Airflow

¢ of Model
Support

¢ of Tunnel

Front View (Downstream)

242

Airflow

74.66

196.58

¢ of support

118

Tunnel Wall

NACA
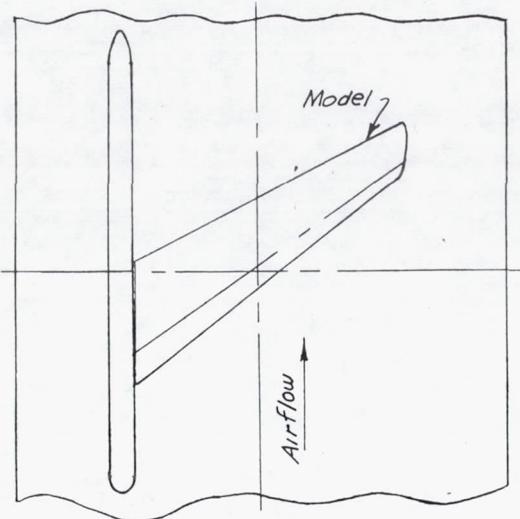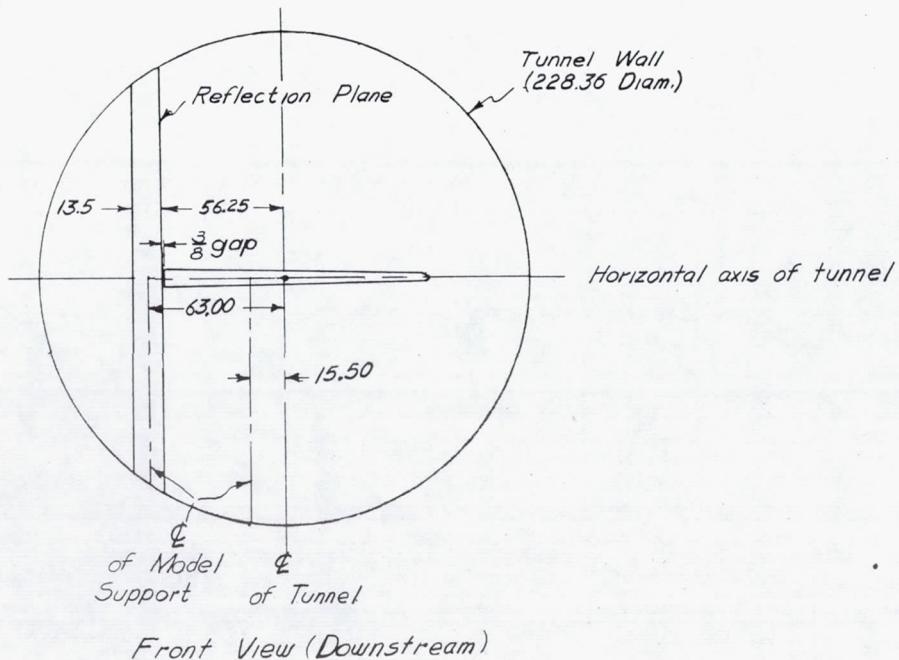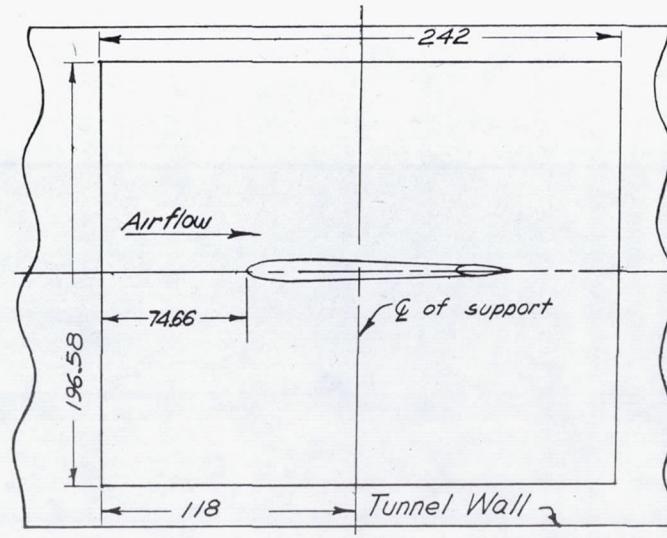
End View

Figure 1.- Details of setup of 37° sweptback semispan wing and reflection plane in Langley 19-foot pressure tunnel.

126.

37.25

15.154

35°

0.27c line

90°

56.

53.339

0.25 c̄

c̄ = 43.550

28.29°

3.15

NACA 64,-212

0.44 b/2

28

(a) Basic wing.

.95 b/2

.45 b/2

0.27c line

A

90°

A

.02c

.140c

.055c

.09c

.02c

Section A-A (Enlarged)

(b) Leading-edge Slat.

.95 b/2

.45 b/2

0.27c line

B

90°

B

.140c

δn

.159c

Section B-B (Enlarged)

(c) Leading-edge Droop.

b/2

.70 b/2

.65 b/2

.50 b/2

.375 b/2

C

90°

0.27c line

C

.05 b/2

5.13

45°

½ Dia.

Section C-C (Enlarged)

(d) Leading-edge Flap.

NACA
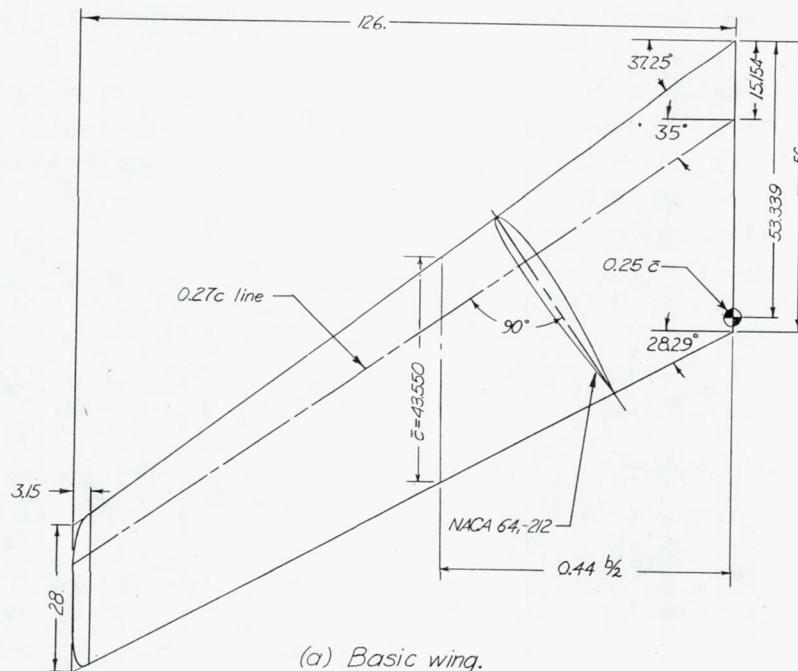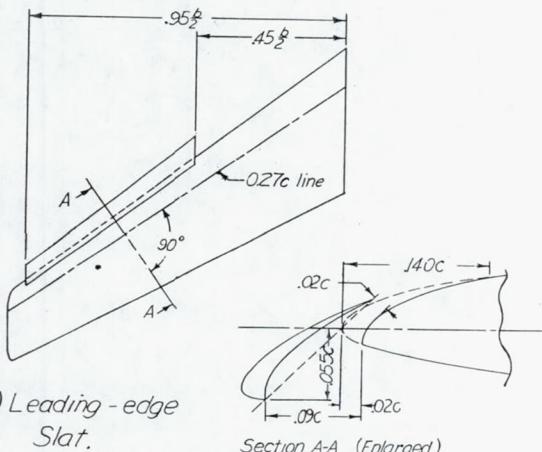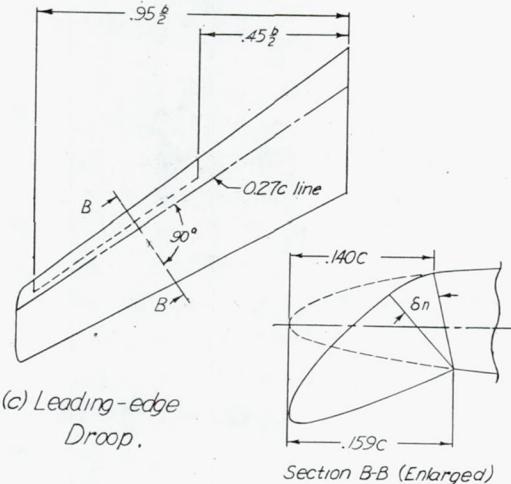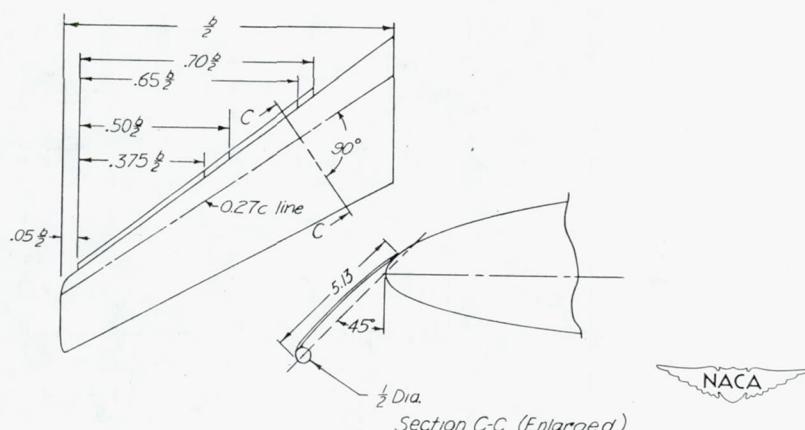
Figure 2.- Details of model, stall-control devices, and trailing-edge flaps. Dimensions in inches except where noted.

0.6 × maximum airfoil thickness

30°

30°
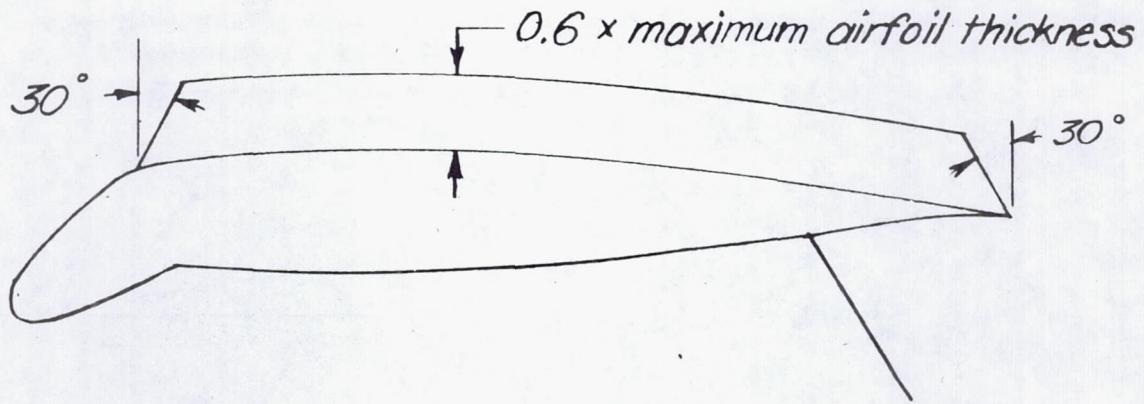
(e) Fence with drooped leading edge and split flap. Spanwise location, 0.5 $\frac{b}{2}$. Parallel to plane of symmetry.
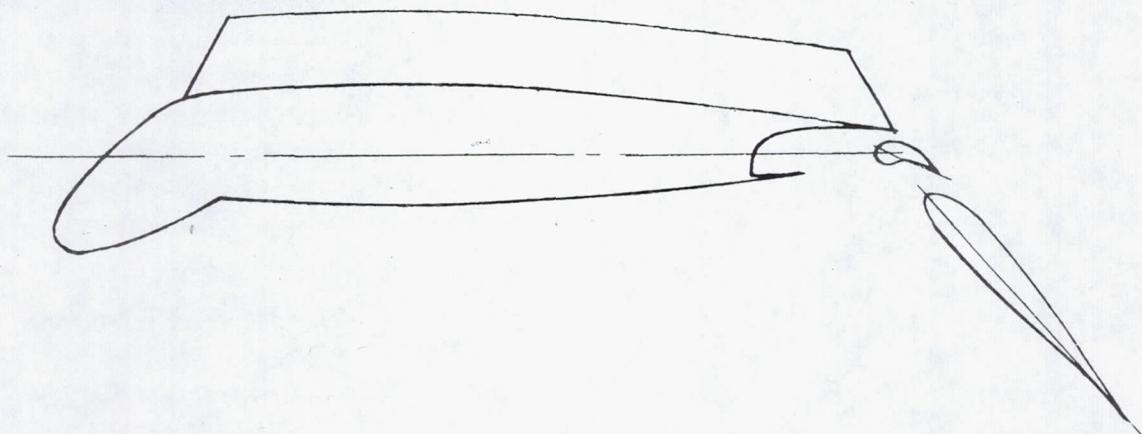
(f) Fence with drooped leading edge and double-slotted flap. Spanwise location, same as (g).

Figure 2.- Continued.

0.27c line

A

90°

A

.018 b/2

.50 b/2

.975 b/2

Section A-A (Enlarged)

60°

.20c

(g) Split flap.

B

90°

0.27c line

B

.018 b/2

.50 b/2

.975 b/2

.84c

.075c

.0201c

.0093c

.683c

.02c   25°

.76c

.0125c

48.85°

.250c

Section B-B (Enlarged)

NACA
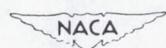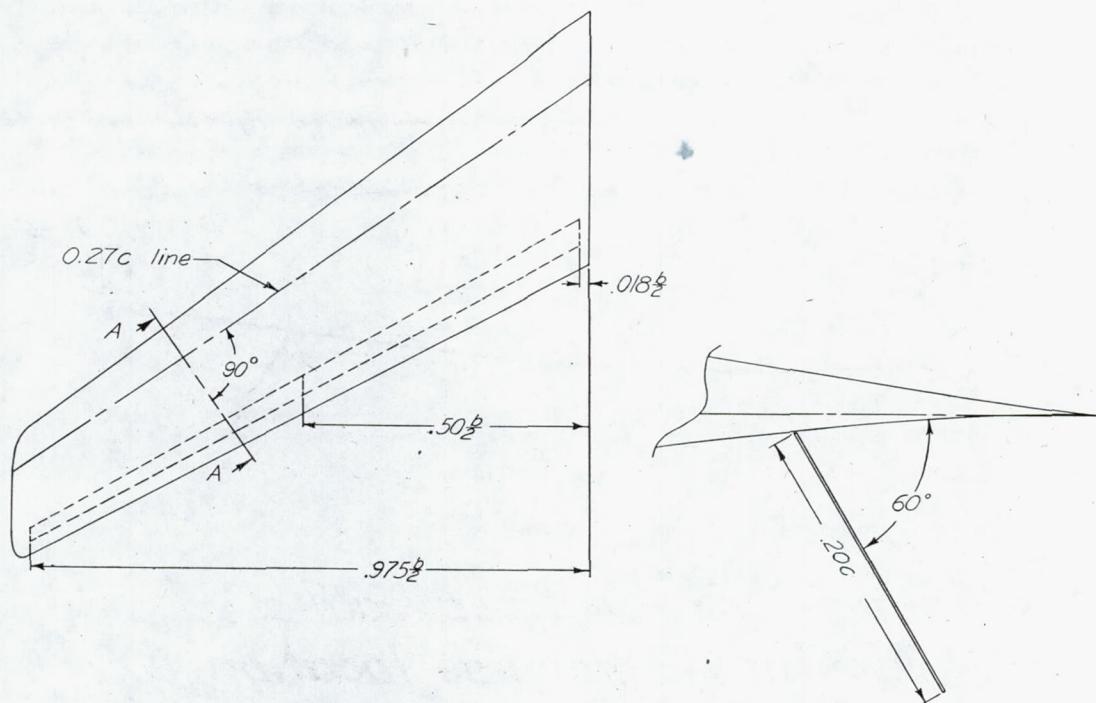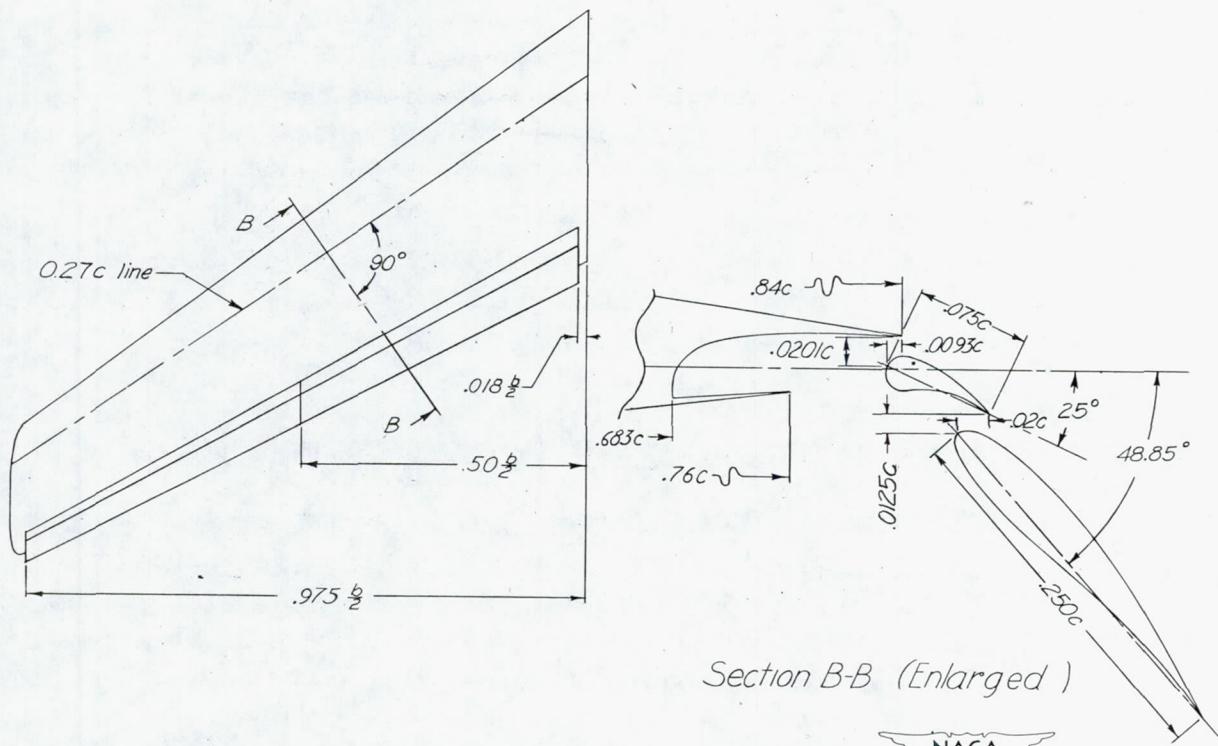
(h) Double-slotted flap.

Figure 2.- Concluded.
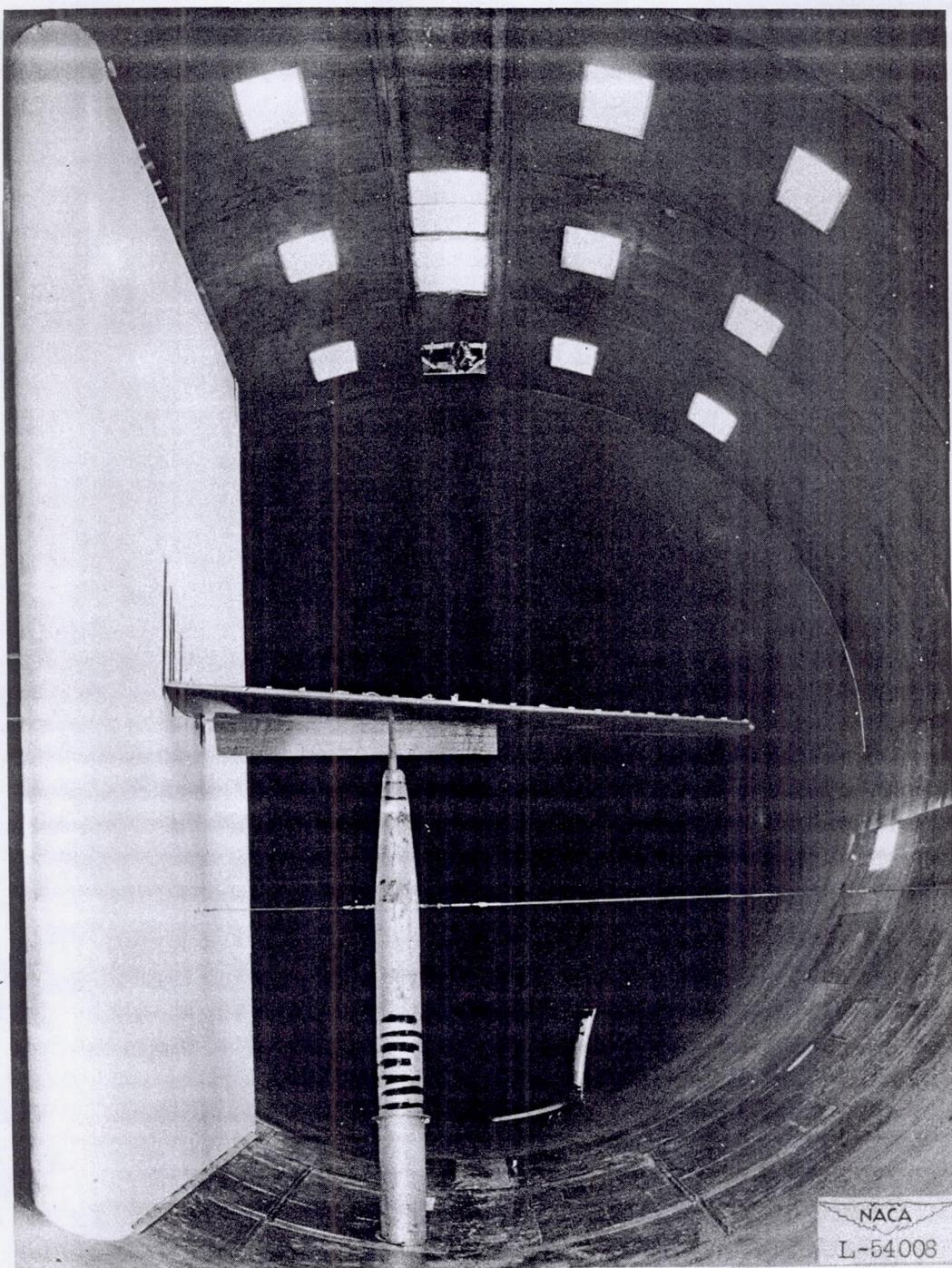
(a)　Model mounted in tunnel.

Figure 3.-　Tunnel setup and various stall-control devices on model.
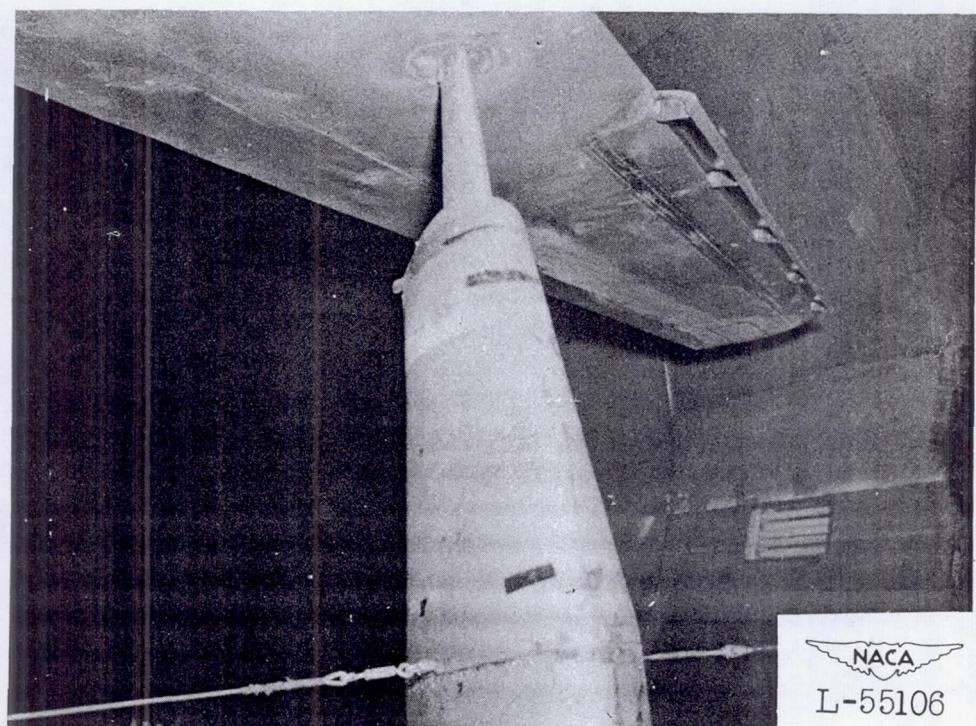
(b)   Leading-edge slat.

Figure 3.- Continued.
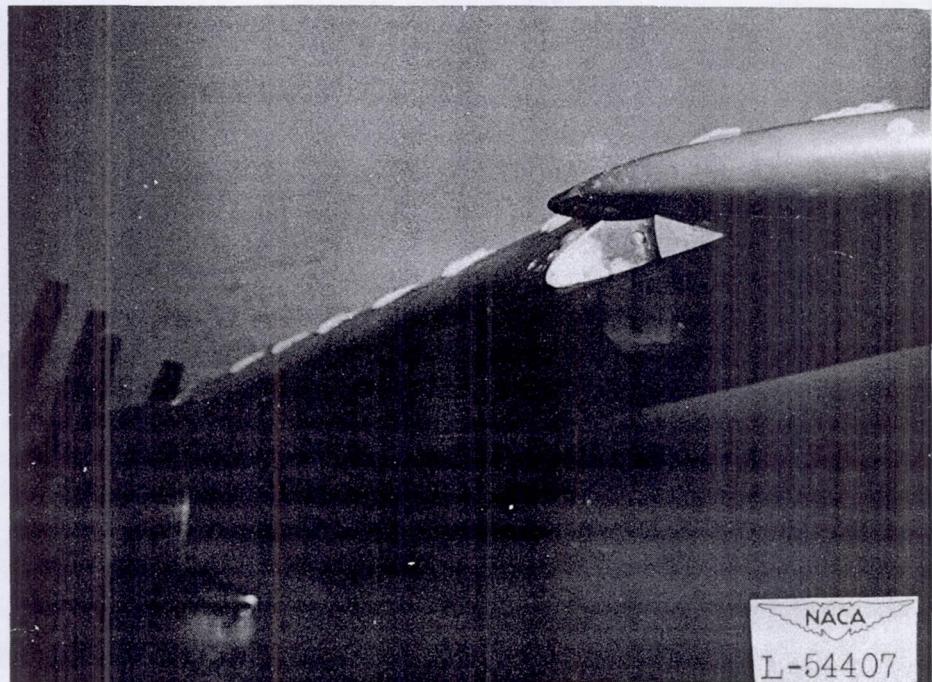
(c) Drooped leading edge.

Figure 3.- Continued.
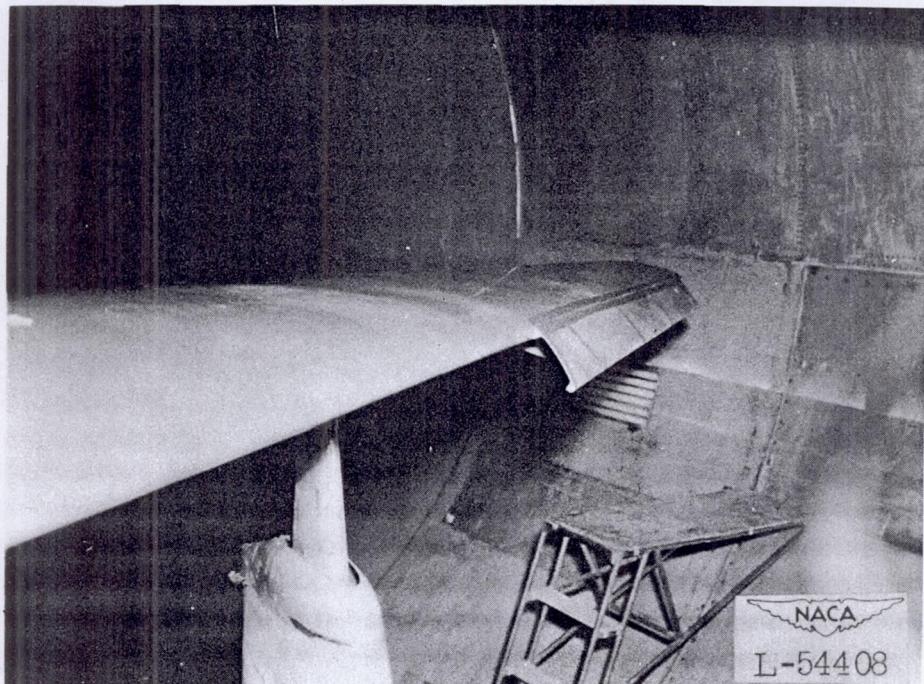
(d)   Extensible round-nose leading-edge flap.

Figure 3.-   Concluded.
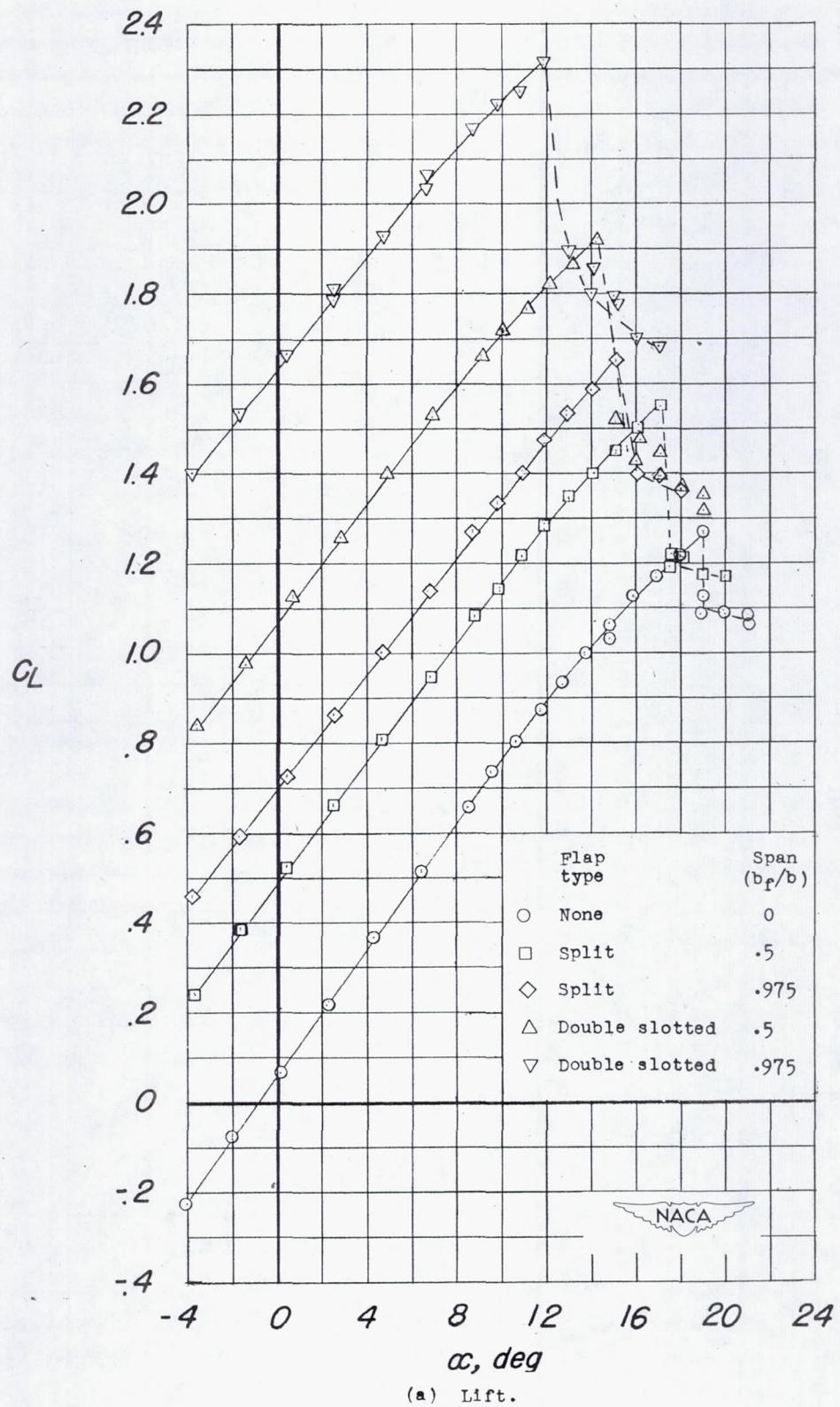
(a) Lift.

Figure 4.— Effects of several trailing edge flap configurations on the aerodynamic
characteristics of 37° sweptback semispan wing. R = 6,800,000.
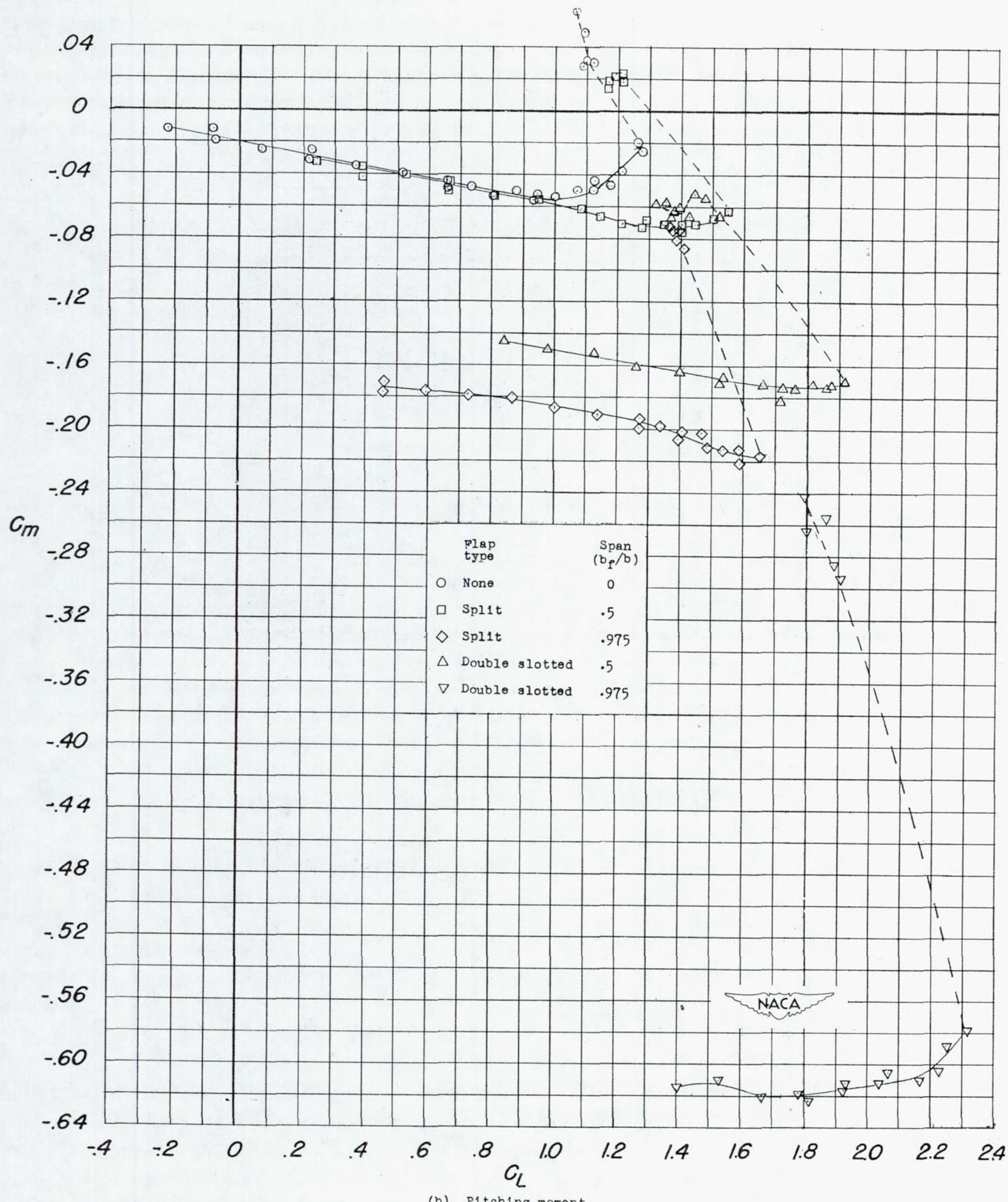
(b) Pitching moment

Figure 4.— Continued.

(c) Drag.
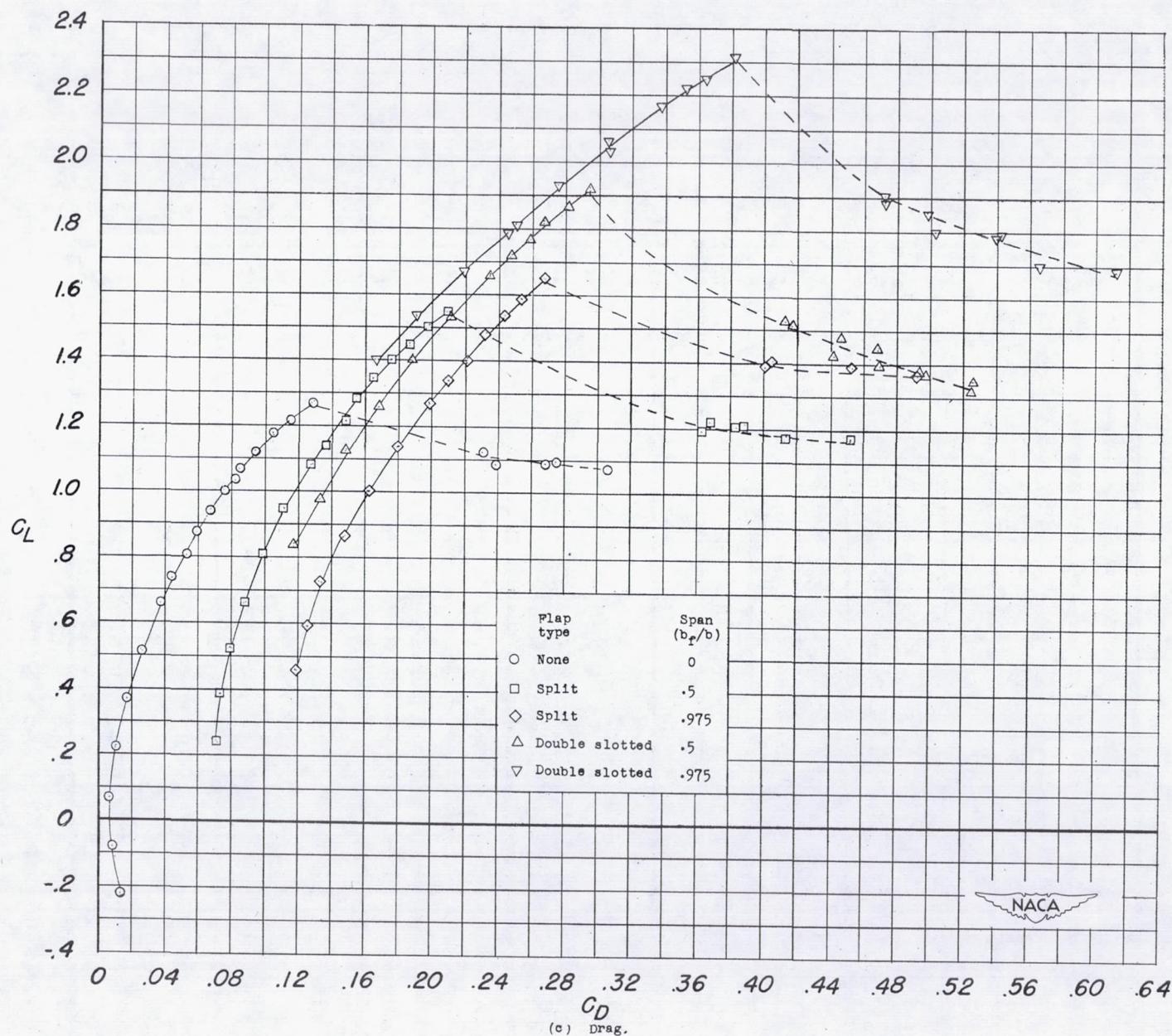
Figure 4.— Concluded.
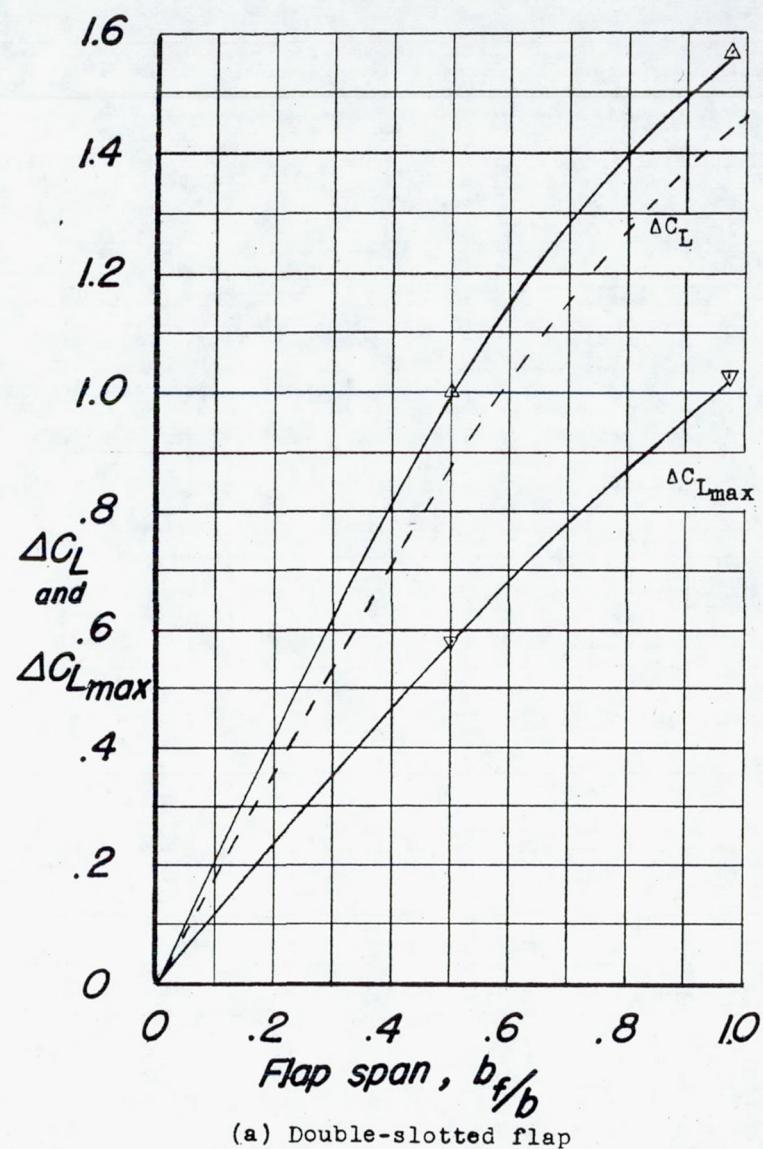
(a) Double-slotted flap
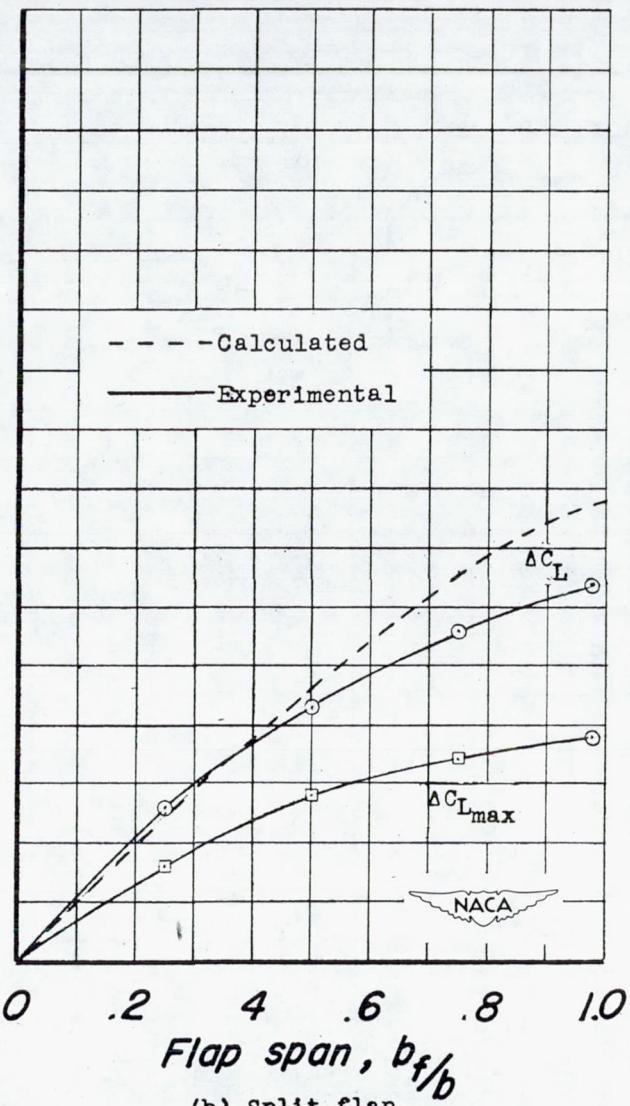
(b) Split flap.

Figure 5.— Effect of flap span on increments in lift due to flap deflection. R= 6,800,000.

(a) Basic wing.

(b) Half-span split flap.

(c) Half-span double-slotted flap.
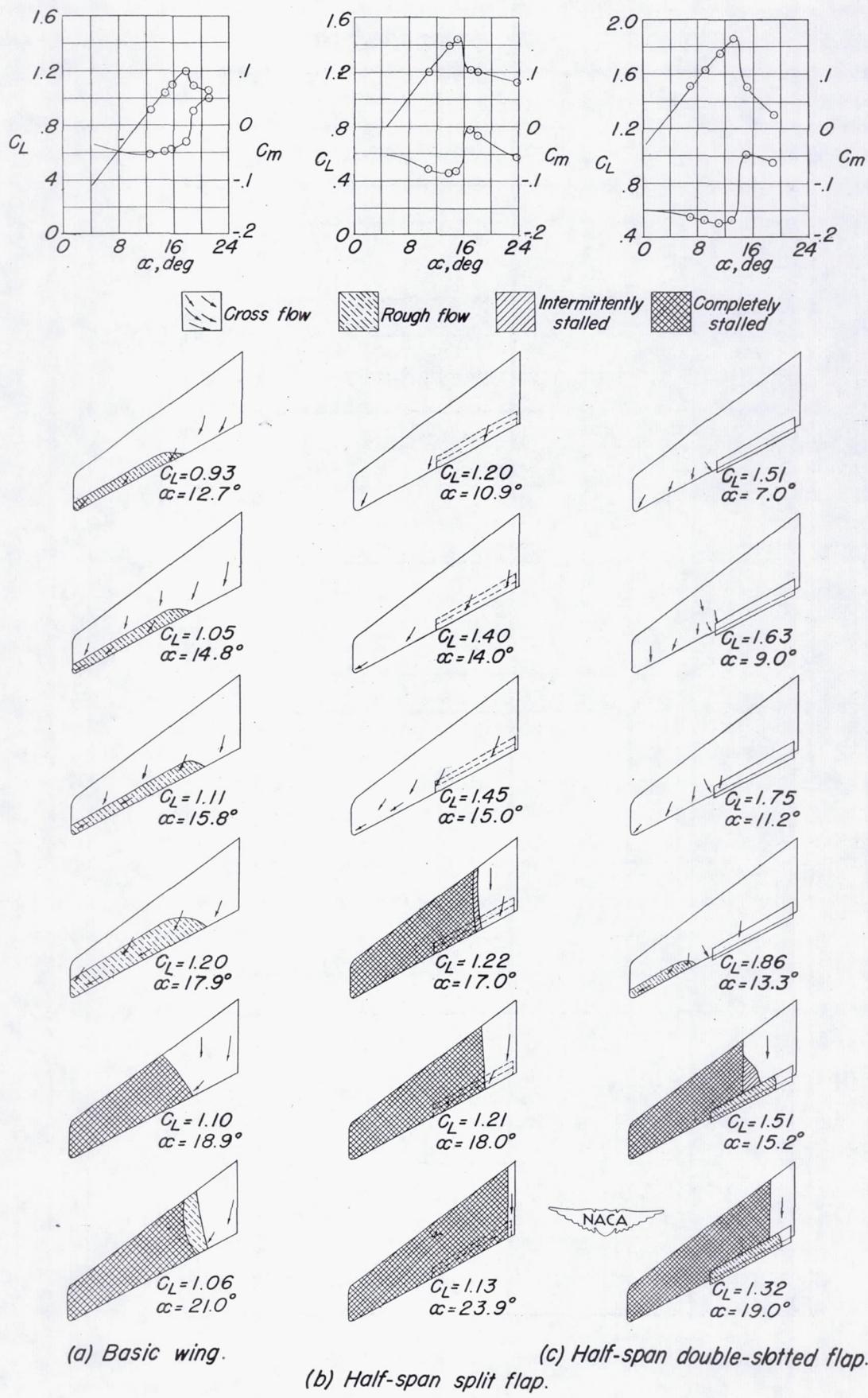
Figure 6.— Stalling characteristics of 37° sweptback semispan wing with and without trailing edge flaps. R = 6,800,000.
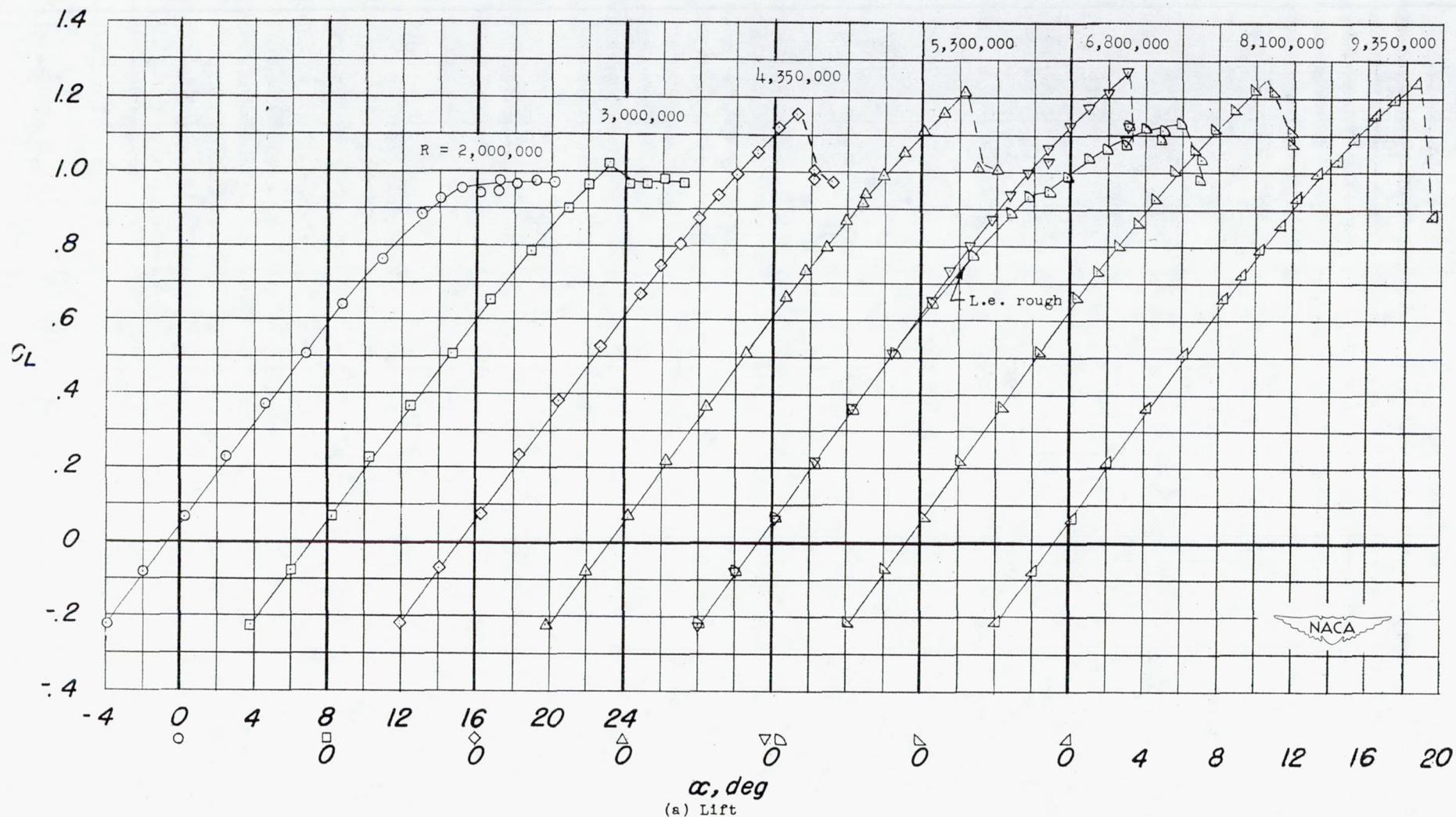
Figure 7.— Effects of Reynolds number variation on the aerodynamic characteristics of 37° sweptback semispan wing.

(b) Pitching moment.

Figure 7.— Continued.

(c) Drag.
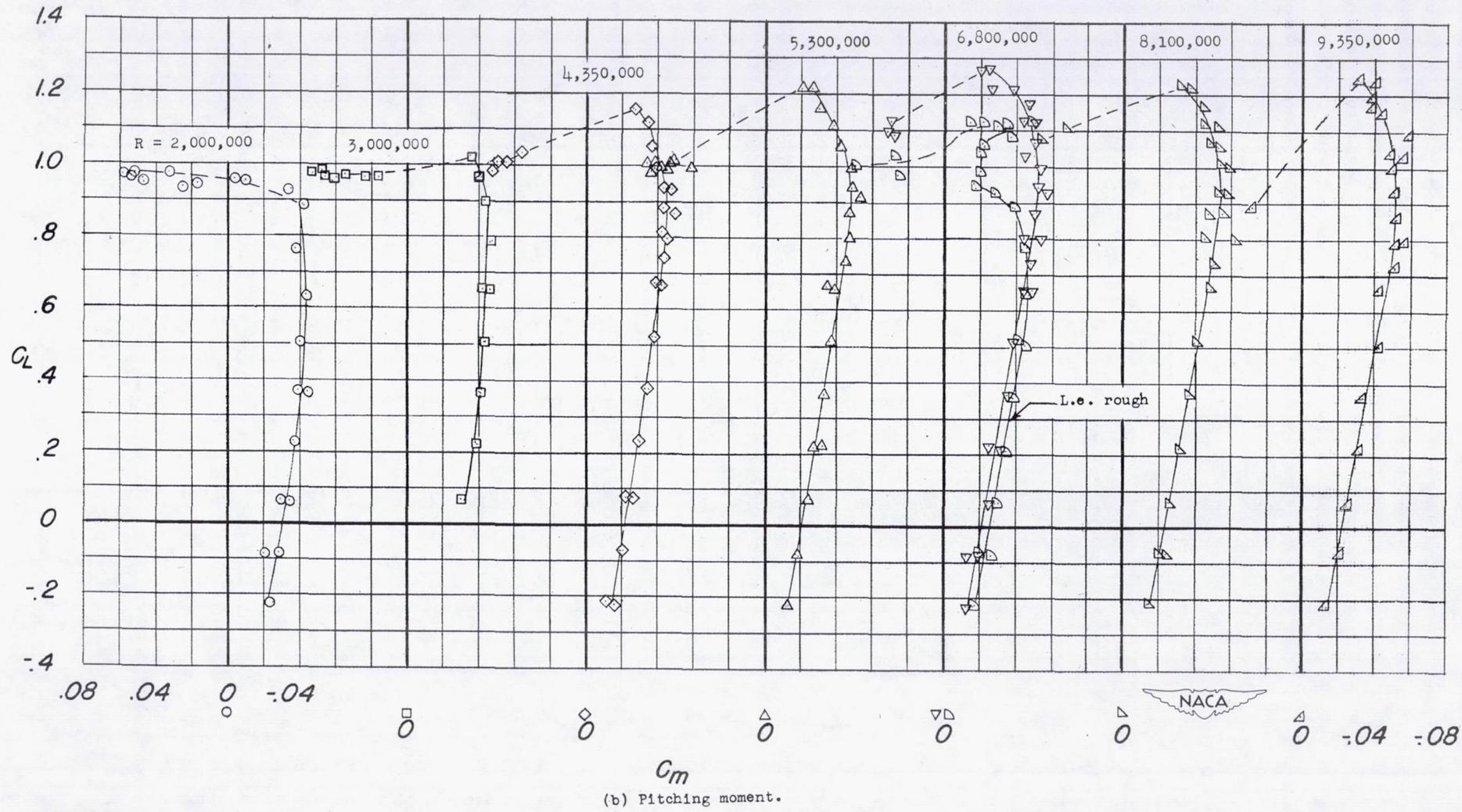
Figure 7.— Concluded.
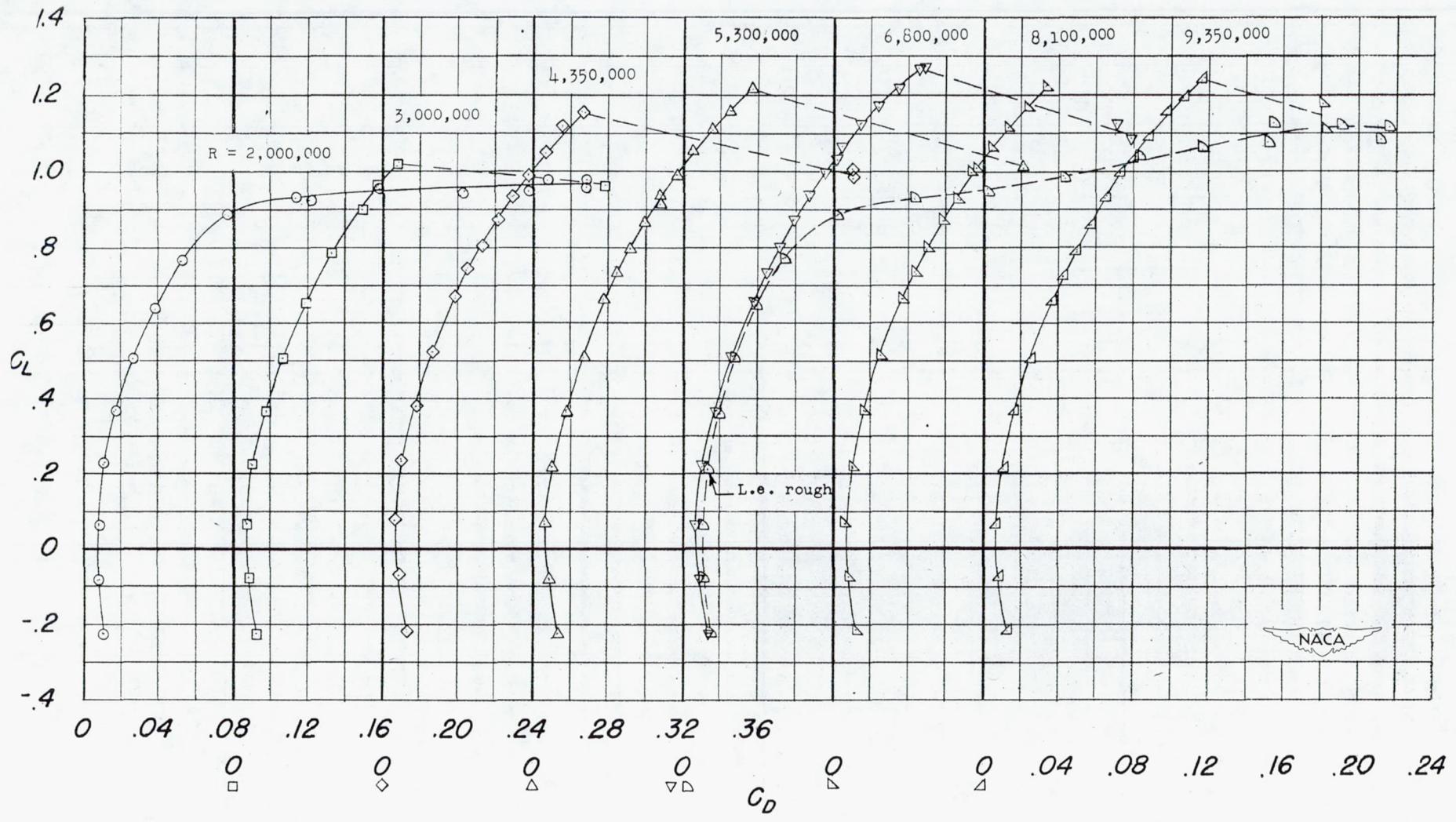
(a) Lift and pitching moment.
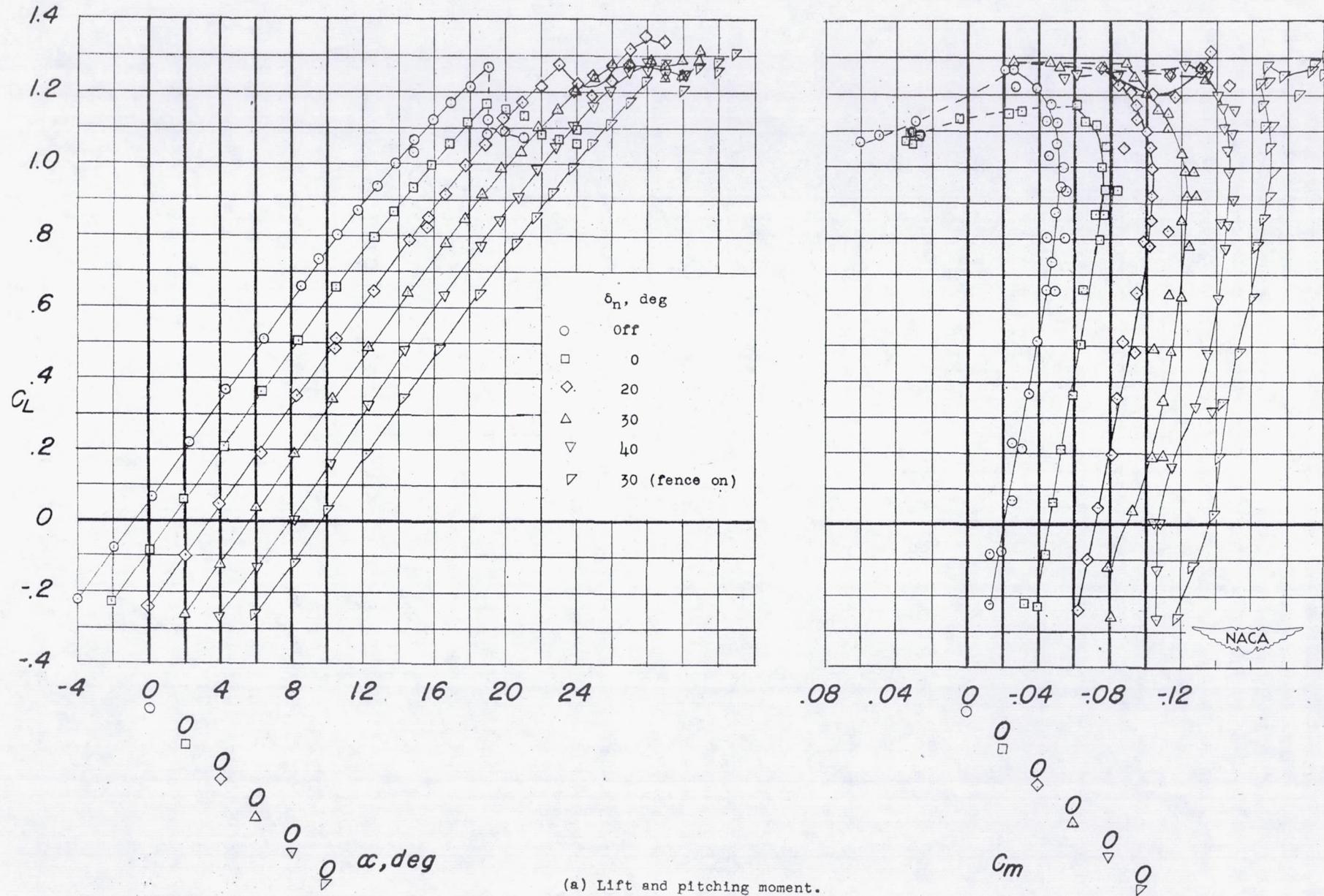
Figure 8.— Effect of drooped leading edge on the aerodynamic characteristics of 37° sweptback semispan wing. R = 6,800,000.

(b) Drag.

Figure 8.— Concluded.

Stall-control
devices | Span (b/2)
○ None | --
□ L.e. flap | 0.50
◇ L.e. flap | .70
△ Slat | .50

α, deg

C_m
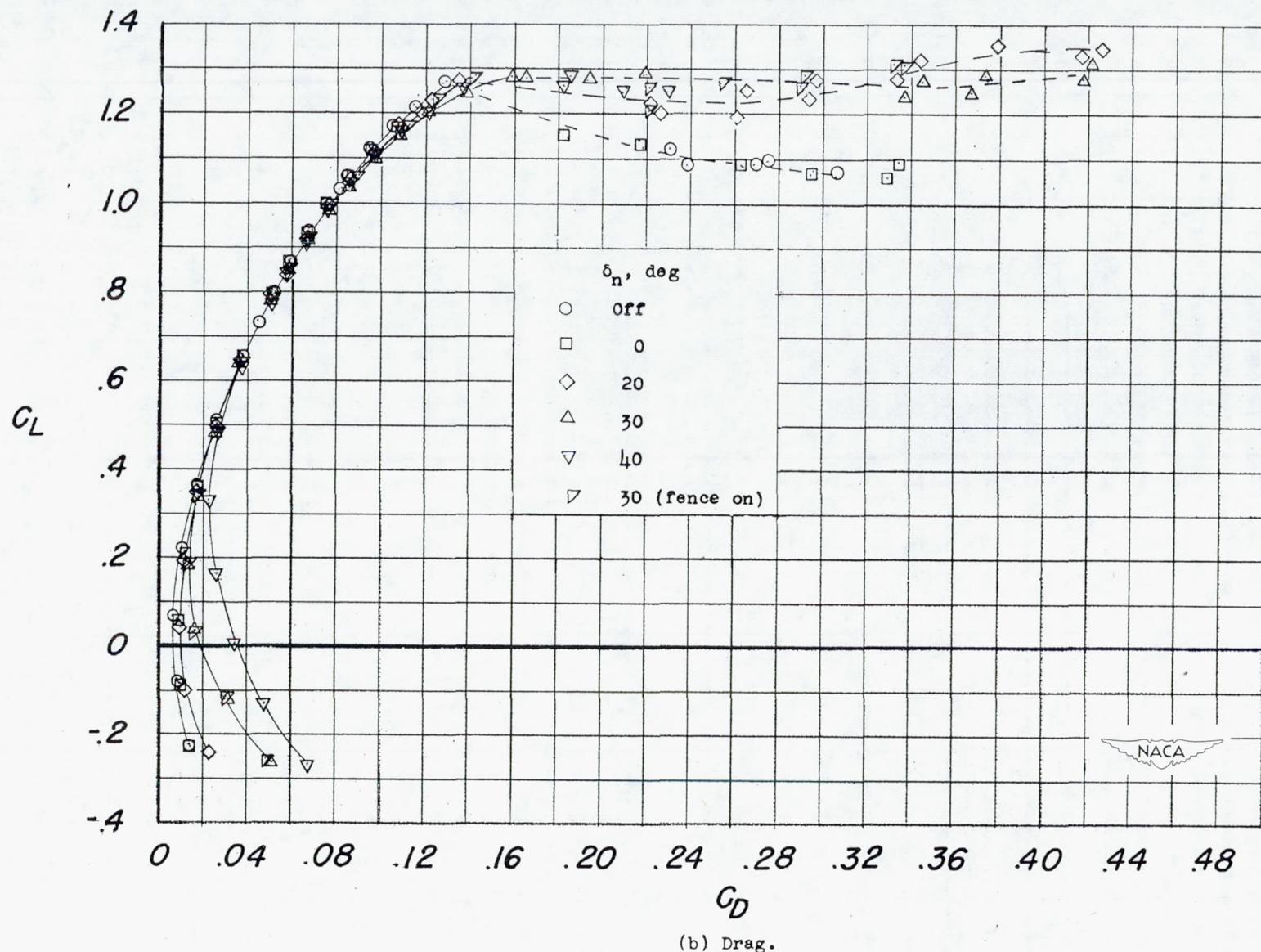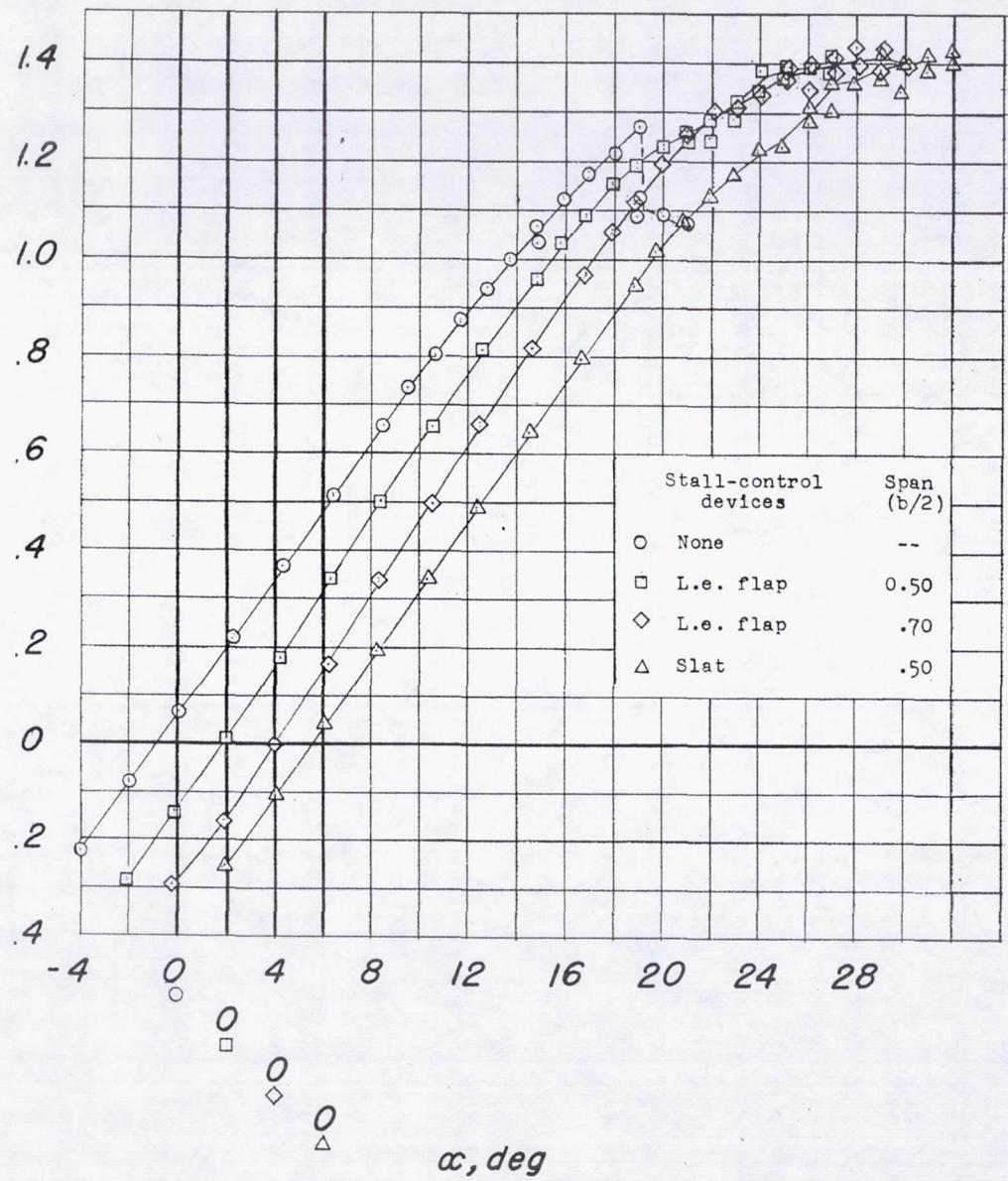
(a) Lift and pitching moment.
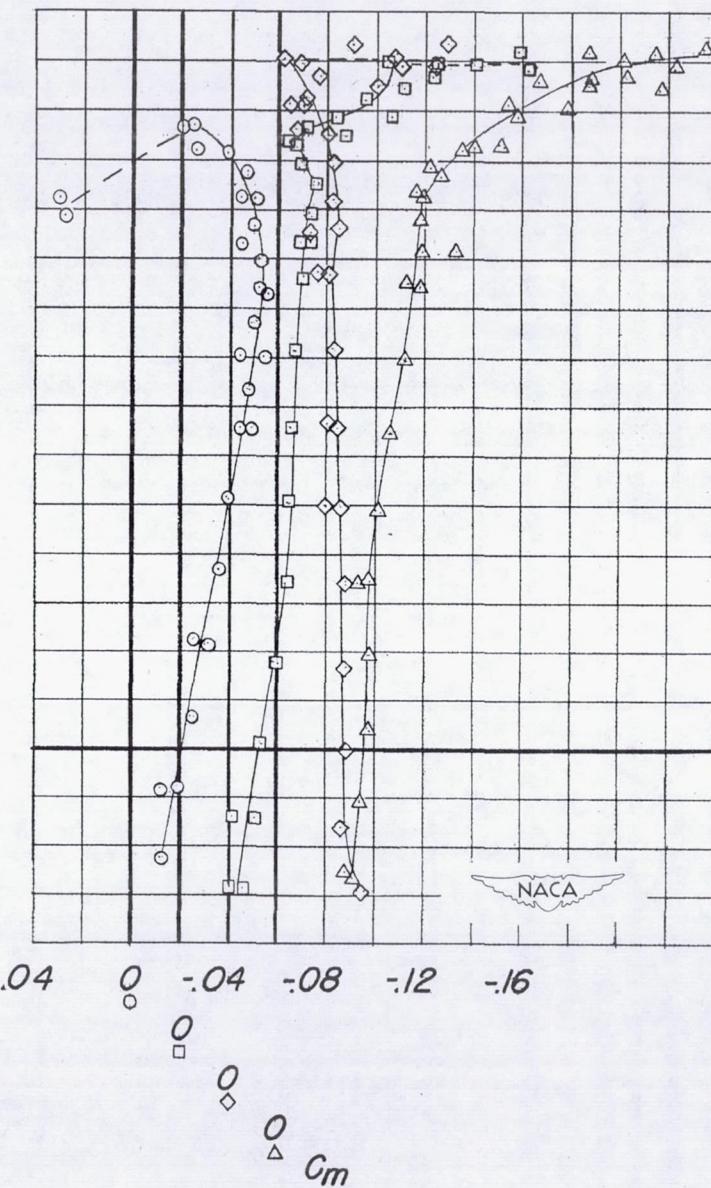
Figure 9.- Effects of leading-edge flap and slat on the aerodynamic characteristics of 37° sweptback semispan wing.   R = 6,800,000.

(b) Drag.

Figure 9.— Concluded.

Cross flow   Rough flow   Intermittently stalled   Completely stalled

$C_L = 1.05$
$\alpha = 14.8°$

$C_L = 0.91$
$\alpha = 12.7°$

$C_L = 1.14$
$\alpha = 15.9°$

$C_L = 1.11$
$\alpha = 15.8°$

$C_L = 1.04$
$\alpha = 14.8°$

$C_L = 1.20$
$\alpha = 17.9°$

$C_L = 1.17$
$\alpha = 16.9°$

$C_L = 1.15$
$\alpha = 16.9°$

$C_L = 1.23$
$\alpha = 19.0°$

$C_L = 1.19$
$\alpha = 17.8°$

$C_L = 1.19$
$\alpha = 17.9°$

$C_L = 1.25$
$\alpha = 19.9°$

$C_L = 1.22$
$\alpha = 18.9°$

$C_L = 1.21$
$\alpha = 19.0°$

$C_L = 1.30$
$\alpha = 21.0°$

$C_L = 1.32$
$\alpha = 20.9°$

$C_L = 1.19$
$\alpha = 19.9°$

$C_L = 1.34$
$\alpha = 22.9°$

(a) Slat.

(b) 30° Drooped leading edge.

(c) Half-span leading edge flap.
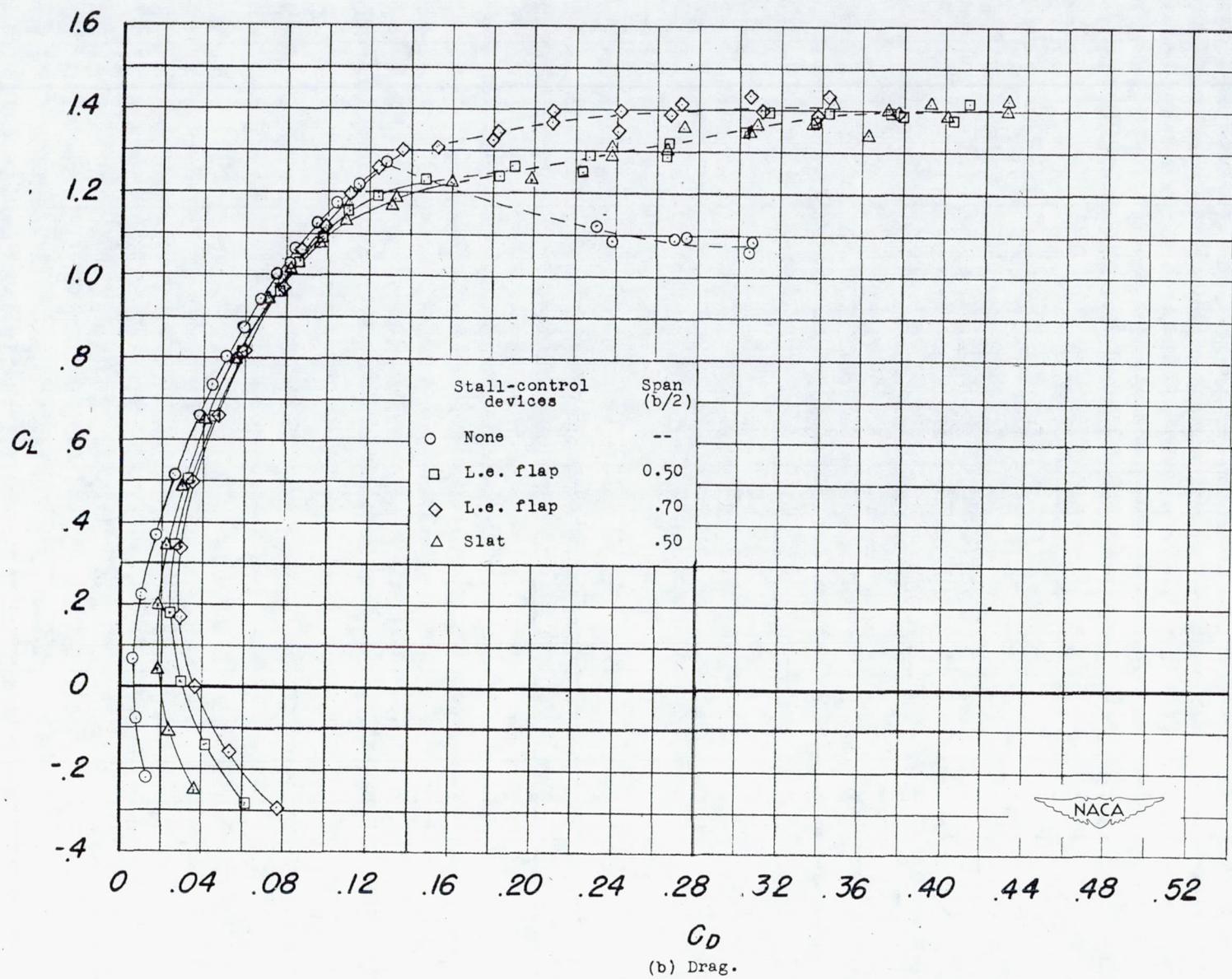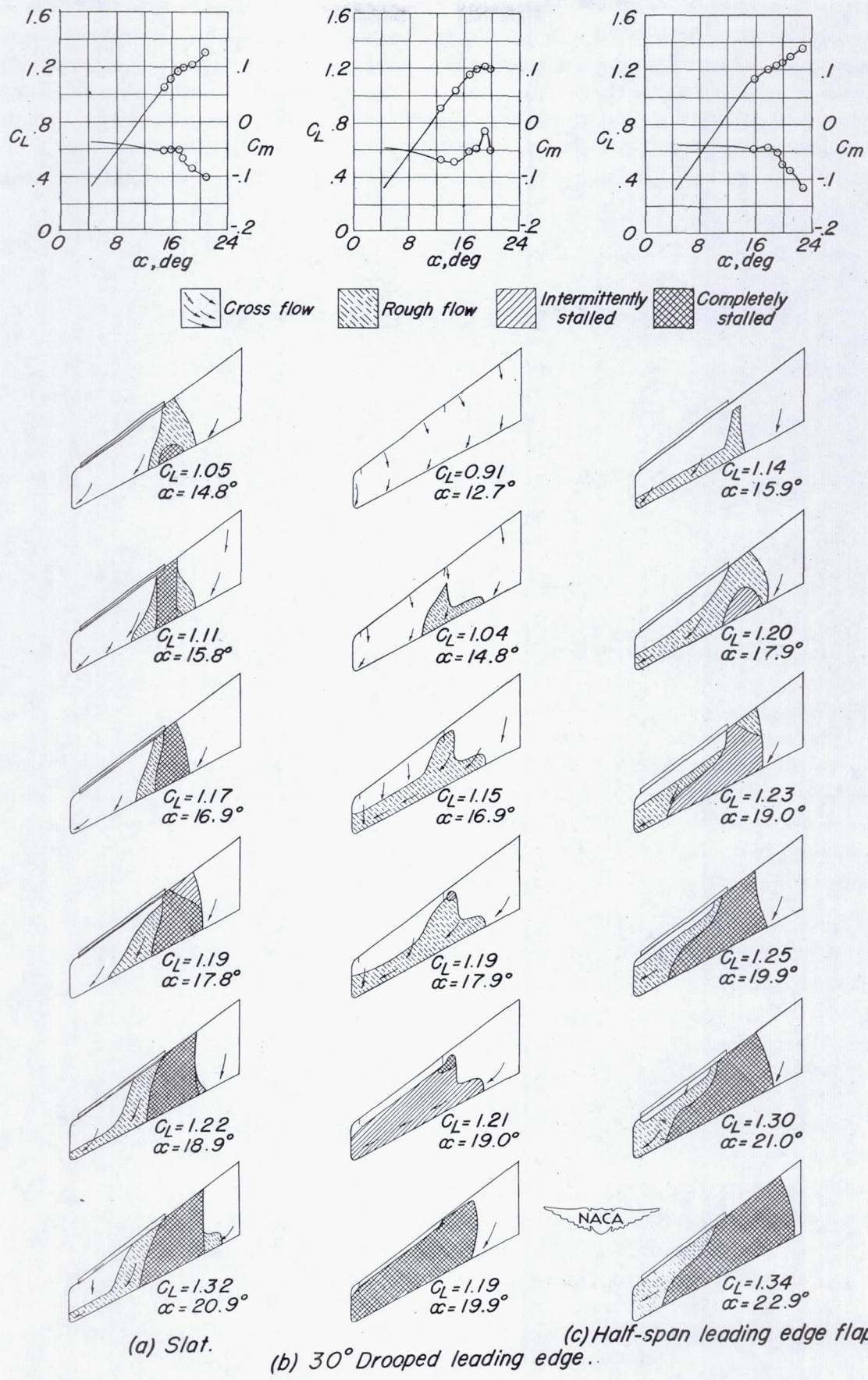
Figure 10.— Effects of various stall-control devices on the stalling characteristics of 37° sweptback semispan wing. R = 6,800,000.
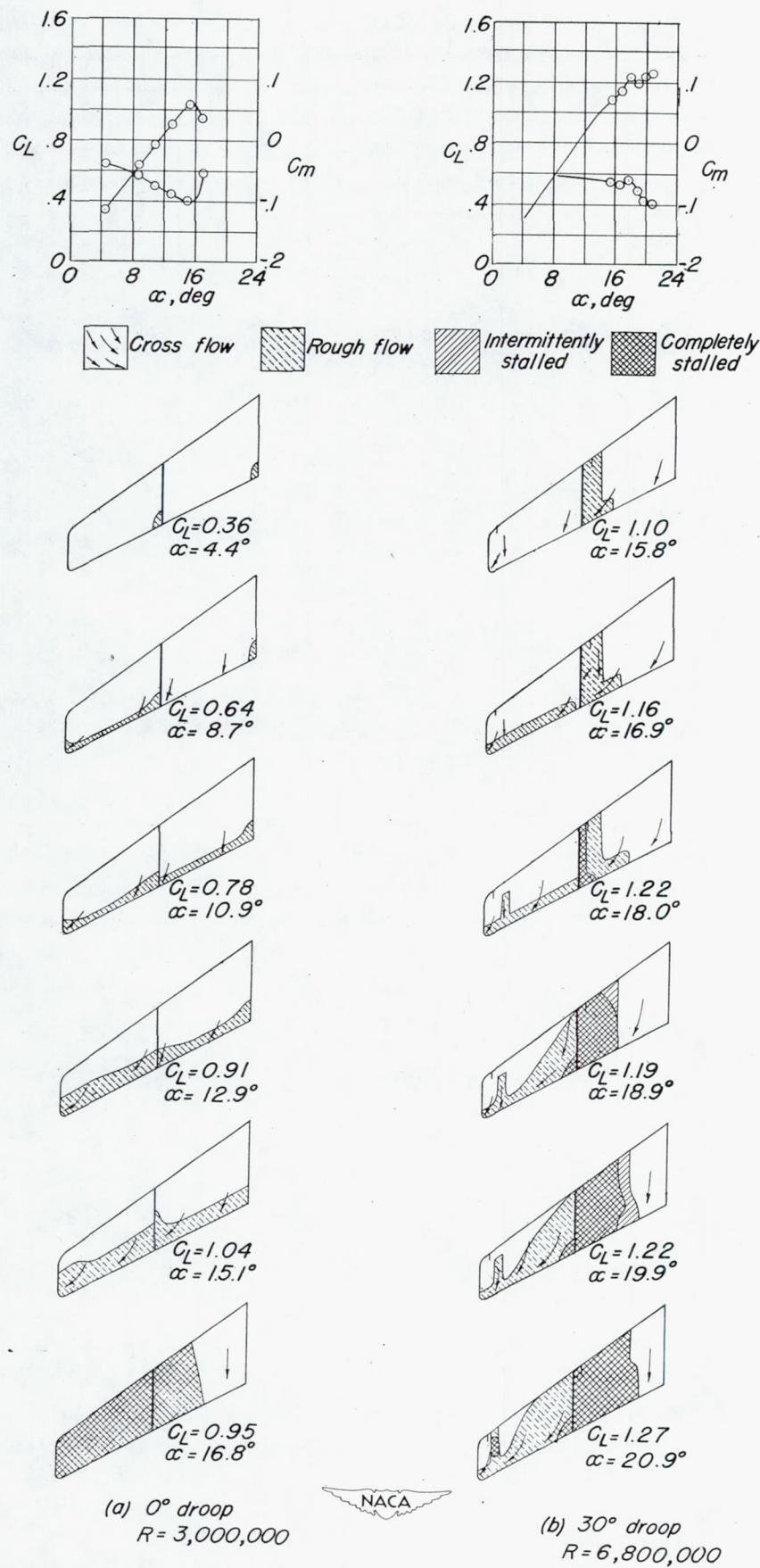
Figure 11.— Effects of a fence on the stalling characteristics of 37° sweptback semispan wing with leading edge droop neutral and 30°.
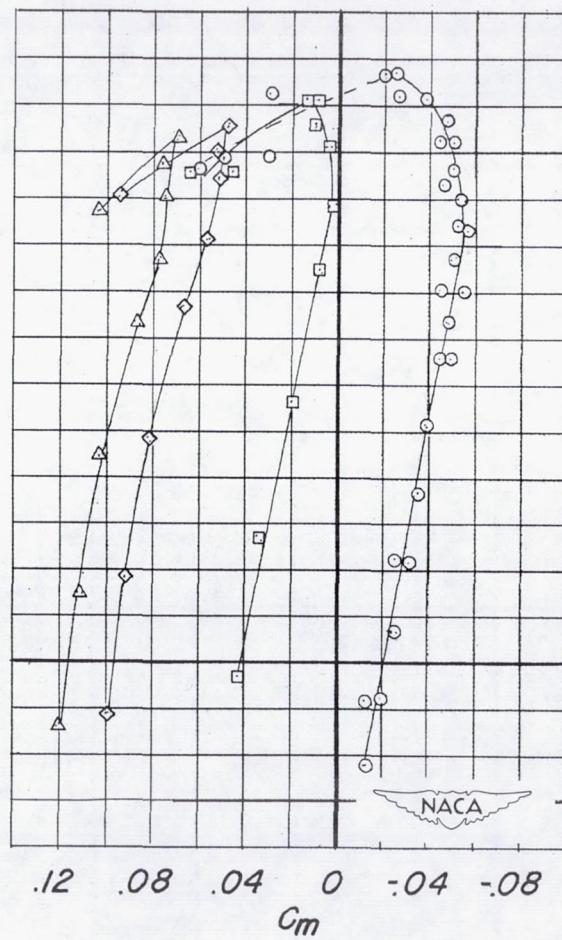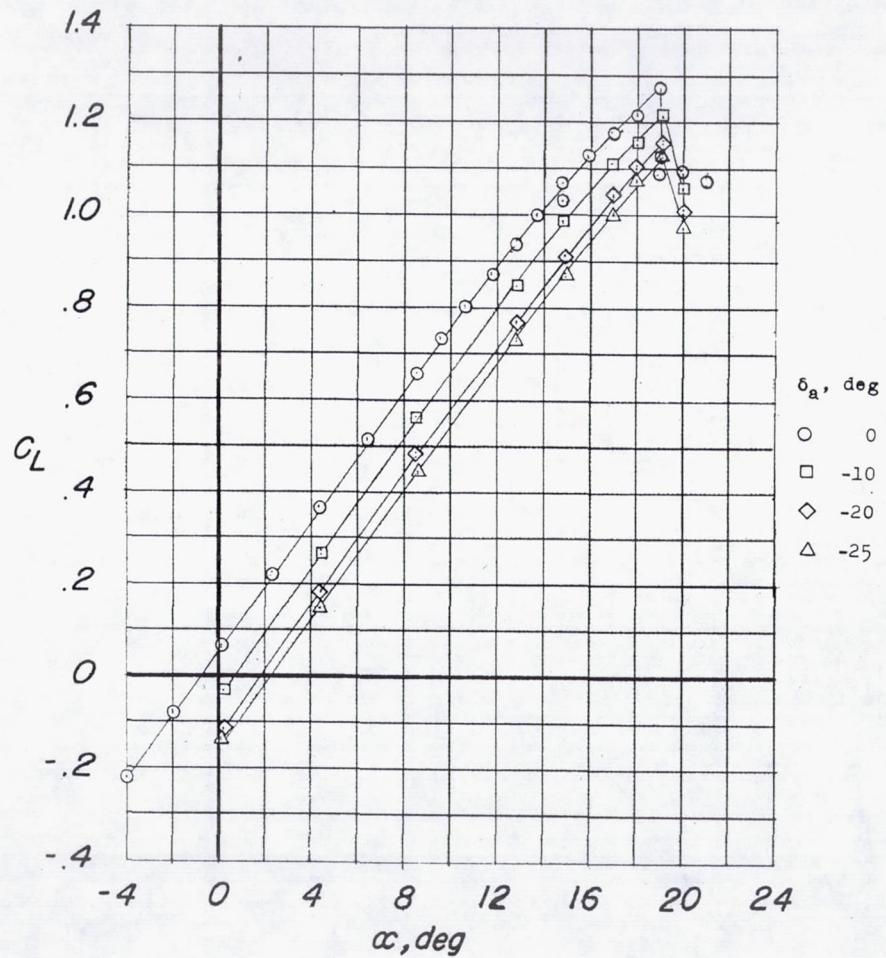
Figure 12.- Effect of outboard flap (aileron) deflection on aerodynamic characteristics of 37° sweptback semispan wing. R = 6,800,000.

(a) Lift and pitching moment
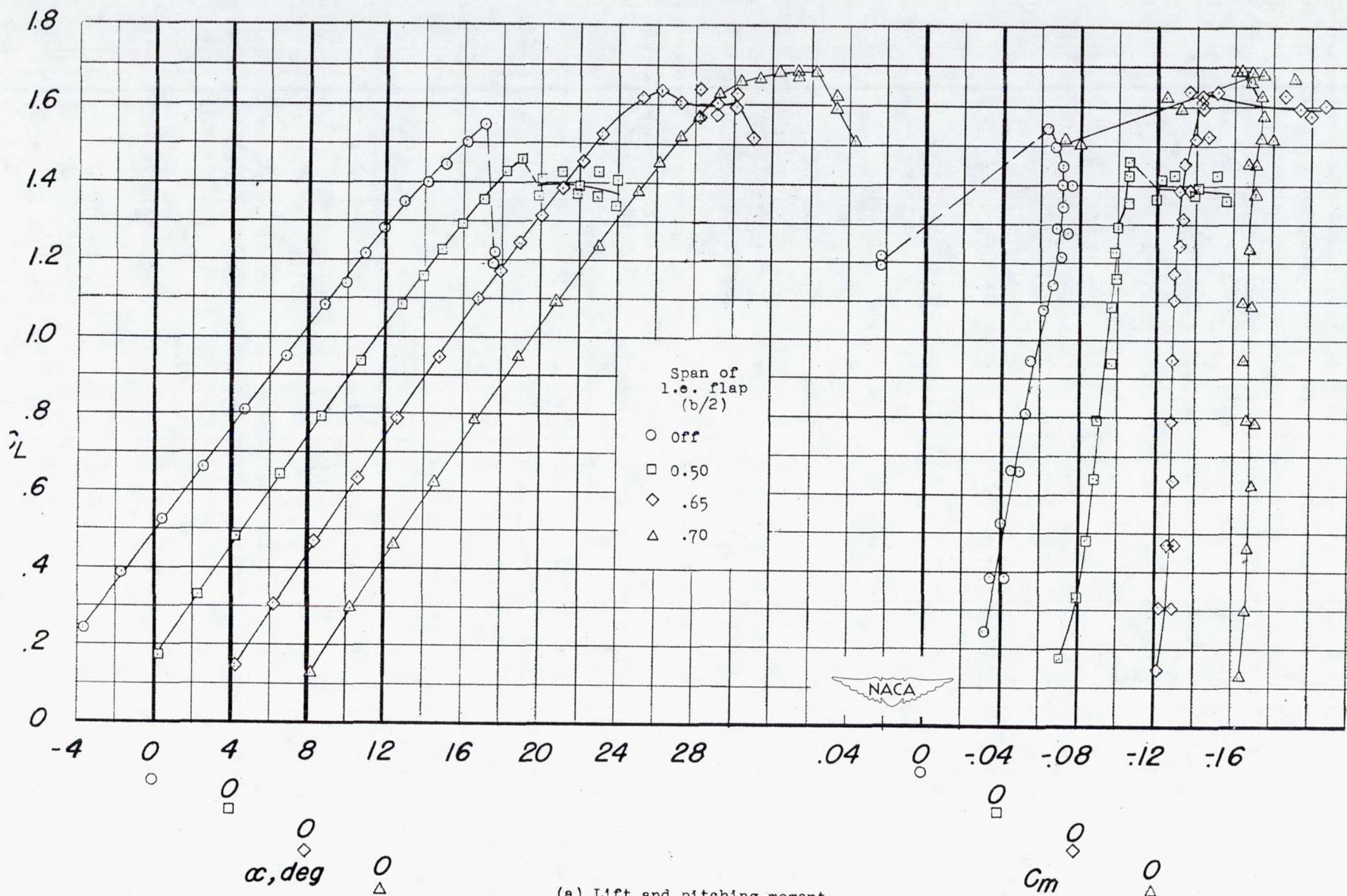
Figure 13.— Effects of varying the span of a leading-edge flap on the aerodynamic characteristics of the 37° sweptback semispan wing with half-span split flaps. R = 6,800,000.
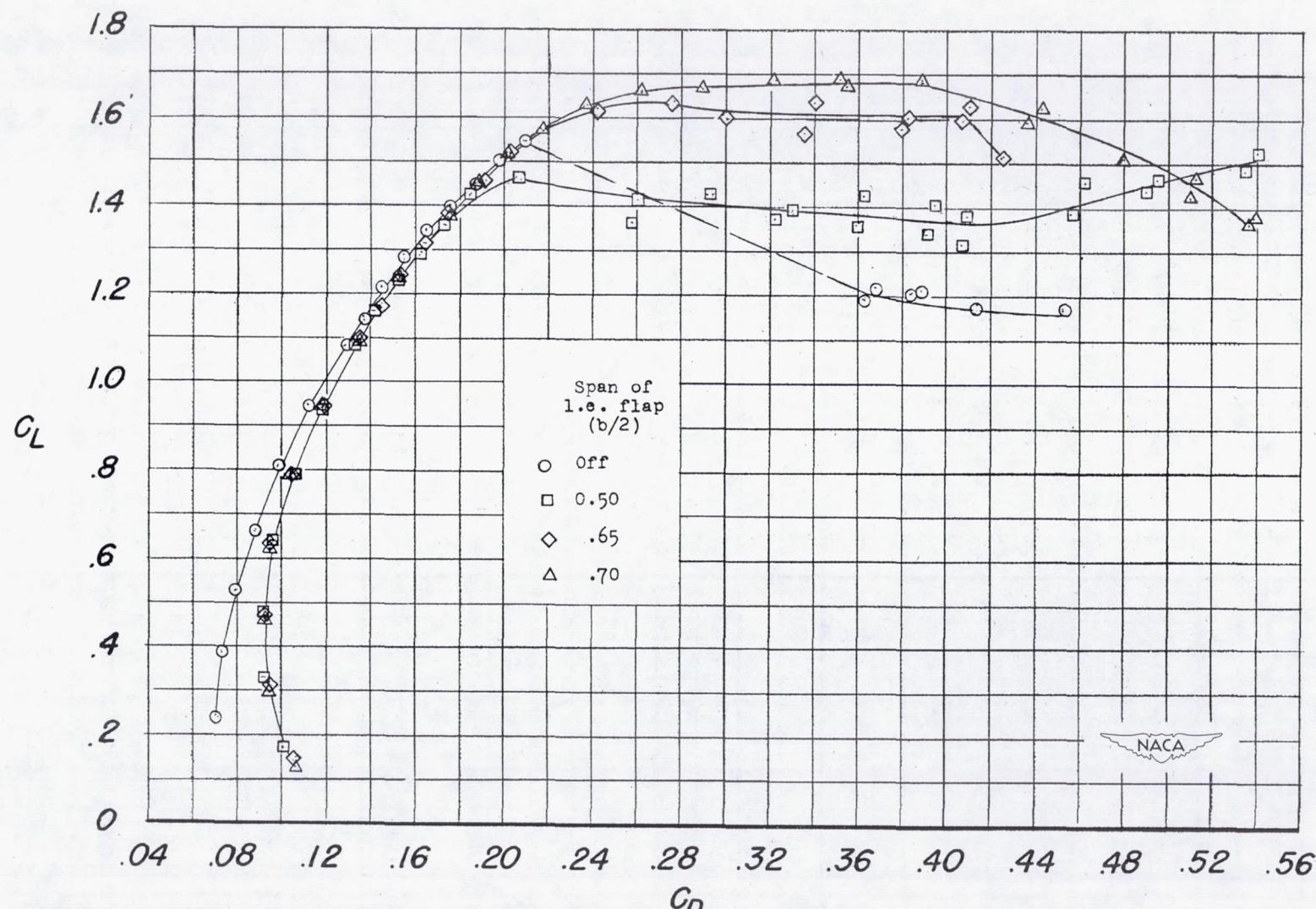
(b) Drag.

Figure 13.— Concluded.
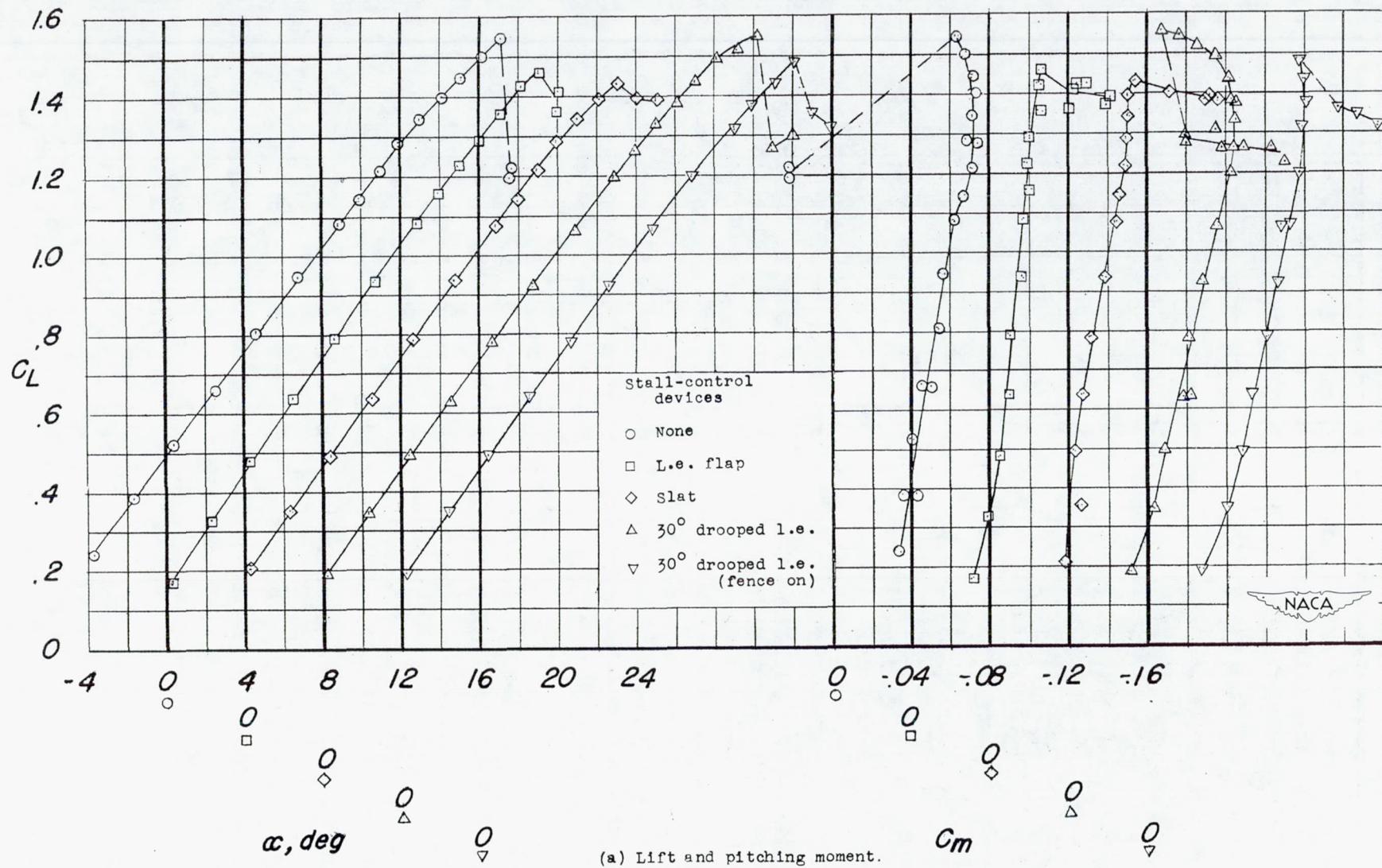
(a) Lift and pitching moment.

Figure 14.— Effects of various half-span stall-control devices on the aerodynamic characteristics of 37° sweptback semispan wing with half-span split flap. R=6,800,000.
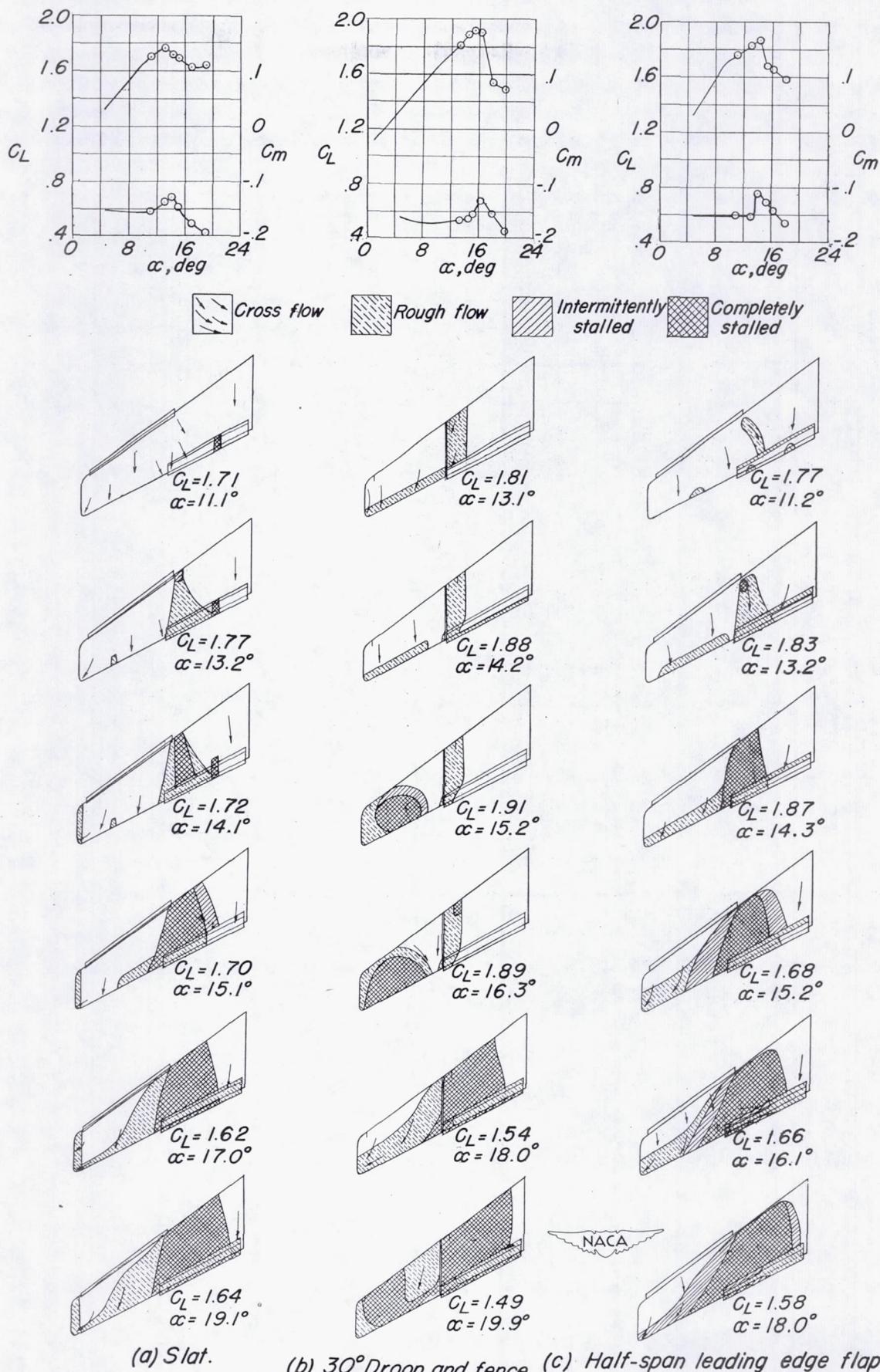
Stall-control
devices

○ None

□ L.e. flap

◇ Slat

△ 30° drooped l.e.

▽ 30° drooped l.e.
    (fence on)

(b) Drag.
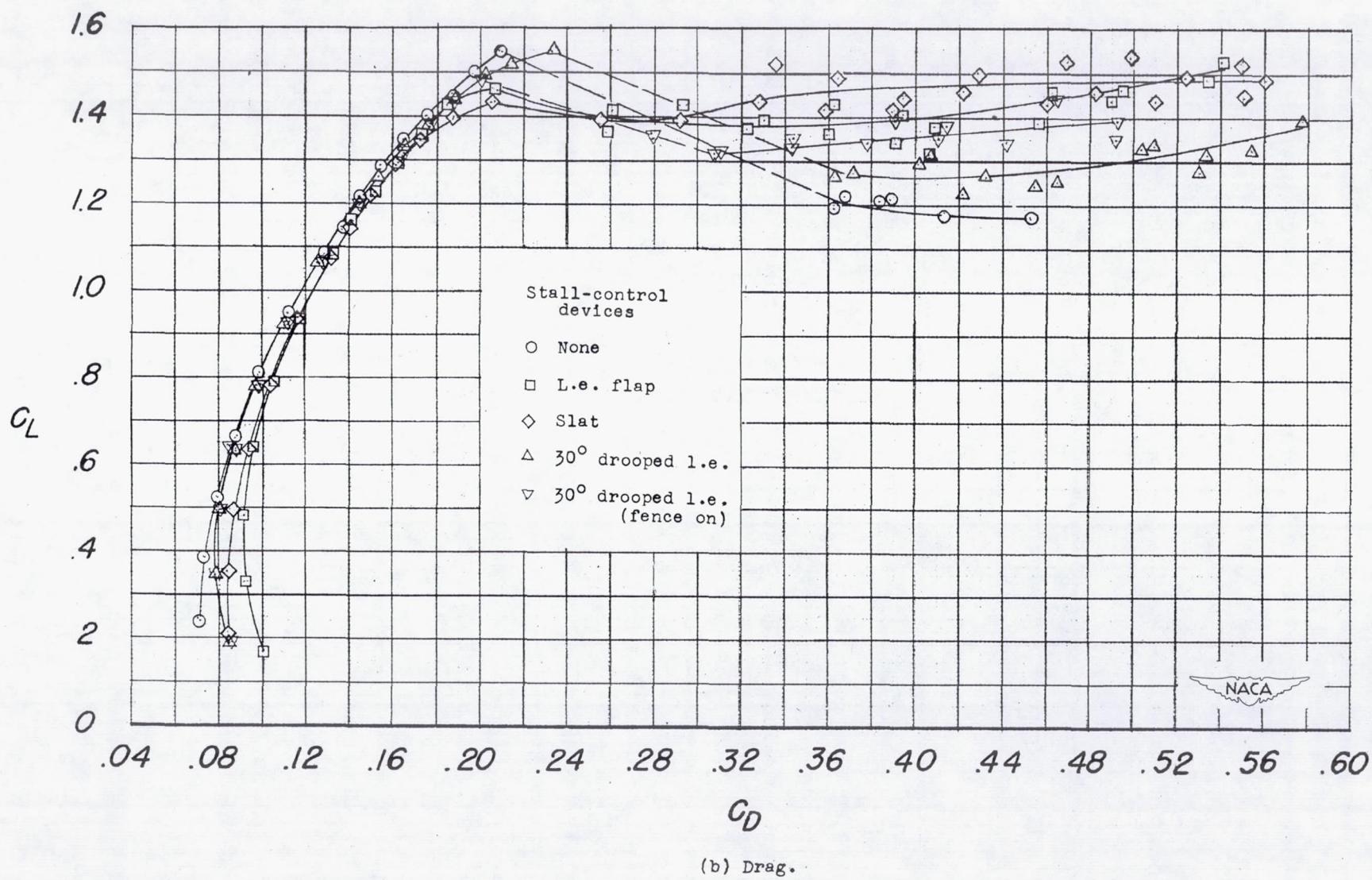
Figure 14.— Concluded.
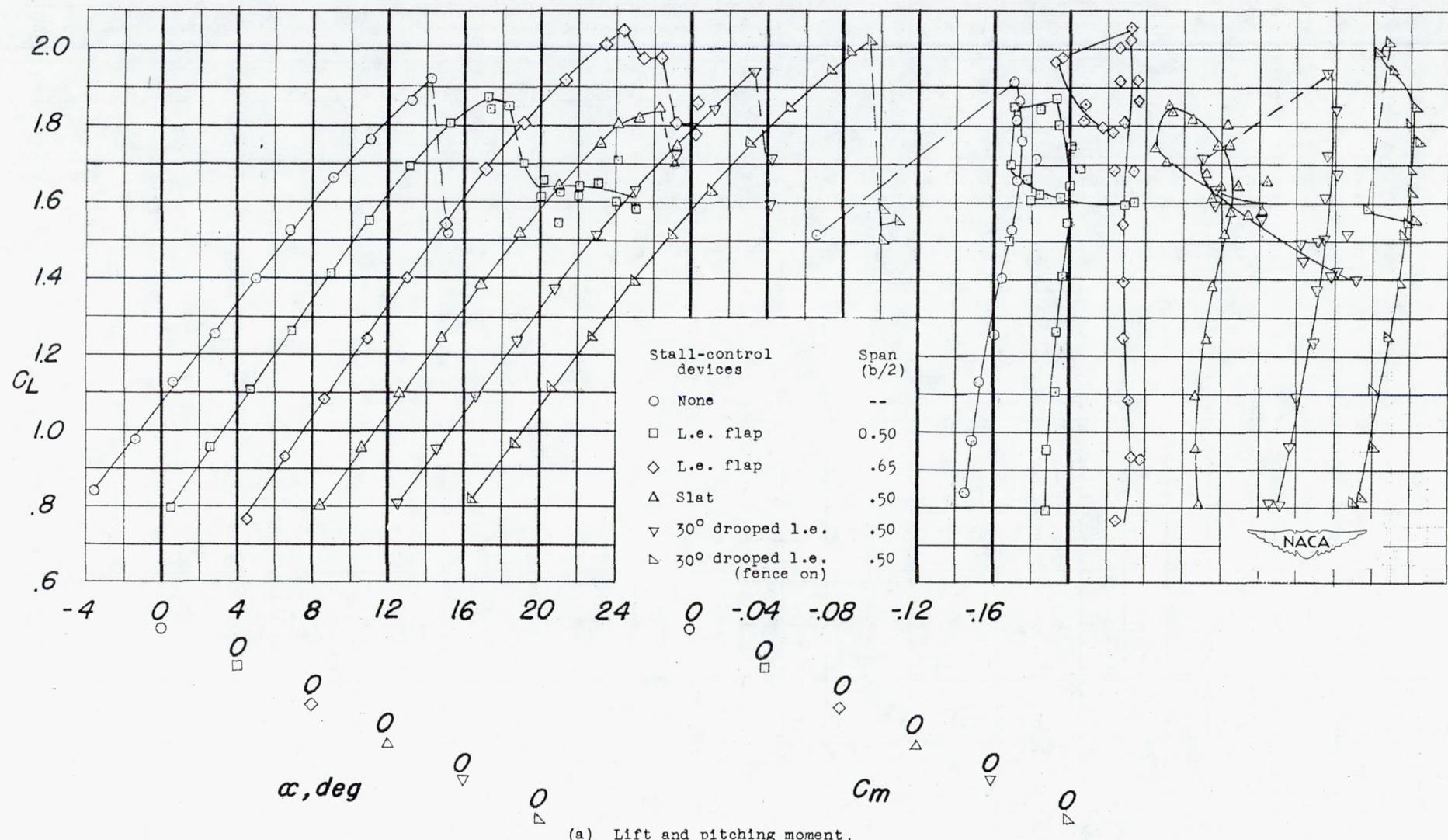
(a) Lift and pitching moment.

Figure 15.— Effects of various stall-control devices on the aerodynamic characteristics of 37° sweptback semispan wing with half-span double slotted flap. R = 6,800,000.

| Stall-control devices	Span (b/2)
○ None	--
□ L.e. flap	0.50
◇ L.e. flap	.65
△ Slat	.50
▽ 30° drooped l.e.	.50
◁ 30° drooped l.e. (fence on)	.50

(b) Drag.
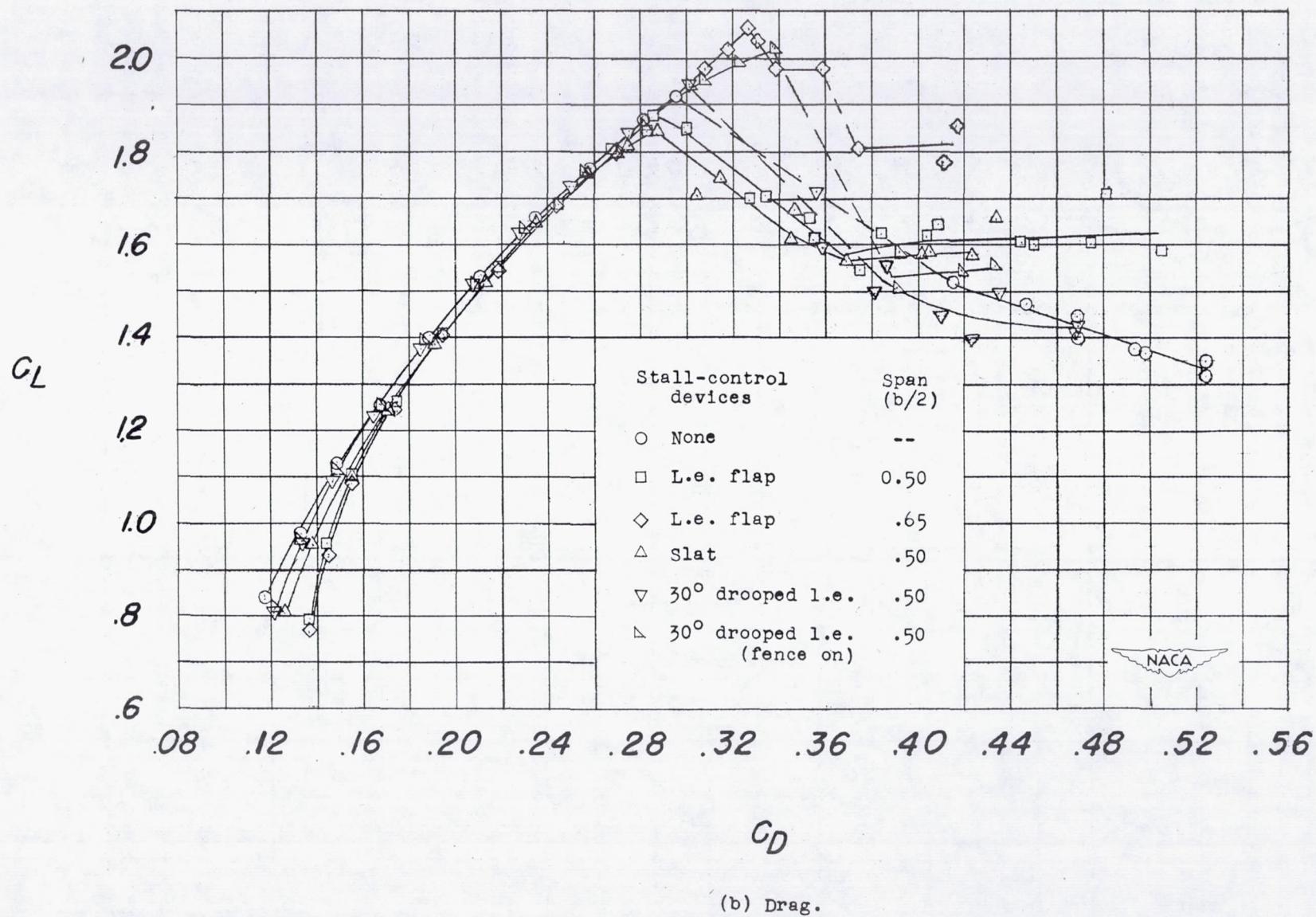
Figure 15.- Concluded.
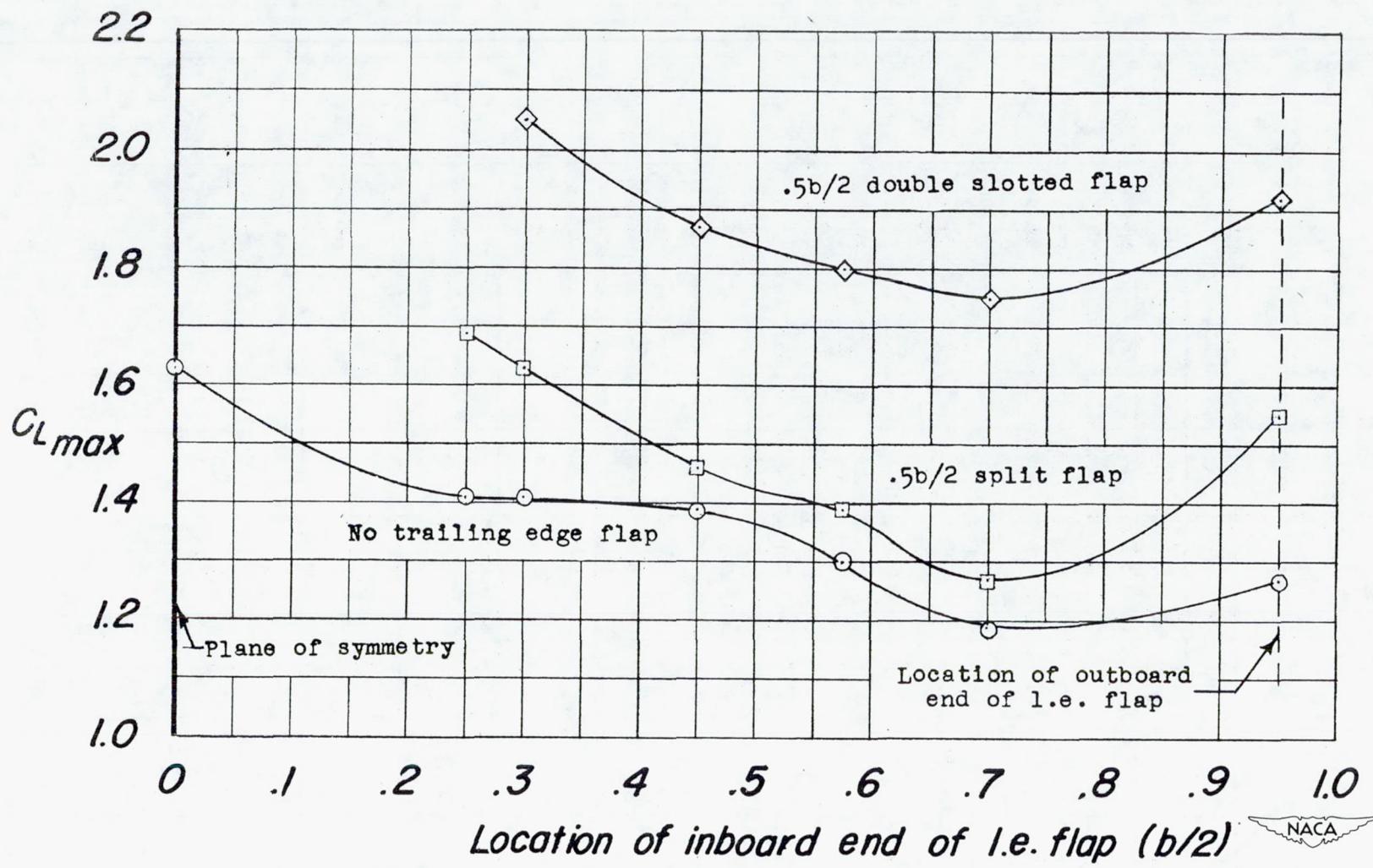
(a) Maximum lift.

Figure 16.- Effect of leading-edge flap span on maximum-lift and pitching-moment characteristics of 37° sweptback semispan wing with various trailing-edge flap configurations. R = 6,800,000.

(b) Pitching moment.

Figure 16.- Concluded.
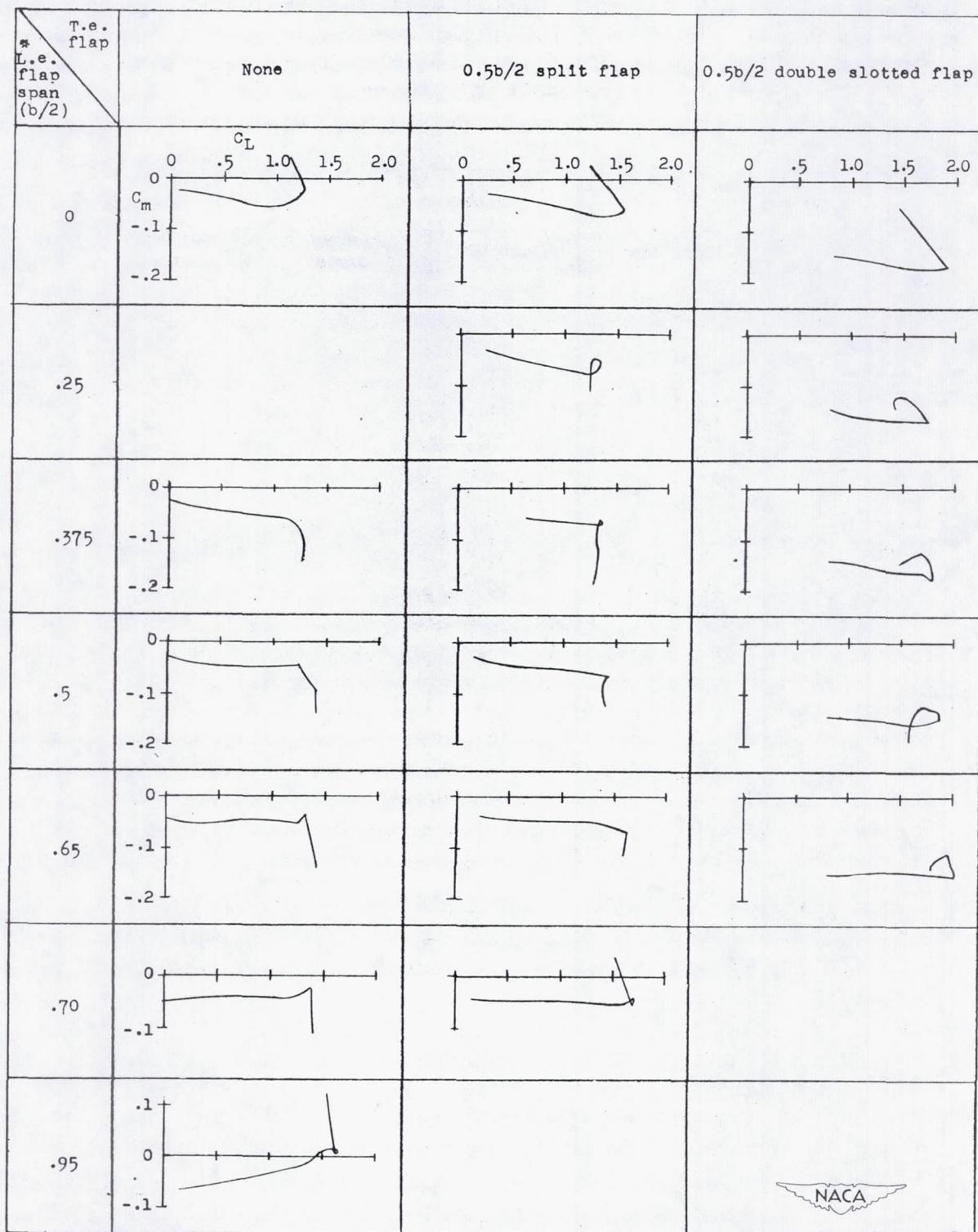
* Outboard end at 0.95b/2

(a) Slat.   (b) 30° Droop and fence.   (c) Half-span leading edge flap.
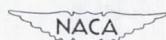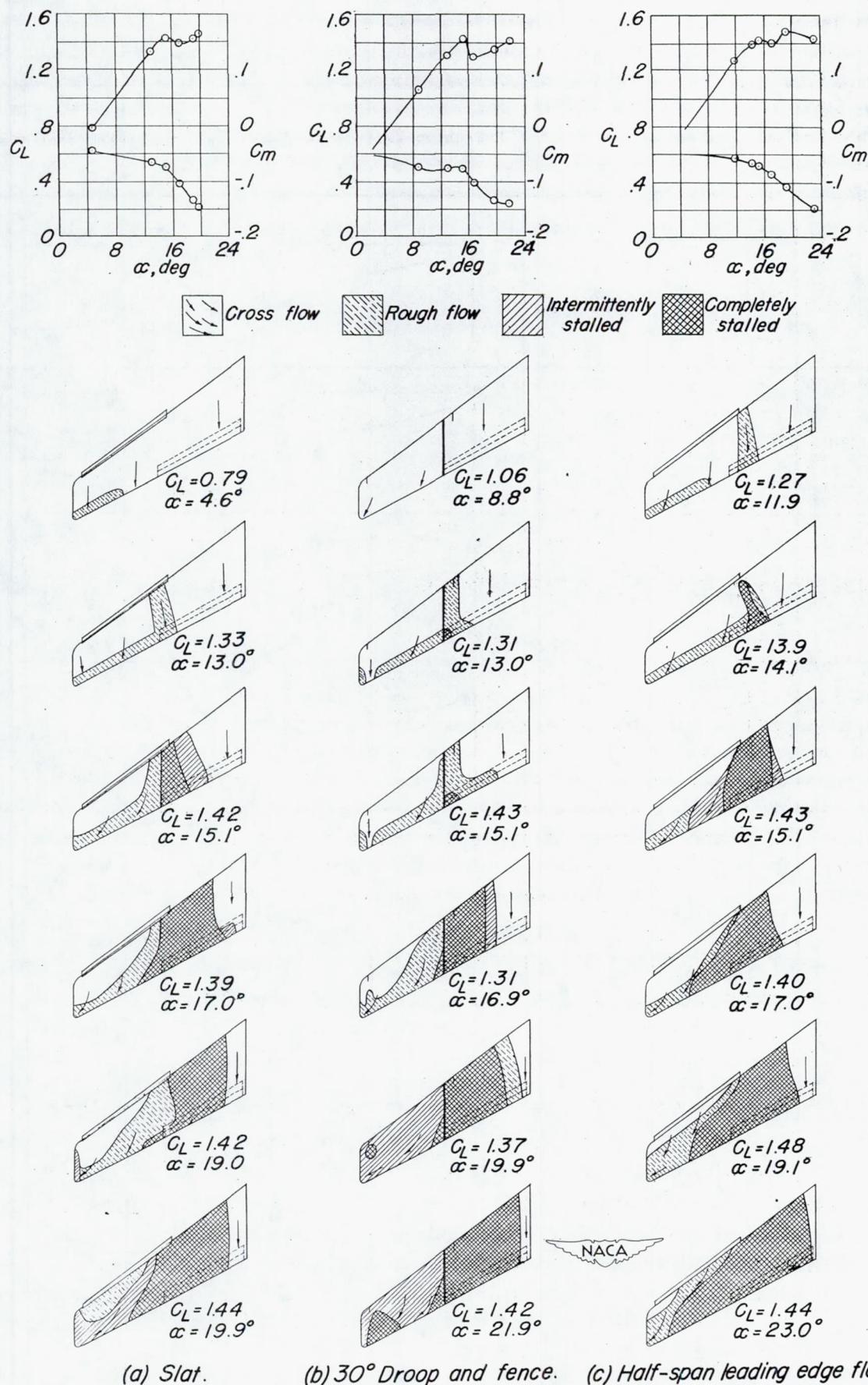
Figure 17.— Effects of stall-control devices on the stalling characteristics of
the 37° sweptback semispan wing with half-span split flap. R=6,800,000.

Cross flow   Rough flow   Intermittently stalled   Completely stalled

$C_L = 1.71$
$\alpha = 11.1°$

$C_L = 1.81$
$\alpha = 13.1°$

$C_L = 1.77$
$\alpha = 11.2°$

$C_L = 1.77$
$\alpha = 13.2°$

$C_L = 1.88$
$\alpha = 14.2°$

$C_L = 1.83$
$\alpha = 13.2°$

$C_L = 1.72$
$\alpha = 14.1°$

$C_L = 1.91$
$\alpha = 15.2°$

$C_L = 1.87$
$\alpha = 14.3°$

$C_L = 1.70$
$\alpha = 15.1°$

$C_L = 1.89$
$\alpha = 16.3°$

$C_L = 1.68$
$\alpha = 15.2°$

$C_L = 1.62$
$\alpha = 17.0°$

$C_L = 1.54$
$\alpha = 18.0°$

$C_L = 1.66$
$\alpha = 16.1°$

$C_L = 1.64$
$\alpha = 19.1°$

$C_L = 1.49$
$\alpha = 19.9°$

$C_L = 1.58$
$\alpha = 18.0°$

(a) Slat.   (b) 30° Droop and fence.   (c) Half-span leading edge flap.

Figure 18.— Effects of stall-control devices on the stalling characteristics of
the 37° sweptback semispan wing with half-span double-slotted flap.
$R = 6,800,000$

Spanwise location

(a) $\alpha = 4.9°$.

Spanwise location

(b) $\alpha = 9.0°$.
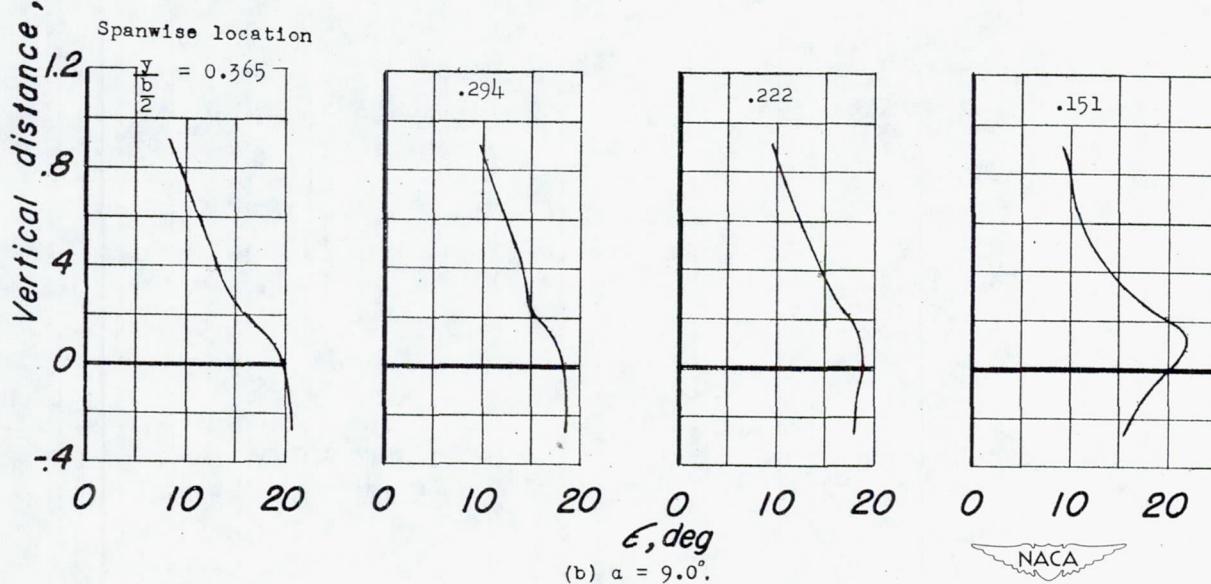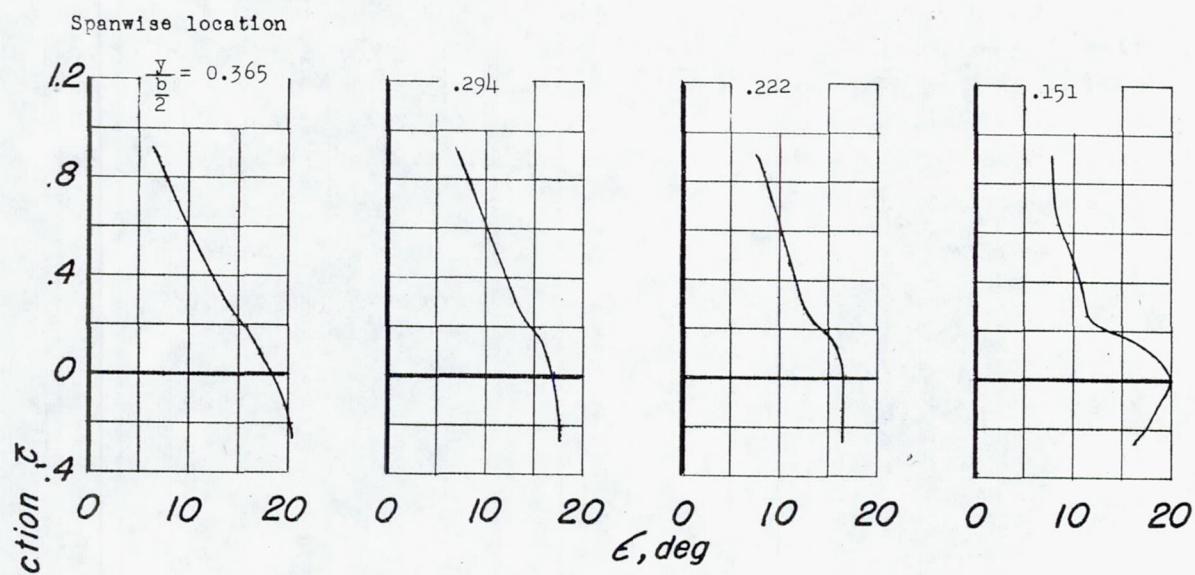
Figure 19.- Downwash surveys in a plane $2.0\bar{c}$ behind the $0.25\bar{c}$ point on 37° sweptback semispan wing with slat and half-span double slotted flap. R = 6,800,000.
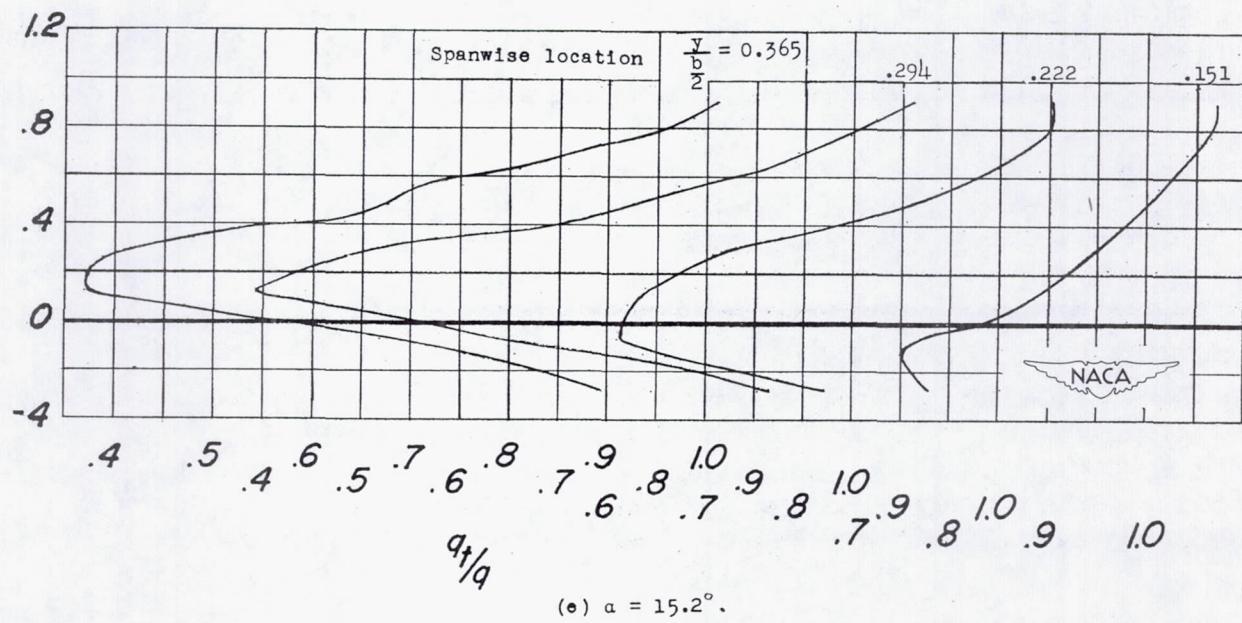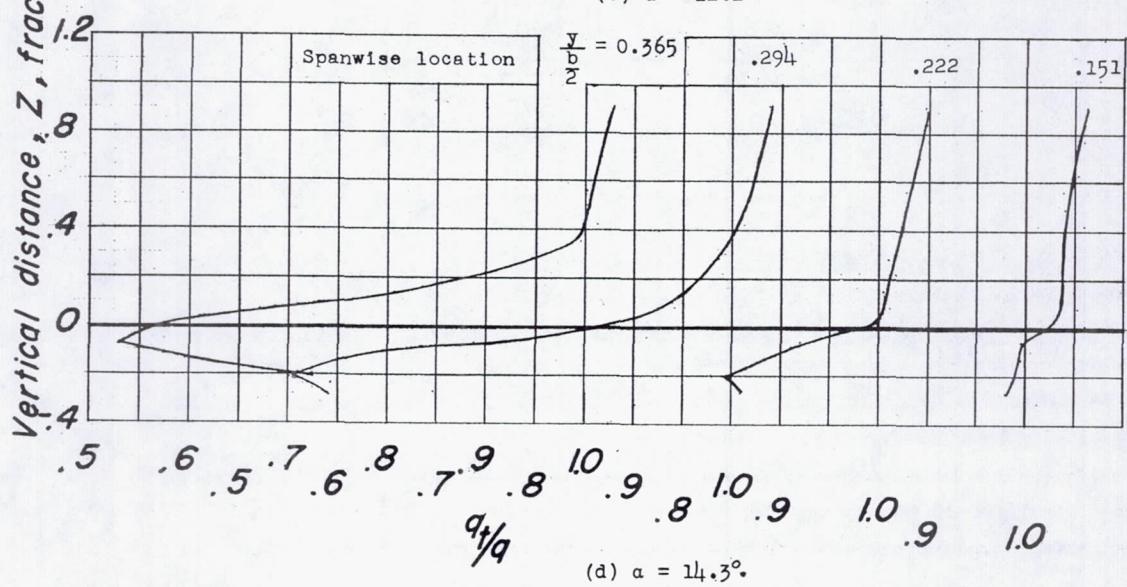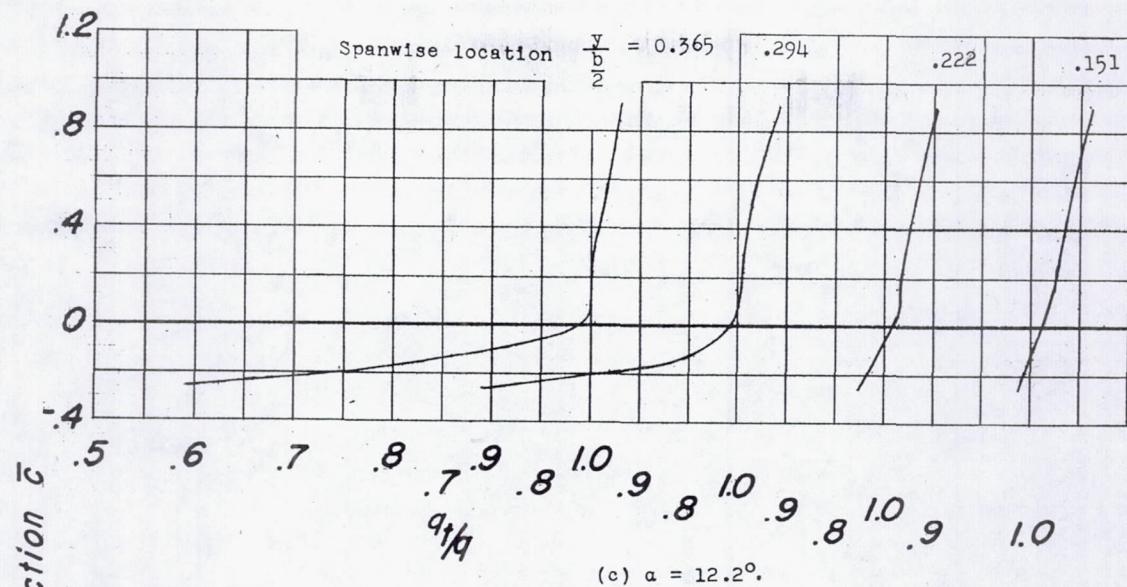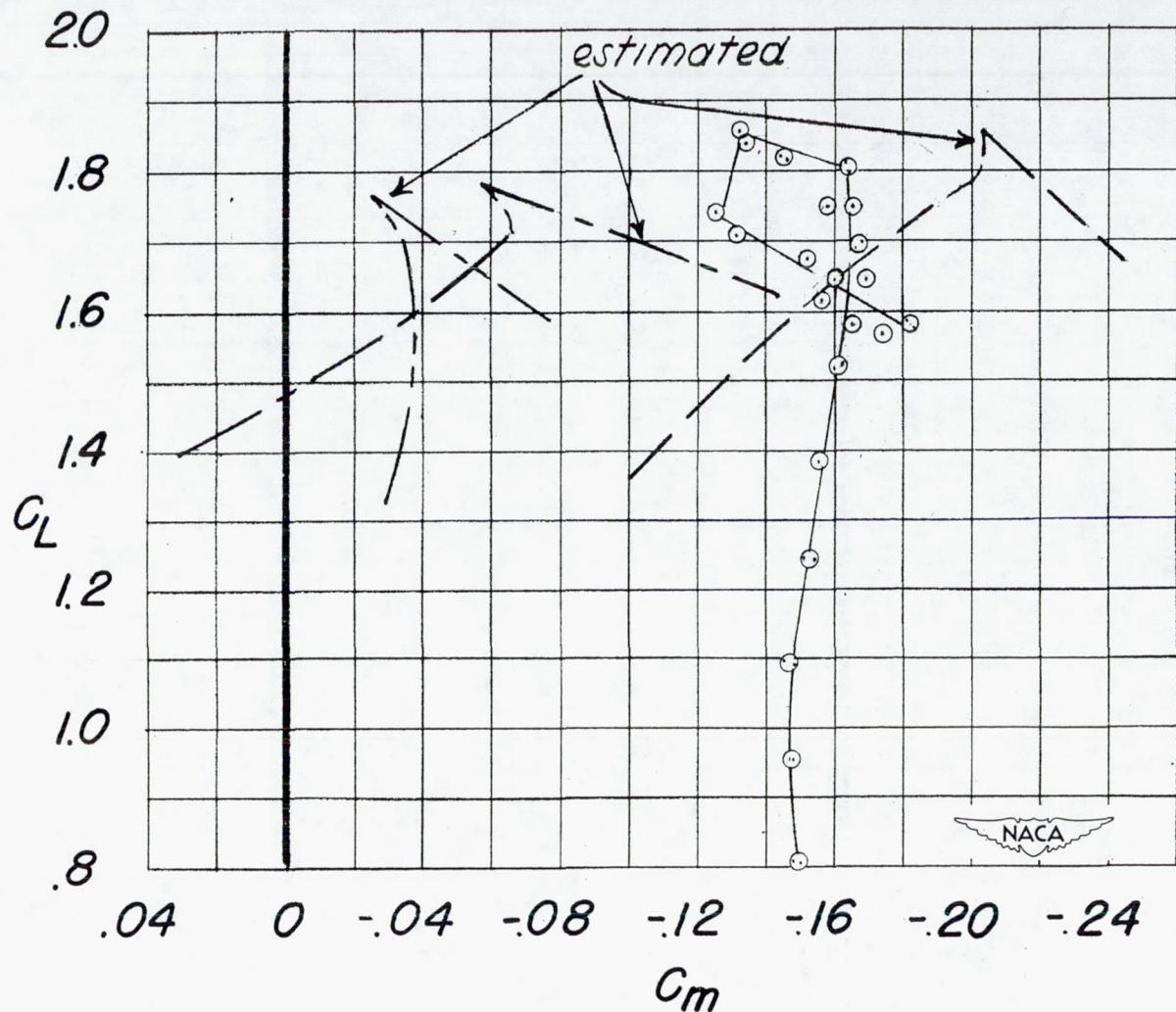
(c) a = 12.2°.

(d) a = 14.3°.

(e) a = 15.2°.

Figure 19.— Concluded.

Spanwise location

$\frac{y}{\frac{b}{2}} = 0.365$ .294   .222   .151

q_t/q

(a) $\alpha = 4.9°$

Vertical distance, Z, fraction $\bar{c}$

Spanwise location

$\frac{y}{\frac{b}{2}} = 0.365$ .294   .222   .151

q_t/q

(b) $\alpha = 9.0°$

NACA
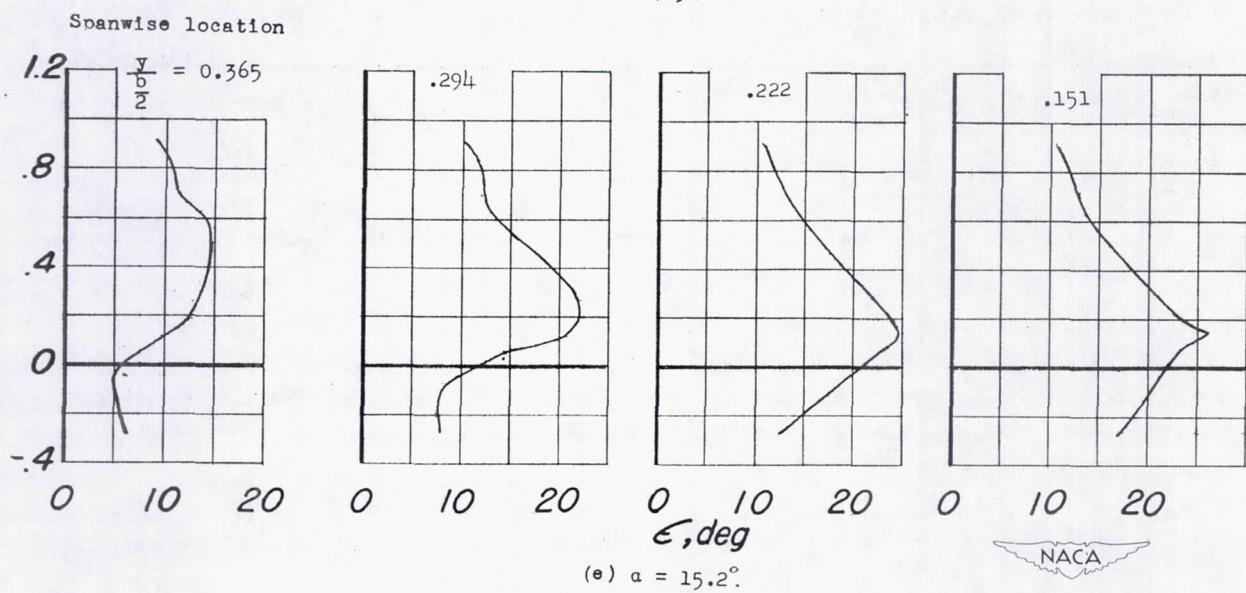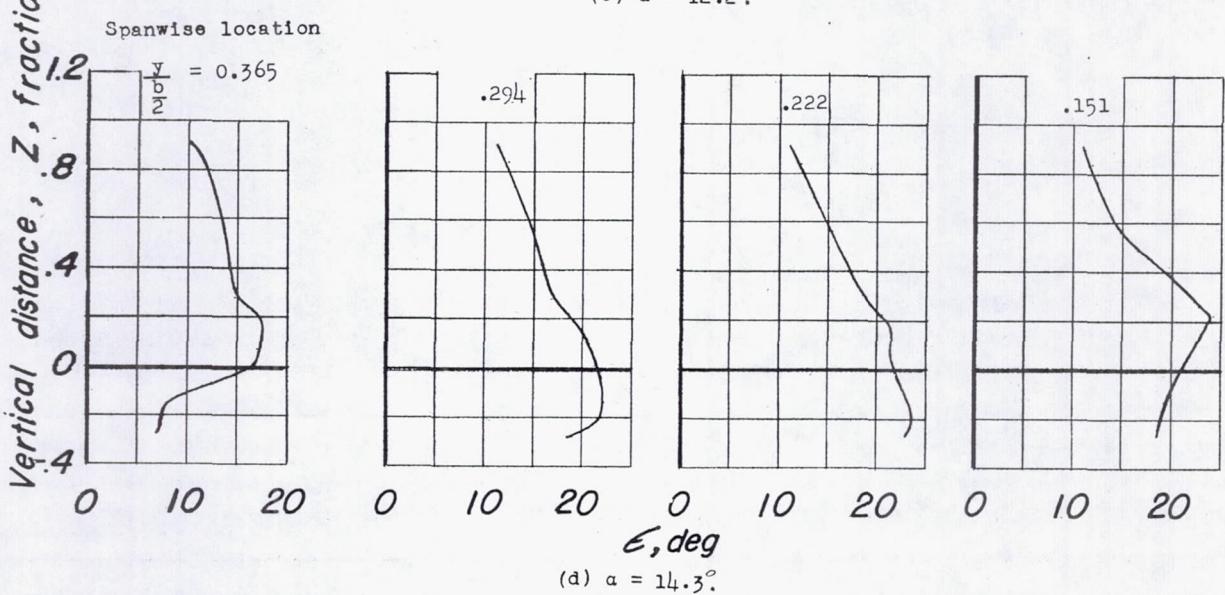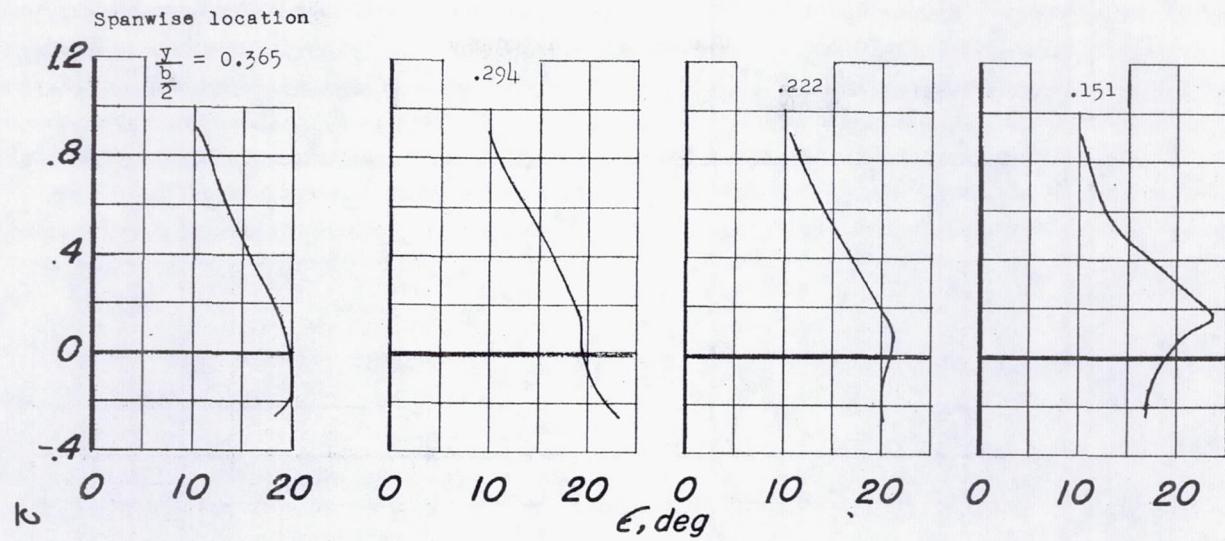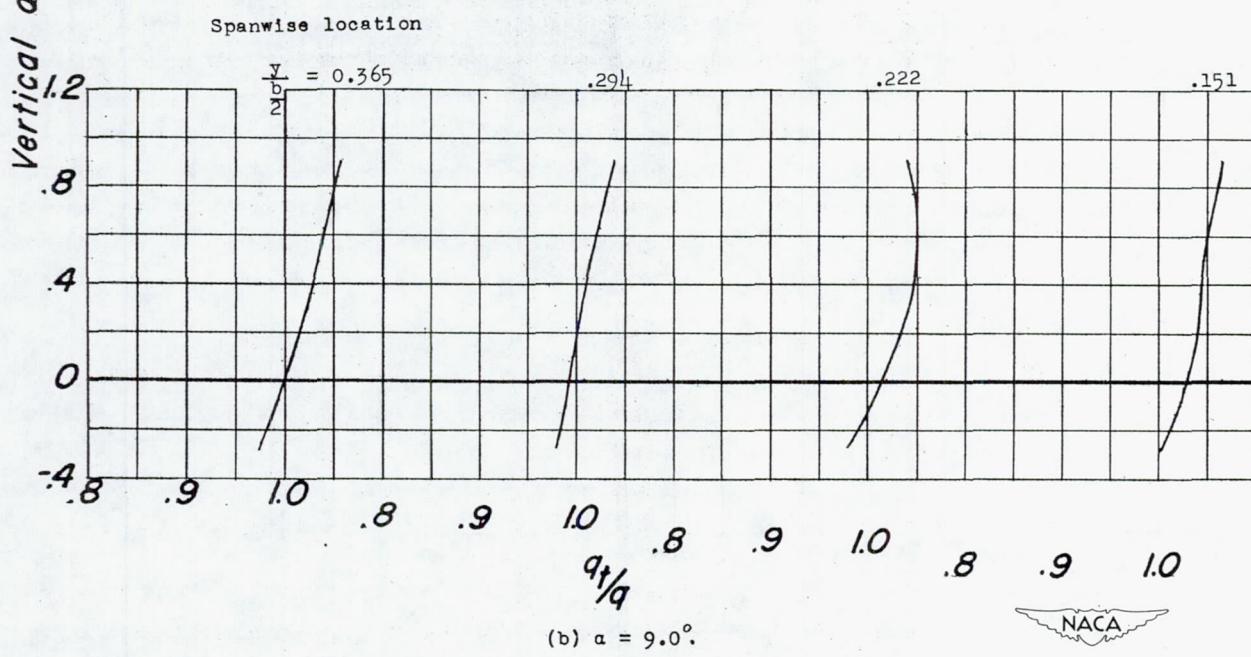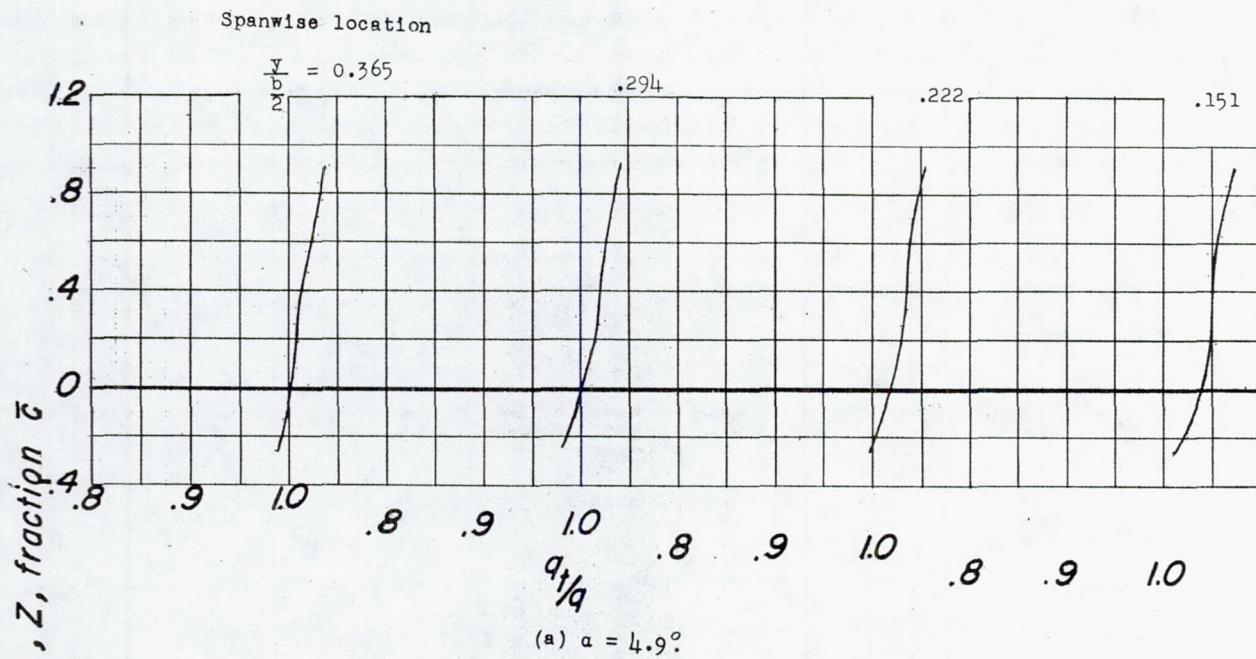
Figure 20.— Dynamic pressure surveys in a plane 2.0 $\bar{c}$ behind 0.25 $\bar{c}$ point on 37° sweptback semispan wing with slat and half-span double slotted flap. R = 6,800,000.

(c) a = 12.2°.

(d) a = 14.3°.

(e) a = 15.2°.

Figure 20.— Concluded.

Figure 21.— Effects of a horizontal tail at various locations on the pitching moment characteristics of the 37° sweptback semispan wing with slat and half-span double slotted flap. $R = 6,800,000$.

(a) Lift.
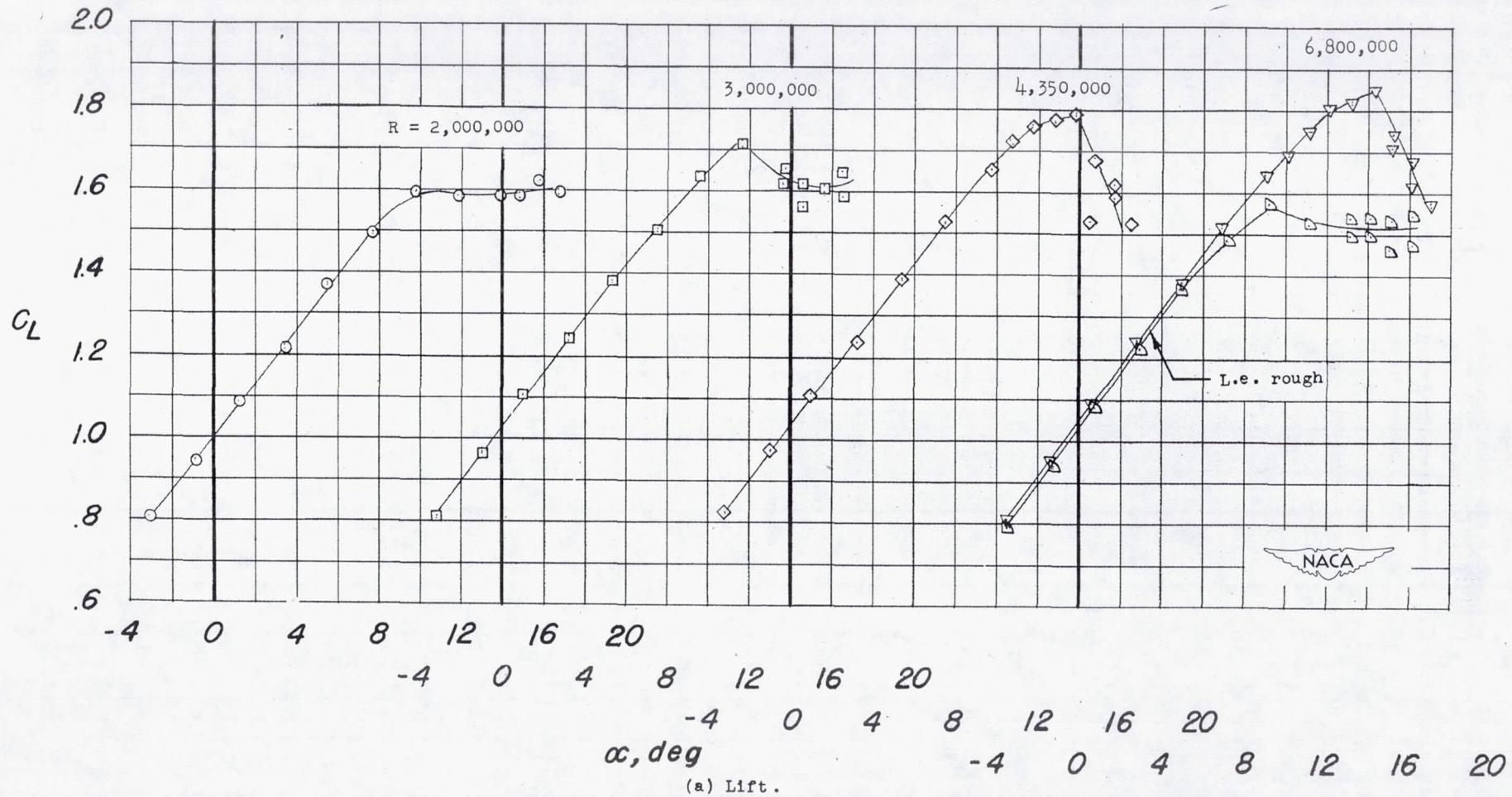
gure 22.— Effects of Reynolds number variation on the aerodynamic characteristics of the 37° sweptback semispan wing with slat and half-span double slotted flap.
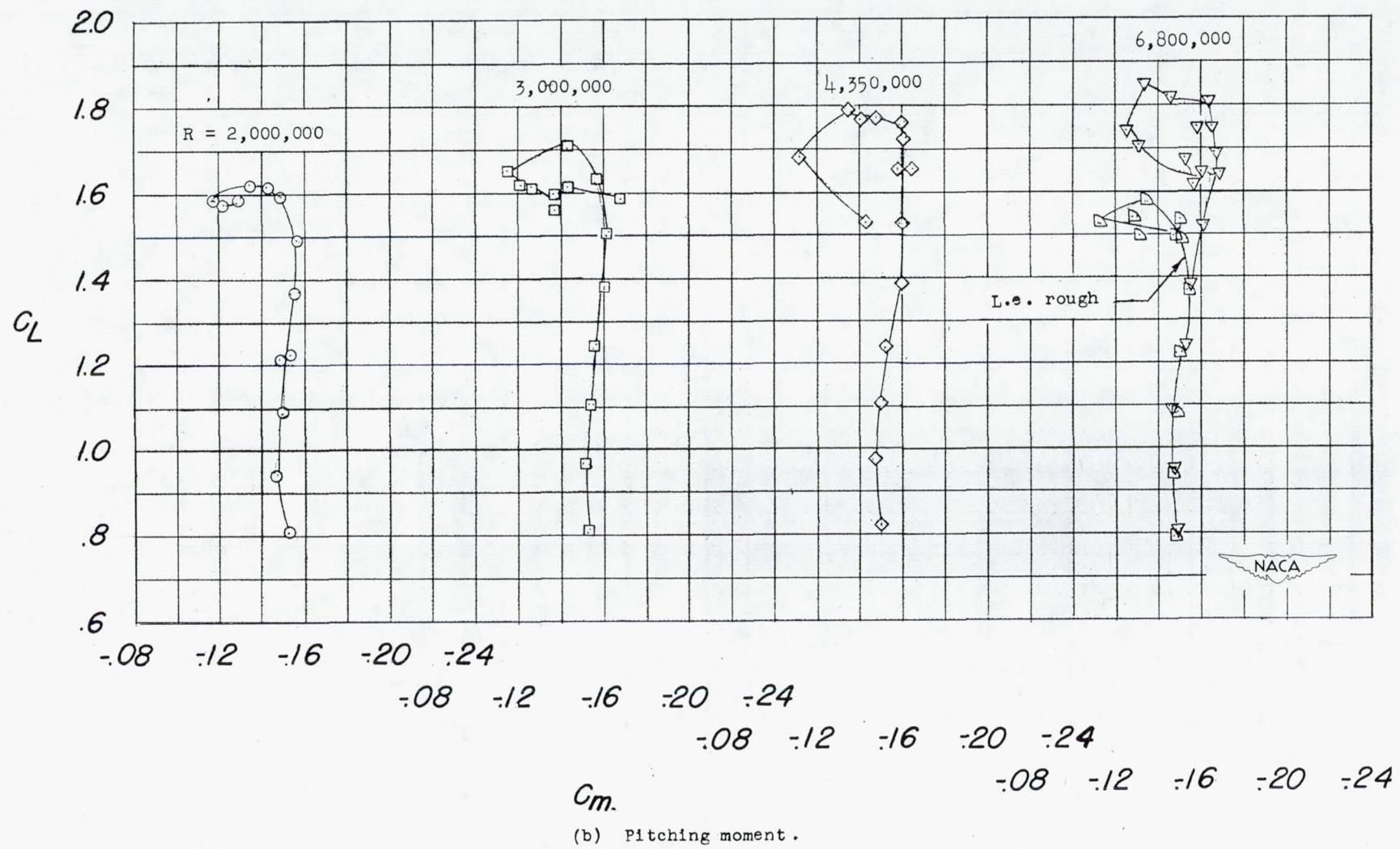
(b) Pitching moment.

Figure 22.— Continued.
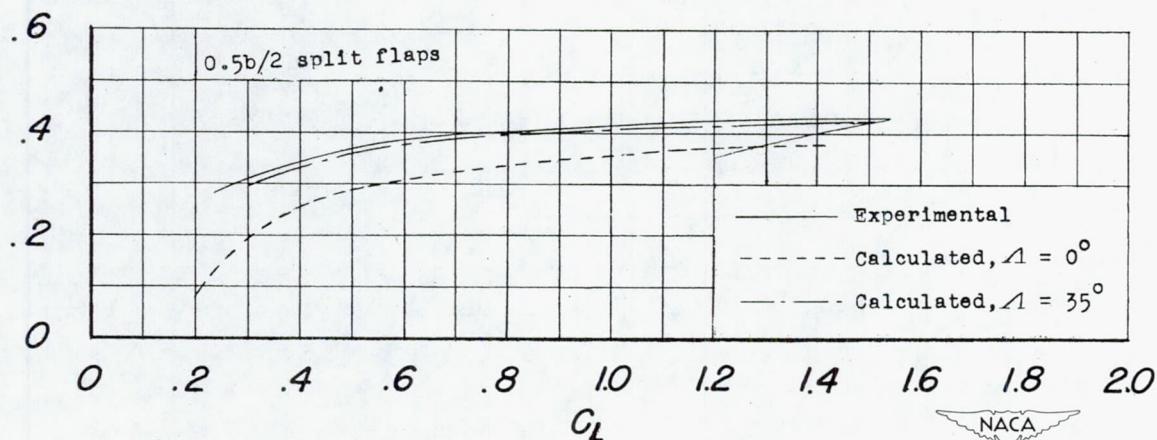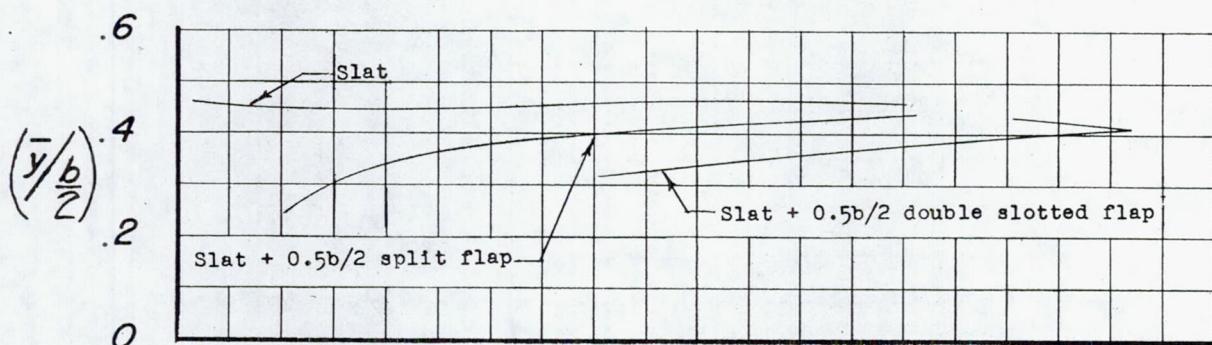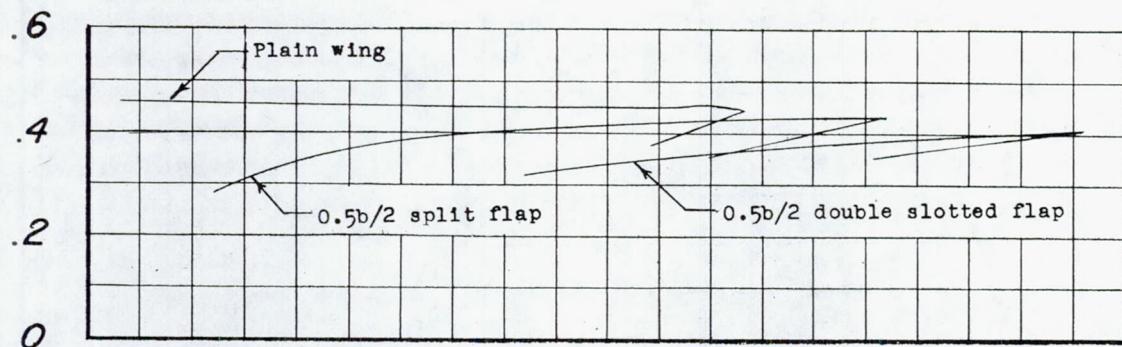
(c) Drag.
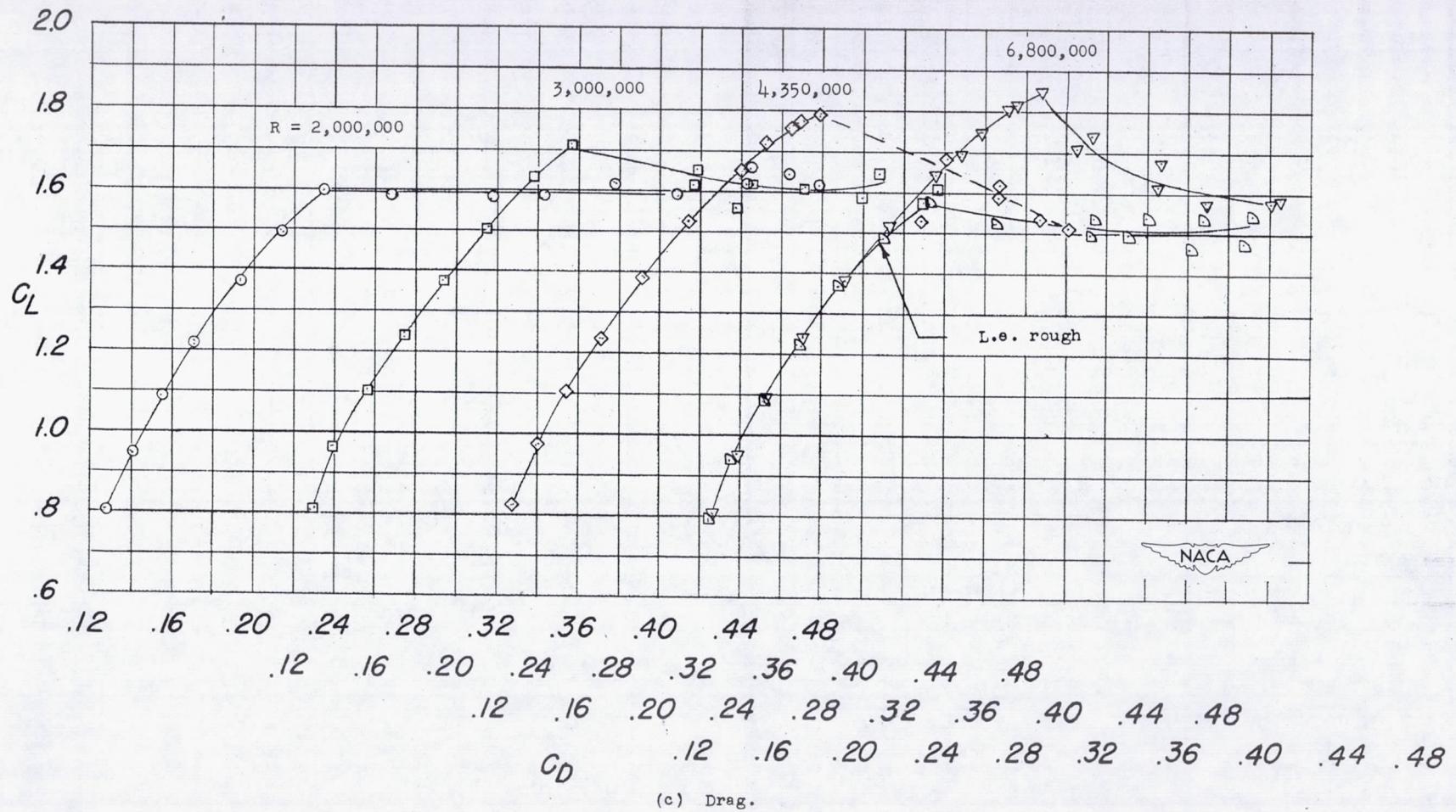
Figure 22.— Concluded.

Figure 23.- Spanwise location of the centroid of load distribution for several configurations of 37° sweptback semispan wing.